National Technical University of Athens

School of Chemical Engineering
Department of Materials Science and Engineering

Investigation and Optimization of Dye-Sensitized Solar Cells under Variable Light Conditions

PhD Thesis

George V. Belessiotis
Physicist, M.Sc.

PhD Supervisors:

C. Karagianni, Ret. Professor NTUA

P. Falaras, Dir. of Research NCSR Demokritos

E. Hristoforou, NTUA Professor

Examination Committee:

K. Kordatos, Prof. NTUA

E. Pavlatou, Prof. NTUA

E. Stefanakos, Prof. University of South Florida

E. Hristoforou, Prof. NTUA

A. G. Kontos, Assoc. Professor NTUA

C. Karagianni, Ret. Professor NTUA

P. Falaras, Dir. of Research NCSR Demokritos

The experimental part of the dissertation took place in the Institute of Nanoscience and Nanotechnology of NCSR "DEMOKRITOS

Approval of the doctoral dissertation from the School of Mechanical Engineering of National Technical University of Athens (NTUA) does not imply acceptance of the opinions of the author (Law 5343/1932, Article 202).

Athens, 2023

Abstract

The aim of this dissertation is the optimization of photovoltaics based on semiconductors for energy production under low intensity visible artificial light while maintaining or enhancing their performance under solar light. This investigation is focused on photovoltaic power generation with Dye Sensitized Solar Cells (DSSCs), specifically on the optimization of their components for good performance, under both simulated solar light and artificial indoor light (tube lamps of 100-1000 lux intensity).

The introductory chapter contains a presentation of the recent advances in the area of photovoltaics, focusing on both lab scale experiments and industrial applications and highlighting the suitability of DSSCs for indoor operation. The "panillumination" perspective for devices that can maintain their performance during radical changes in their lighting environment, is introduced. Furthermore, there is a great focus on DSSCs and their components of interest. After a description of the experimental details of this research in the first chapter, the experimental results are presented. In the second chapter, the electrolyte is the target component for DSSC optimization: a I^-/I_3^- redox electrolyte solution for well performing DSSCs under both indoor and outdoor lighting conditions, is characterized. Electrolyte attributes, including optical and mass transport properties, have been tailored and a good synergy between triiodide content, organic solvent mixture and additives in the electrolyte has been achieved, allowing DSSC adaptability under different lighting types and illumination intensities. The optical and redox properties were evaluated and the electrolyte was tested in DSSCs under different illumination conditions: simulated solar light (from 0.1 to 1 sun) and indoor light (from 100 to 1000 lux). Under indoor lighting, the optimized electrolyte leads to good power conversion efficiency (PCE) values. Moreover, significantly superior performance -compared to iodide-based indoor DSSCs reported in the literature- along with a constantly high fill factor was achieved under 100 mW/cm^2 (1 sun) simulated solar light.

The focus of the third chapter, is the suitability of the new electrolyte in relation to the sensitizer component, with a study covering several common organic and organometallic dyes. The sensitizers were studied in DSSCs under both sunlight (1 sun, 0.1 sun) and indoor fluorescent (200 lux) light sources: The most important factors, with respect to sensitizers, for a good "pan-illumination" performance under radically different light conditions, were deemed to be the suppression of recombination followed by the good spectral matching between absorber and emission source. Good recombination suppression was found to significantly improve the performance under low light.

The fourth chapter focuses on a more stable alternative panillumination electrolyte based on the Cs_2SnI_6 perovskite. Initially, a temperature-variable Raman investigation was performed, providing insight to its stability. After showing excellent stability without no phase change or significant restructuring in this characterization, it performed well as part of a quasi-solid DSSC under indoor light conditions. Finally, in the fifth chapter, general conclusions and perspectives on future research are presented.

Περίληψη

Στόχος της παρούσας διδακτορικής διατριβής είναι η βελτιστοποίηση φωτοβολταικών που βασίζονται σε ημιαγωγούς για παραγωγή ενέργειας κάτω από ορατό τεχνητό φως χαμηλής έντασης με παράλληλη διατήρηση ή ενίσχυση της απόδοσής τους κάτω από ηλιακό φως. Η έρευνα επικεντρώνεται στην παραγωγή φωτοβολταϊκής ενέργειας απο ηλιακά κελιά φωτοευαισθητοποιημένων ημιαγωγών (DSSCs) και συγκεκριμένα στη βελτιστοποίηση των επιμέρους στοιχείων τους με στόχο την καλή απόδοση, τόσο υπό προσομοιωμένο ηλιακό φως όσο και υπό τεχνητό φως εσωτερικού χώρου (σωληνοειδείς λαμπτήρες έντασης 100-1000 lux).

Το εισαγωγικό κεφάλαιο περιέχει μια παρουσίαση της πρόσφατης προόδου στον τομέα των φωτοβολταϊκών, εστιάζοντας τόσο σε πειράματα εργαστηριακής κλίμακας όσο και σε βιομηχανικές εφαρμογές και εξετάζοντας την καταλληλόλητα των DSSC για λειτουργία σε εσωτερικούς χώρους. Παράλληλα εισάγεται η προοπτική πανφωτισμού (“panillumination”) που αφορά διατάξεις που είναι σε θέση να διατηρήσουν την απόδοσή τους κατά τη διάρκεια ριζικών μεταβολών στις συνθήκες φωτισμού τους. Επιπλέον, ιδιαίτερη έμφαση δίνεται στην τεχνολογία DSSCs και στα χαρακτηριστικά των υλικών για την ανάπτυξη των διατάξεων αυτών. Μετα από μια περιγραφή των πειραματικών μεθόδων που εφαρμόστηκαν για την έρευνα αυτή στο πρώτο κεφάλαιο, παρουσιάζονται τα πειραματικά αποτελέσματα. Στο δεύτερο κεφάλαιο, παρουσιάζεται η βελτιστοποίηση του ηλεκτρολύτη: Χαρακτηρίζεται ένα διάλυμα ηλεκτρολύτη οξειδοαναγωγής I^-/I_3^- για καλές επιδόσεις DSSC τόσο σε συνθήκες εσωτερικού όσο και σε εξωτερικού φωτισμού. Έγινε ρύθμιση οπτικών ιδιοτήτων, ιδιοτήτων μεταφοράς μάζας και άλλων χαρακτηριστικών του ηλεκτρολύτη ώστε να επιτευχθεί μια καλή συνέργεια μεταξύ της περιεκτικότητας σε τριώδιο, του μείγματος οργανικών διαλυτών και των προσθέτων στον ηλεκτρολύτη, επιτρέποντας την προσαρμοστικότητα DSSC σε διαφορετικούς τύπους και εντάσεις φωτισμού. Οι οπτικές και οξειδοαναγωγικές ιδιότητες αξιολογήθηκαν και ο ηλεκτρολύτης δοκιμάστηκε σε DSSC υπό διαφορετικές συνθήκες ακτινοβόλησης: προσομοιωμένο ηλιακό φως (από 0,1 έως 1 ήλιο) και φως εσωτερικού χώρου (από 100 έως 1000 lux). Κάτω από τεχνητό φωτισμό χαμηλής έντασης, ο βελτιστοποιημένος ηλεκτρολύτης οδηγεί σε υψηλές τιμές απόδοσης μετατροπής ισχύος (PCE). Επιπλέον, σημαντικά ανώτερη απόδοση επιτυγχάνεται -σε σχέση με βιβλιογραφικά αναφερόμενα DSSCs

για εσωτερικούς χώρους με βάση το ιώδιο- μαζί με έναν συνεχώς υψηλό συντελεστή πλήρωσης (fill factor), υπό προσομοιωμένο ηλιακό φως (100 mW/cm^2).

Στόχος διερεύνησης του τρίτου κεφαλαίο, είναι η καταλληλόλητα του νέου ηλεκτρολύτη σε σχέση με τον ευαισθητοποιητή (χρωστική), με μελέτη μιας σειράς από τις πιο συνήθεις οργανικές και οργανομεταλλικές χρωστικές. Οι χρωστικές μελετήθηκαν σε DSSC υπό ηλιακό φως (1 ήλιος, 0,1 ήλιος) και υπο τεχνητή πηγή φωτός (200 lux): Οι πιο σημαντικοί παράγοντες όσον αφορά τους ευαισθητοποιητές για μια καλή απόδοση "panillumimation" κάτω από ριζικά διαφορετικές συνθήκες φωτισμού, βρέθηκαν ότι είναι η αποφυγή της επανασύνδεσης φορέων και η καλή φασματική συμφωνία μεταξύ απορροφητή και πηγής εκπομπής φωτός. Η υψηλή αντίσταση στην επανασύνδεση φορέων βρέθηκε να ενισχύει σημαντικά την απόδοση υπό χαμηλό φωτισμό.

Το τέταρτο κεφάλαιο επικεντρώνεται σε έναν πιο σταθερό εναλλακτικό ηλεκτρολύτη πανφωτισμού με βάση τον περοβσκίτη Cs_2SnI_6. Αρχικά πραγματοποιήθηκε μελέτη του περοβσκίτη με τεχνική Raman σε μεταβαλλόμενη θερμοκρασία για τον έλεγχο της σταθερότητας του. Ο περοβσκίτης παρουσίασε εξαιρετική σταθερότητα χωρίς καμία αλλαγή φάσης ή σημαντική αναδιάρθρωση στην μελέτη αυτή και, στην συνέχεια, παρουσίασε αξιοσημείωτη απόδοση σε ημι-στερεό DSSC υπό συνθήκες φωτισμού εσωτερικού χώρου. Τέλος, στο πέμπτο κεφάλαιο παρουσιάζονται γενικά συμπεράσματα και προοπτικές για μελλοντική έρευνα.

Journal Publications that resulted from this work

[1] G. V. Belessiotis, I. Ibrahim, C.S. Karagianni, P. Falaras, DSSCs for Indoor Environments: From Lab Scale Experiments to Real Life Applications, SVOA Mater. Sci. &Technology. 3 (2020) 01–05.

[2] G. V. Belessiotis, M. Antoniadou, I. Ibrahim, C.S. Karagianni, P. Falaras, Universal electrolyte for DSSC operation under both simulated solar and indoor fluorescent lighting, Mater. Chem. Phys. 277 (2021) 125543. https://doi.org/10.1016/j.matchemphys.2021.125543.

[3] G. V. Belessiotis, I. Ibrahim, P. Falaras, Sensitizer effects on DSSC performance under pan-illumination conditions, J. Photochem. Photobiol. A Chem. 433 (2022). https://doi.org/10.1016/j.jphotochem.2022.114201.

[4] G. V. Belessiotis, M. Arfanis, A. Kaltzoglou, V. Likodimos, Y.S. Raptis, P. Falaras, A.G. Kontos, Temperature effects on the vibrational properties of the Cs2SnX6 ‘defect’ perovskites (X = I, Br, Cl), Mater. Chem. Phys. 267 (2021) 124679. https://doi.org/10.1016/j.matchemphys.2021.124679.

Table of Contents

Introduction and Theory

Experimental Details

Results and Discussion

Introduction and Theory

1. The significance of green light-activated semiconductor technologies

As we advance into the 21st century, the need and urgency for conscious strategies for environmental protection increases. One such strategy with the aim to prevent further environmental damage is adopting green environmentally friendly technologies for our various resource requirements, an example being green renewable energy production. The field of light-activated semiconductor technologies serves this purpose. Such technologies are based on charged pair (e^-/h^+) generation and transfer, caused by a light source irradiating a semiconducting material. A main advantage is the utilization of naturally occurring light sources for their function.

With the depletion of fossil fuel energy sources and the urgent demands for green renewable energy production technologies, the field of photovoltaics has been attracting significant attention recently. Photovoltaics (PV) utilize light to produce electricity and have the potential to satisfy energy demands around the globe with sufficiently large deployment area [1]. A common trend is the application of BIPV and BAPV (Building integrated/applied photovoltaics). With BAPV, a retrofitting of photovoltaic technologies onto building areas is performed, while with BIPV typical building materials such as facades are replaced with PV capable devices [1]. The use of BIPV/BAPV, assures energy generation close to its intended destination, avoiding energy transportation and storage issues. BIPV/BAPV have been thought to be especially promising applications (estimated over 30 million USD net worth by 2022 [2]). Additionally, some PV technologies have considerable performance under indoor light conditions making them especially suitable for BIPV/BAPV and PIPV (Product integrated PV [3]) applications.

2. Dye Sensitized Solar Cells (DSSCs): Basic Principles

As a part of the 3rd generation of photovoltaic technologies, Dye Sensitized Solar Cells (DSSCs) have paved the way for efficient low-cost energy production. A typical DSSC is comprised of a working electrode (W.E.), a counter electrode and a charge transfer medium in-between them (Fig. 1). The working electrode consists of a conductive substrate (usually glass with a conductive layer on top of it), onto which the semiconductor film (most commonly TiO_2) has been deposited, with the dye being chemisorbed to the semiconductor molecules. On the other end, there is a catalyst-covered (e.g. Pt) counter electrode (C.E.) and both electrodes are connected to an external circuit. Finally, in liquid-based DSSCs, a solution of electrolyte exists between the two electrodes preventing their direct contact and facilitating charge transfer between them through ionic diffusion.

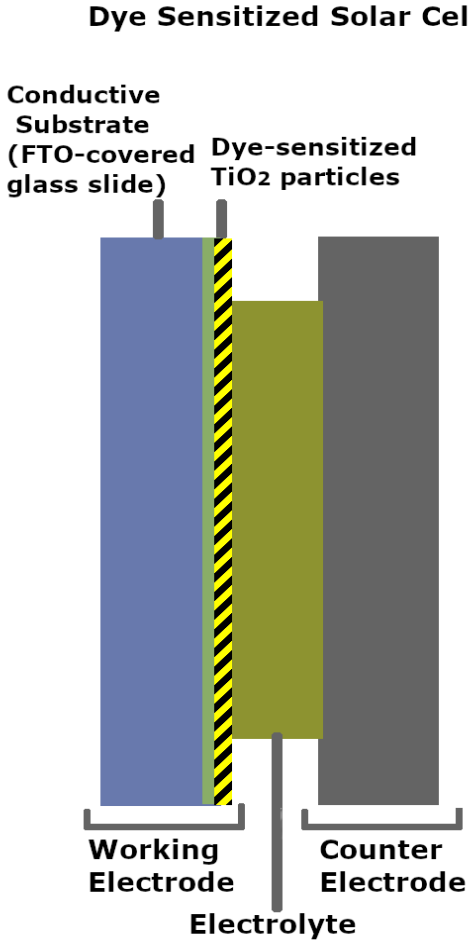

Fig. 1 DSSC components

The basic operation of a DSSC [4] is described below (Fig. 2): The semiconductor material rests on top of the working electrode's substrate as a conductive network of nanoparticles onto where the dye molecules adsorb. Photoexcitation (excitation by light irradiation) of the dye molecules, leads to the injection of their electrons into the conduction band of the adjacent semiconductor. These electrons, then, proceed to the external circuit. For the cycle to continue, the dye's electrons need to be replaced, for it to return to the ground state and be in a position for photoexcitation yet again. This is the role of the electrolyte. The dye's electrons are "regenerated" by the oxidation of electrolyte species, which in turn receive electrons from the counter electrode.

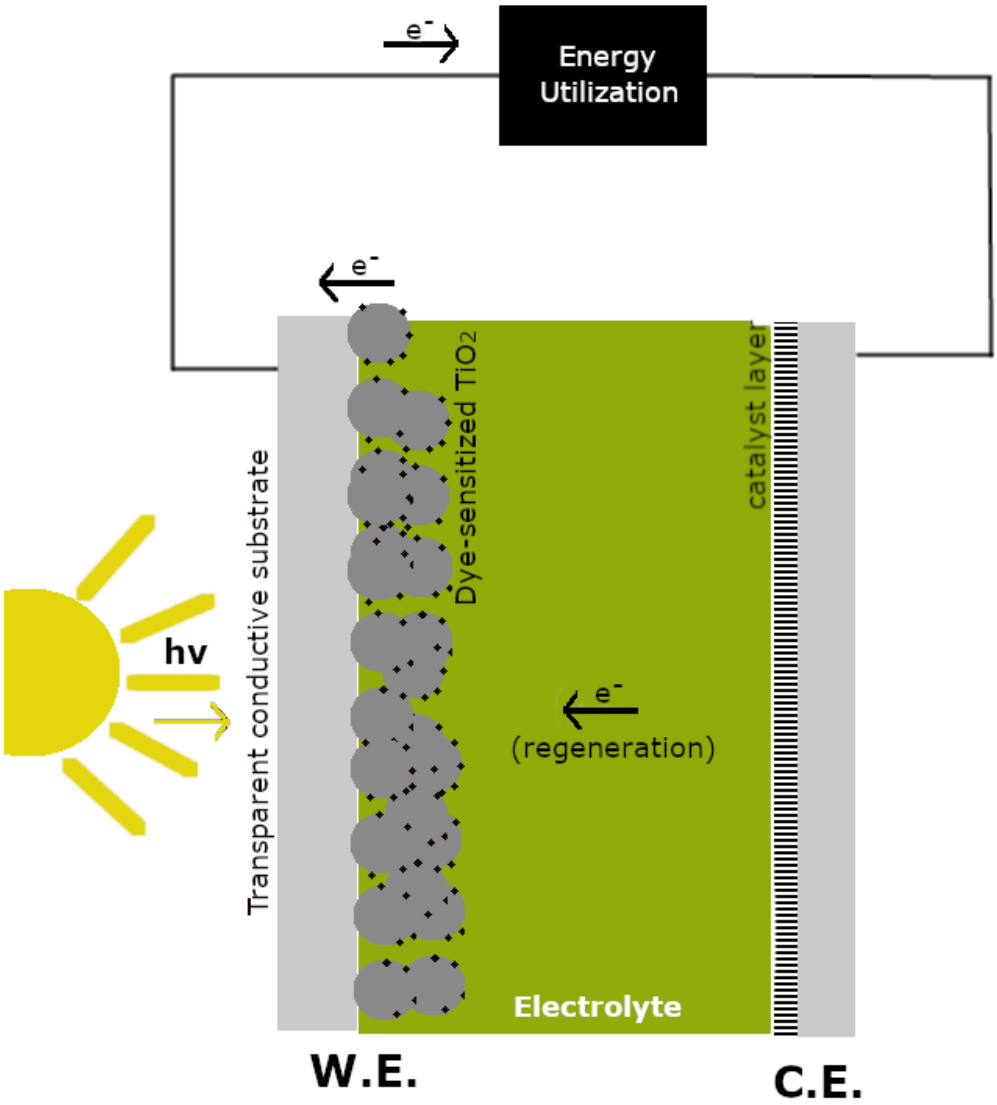

Fig. 2. Basic operating principle of a DSSC

More specifically, with a I^-/I_3^- redox couple electrolyte (Fig. 3i), iodide anions (I^-) are oxidized, providing electrons so that the oxidized dye can be regenerated, and this oxidation reaction of iodide leads to triiodide (I_3^-) ions. These triiodide ions, then, need to diffuse through the solution, in order to reach the C.E., receive electrons from the external circuit and be reduced back to I^-, thereby renewing the cycle with these I^- heading back to regenerate newly oxidized dye molecules. It is evident that proper electrolyte function in a DSSC, requires sufficient ion mobility in the electrolyte solution. This mobility is usually ensured via an ion concentration gradient, a higher number of ions at a point A of the liquid compared to a point B, creates the conditions for ion diffusion towards point B. The steeper the concentration gradient, the greater the speed of ion diffusion.

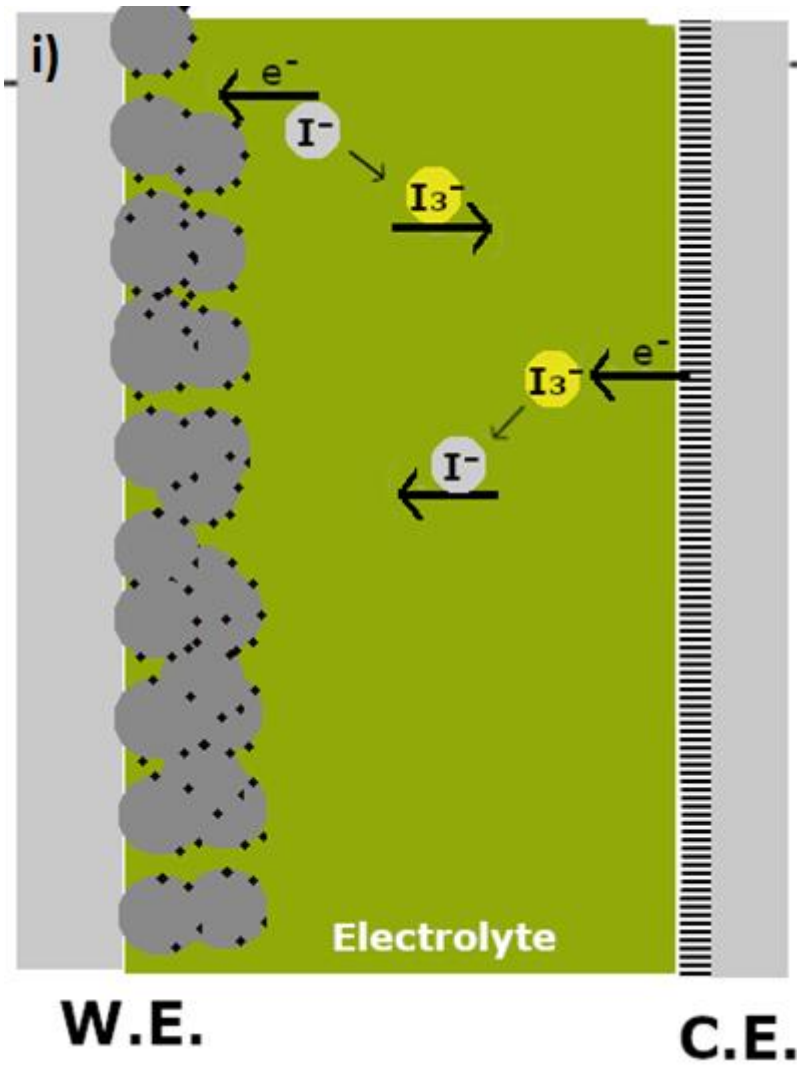

Fig. 3 i) Cycle of regeneration in a Γ/I3- electrolyte-based DSSC ii) Recombination of TiO_2 CB electrons to triiodide ions.

A prominent characterization method for a DSSC is its current-voltage (or current density-voltage) curve, also known as JV curve, commonly used for the evaluation of the cell's operation under illumination (Fig. 4). This curve is the result of the recording of current values (produced from the cell when under irradiation by a light source) during the linear change of the applied voltage value (at a specific V/s rate). DSSCs are characterized by a number of specific values that are derived from such a plot: such as their photo-conversion efficiency (PCE), their voltage at open circuit conditions (Voc), their current density at short circuit conditions (Jsc) and their fill factor (FF). Voc, which is determined by the difference between the electrons' quasi-Fermi level in the semiconductor and the electrolyte's redox potential [5], can be identified at open circuit conditions (where the produced current is zero). Jsc, is identified as the maximum produced current density value at zero voltage conditions. Current density values are calculated by dividing the current values by the illuminated area of the cell (known as "active cell area"), usually in mA/cm^2 units, and is often used instead of the current value itself as it allows for comparisons between cells regardless of active areas. As the generated power is derived from the product of current and voltage, the point on the curve where the product of the generated current (or current density) and the voltage has its maximum value, is defined as the maximum power point (Mpp).

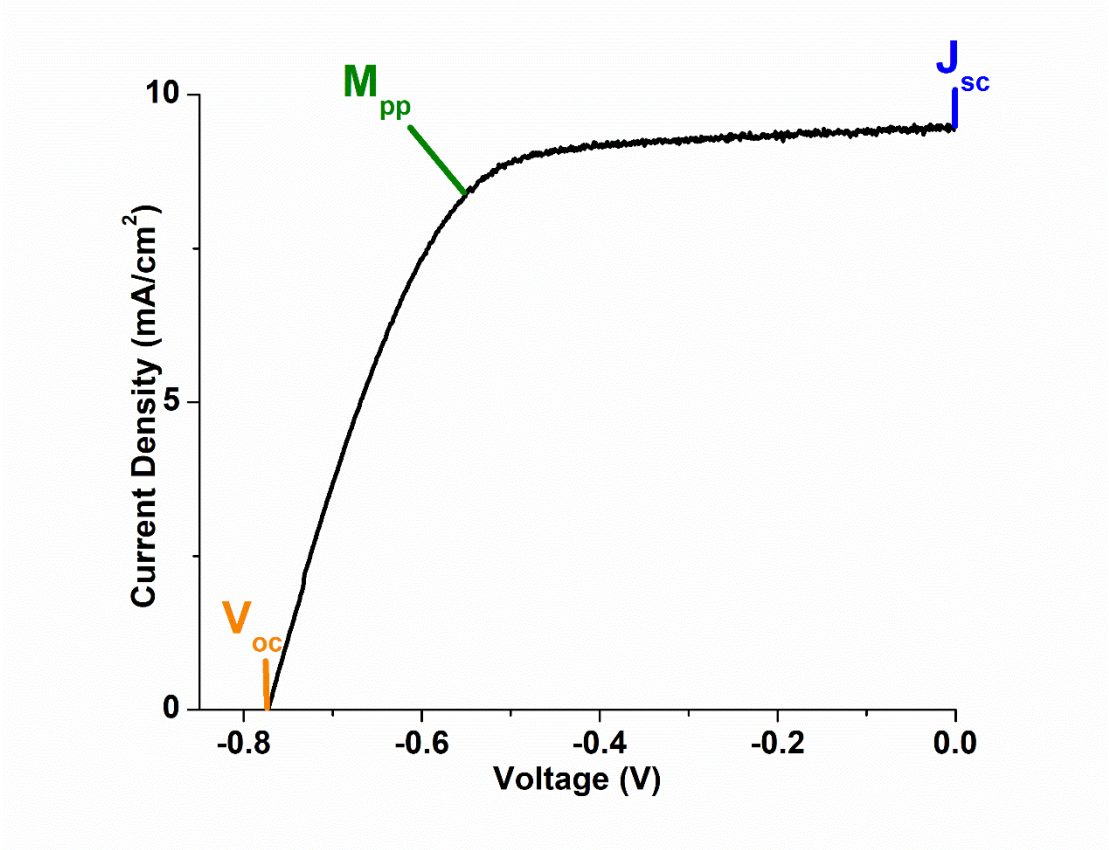

Fig. 4 A characteristic J-V curve for a DSSC under 1 sun illumination

The most important DSSC evaluation metric is its photo-conversion efficiency (PCE), showing the efficiency of the DSSC device during the conversion of incident light energy to electrical energy. It is defined as the ratio of the maximum produced power (power at the Mpp point) to the incident light's power. Under 1 sun illumination at standard test conditions (STC), incident light is considered to irradiate the device with 100 mW/cm^2. Thus, using power densities, PCE is the ratio of maximum produced power density from the device divided by 100 mW/cm^2. Finally, another significant characteristic value is the fill factor (FF), defined as the ratio of maximum produced power density to the product of Jsc and Voc. This value represents the quality of the device and how close the actual produced power is to the ideal power value (The power value of Jsc*Voc=Jmax*Vmax is unobtainable due to one of the parameters being zero at short circuit or open circuit conditions). The fill factor parameter, whose value ranges from 0 to 1 [4], is representative of the current-voltage curve shape. A shape closer to the ideal rectangle is related to higher FF values. Power dissipation

during operation e.g. through the contacts' resistance, are represented by electrical resistances and can lead to a drop in FF values.

Finally, potential undesirable reactions can occur inside a DSSC and a prominent issue is the competitive nature between charge transfer and the undesirable charge recombination process [6]. TiO_2 injected electrons can recombine into the oxidized dye (a) or into the electrolyte (b) and there can even be direct dye recombination from its excited state (c) [7] and the process of recombination can lead to Voc loss [8]. The recapture of electrons by electrolyte species such as triiodide (b, Fig. 3ii) is an especially significant recombination route and its suppression can lead to higher Voc [9,10]. Also, in areas on the anode exposed to the electrolyte, I_3^- species can capture electrons necessitating the use of a compact blocking layer. Thus, it is evident that electron recombination issues can arise from an excessive triiodide concentration in the electrolyte.

3. Utilization of low intensity irradiation and low energy visible photons

In the photovoltaic research field, there is a trend for the utilization of visible light of even the smallest intensity for the well performing operation of the devices. Direct full intensity solar light is not guaranteed in every case due to weather phenomena or issues of shading etc. Thus, the ability to take advantage of all available photons with efficiency is important. Furthermore, the effort for the further extension of light response from photovoltaic cells, into the visible wavelength region has already a lot of history behind it due to the challenges of utilizing lower energy photons by the (usually) wide band gap semiconductors. Thus, there is increased interest in the proper utilization of light both of low intensity and of low energy (aka visible wavelength range). This goal is represented in the effort for the efficient utilization of low power artificial visible light sources.

Beyond solar light, low power artificial lighting sources can be used to activate photoelectrochemical energy production, thereby achieving maximum utility of the available light sources and continuing operation even without the sun's presence.

Ideally, a photoelectrochemical device should be able to fully utilize both natural and artificial light sources to maximize the total operation efficiency. The difference in intensity and wavelength spectra between solar and artificial light sources creates some challenges however. Indoor light sources are mostly active in the visible part of the wavelength spectrum [11], whereas solar light has a significant infrared component and indoor light intensity is several orders of magnitude bellow solar light. Thus, the pursuit for the efficient operation under low power artificial irradiation sources, besides offering greater flexibility of usage for the device, also serves the aforementioned purposes of extended light wavelength response and maximized photon utilization.

Regarding photovoltaic solar cells, as the indoor lighting conditions are radically different from the Standard Test Conditions (STC) that are commonly used for testing as a way to simulate solar light [12], tailored architecture and components are needed for the photovoltaic devices in order to account for the reduced intensity and the primarily visible emission spectrum. Among the 3rd generation PVs, DSSCs have been proven to be especially suitable and many DSSC-integrated products can already be found on the market. Especially important are adaptable PV devices able to operate efficiently under both solar and artificial indoor light. The usage flexibility due to their adaptability to changing light conditions can consolidate their position as prime BIPV, BAPV and PIPV application candidates for usage regardless of the lighting conditions applied.

4. DSSCs for indoor environments

DSSCs can be easily manufactured using low-cost wet-chemistry processes, they have an eco-friendly profile, their efficiency is independent from the light's angle of incidence and they present a variety in color and transparency [13–15]. However, what makes them especially attractive is their excellent performance under low intensity light. A key factor in the recent re-emergence of Dye Sensitized Solar Cells (DSSCs [16]) is their suitability for operation under indoor lighting environments. This is especially evident in their potential applications in buildings and devices. Building applied and building integrated photovoltaics (BAPV/BIPV) [2] as well as product integrated photovoltaics (PIPV) [3]-especially for low power electronics- are

some of the more promising applications for DSSC. Dye Sensitized Solar Cells (DSSCs) [16], a green [15] and low cost [14] technology with proven potential for BIPV and PIPV: For example, with proper incorporation in windows, BIPVs can be developed which can produce photovoltaic power, while regulating the indoor environment's thermal and visual comfort levels [17–19]. These applications require novel technologies that perform well, when operating under low intensity light environments, most often indoors or under diffuse light (Images 1 and 2). However, several industrial products have specific operational environment designations (for direct sun, outdoor or indoor conditions [14,20]) and, as PVs are most often designed with a specific lighting environment in mind, many indoor optimized devices underperform under 1 sun illumination [12]. It is obvious that DSSCs need to be adaptable to changes in lighting conditions (e.g. daily or yearly solar light variations) and to maintain performance under any possible lighting environment (e.g. for mobile PIPV applications) [12,21]. Thus, an optimization method that boosts low intensity/indoor DSSC efficiency without negatively impacting outdoor/solar performance is needed.

Image 1. 100 lux of artificial light (near street level) from a public lighting pylon

Image 2. 580lux of natural light (near ground level) during clouded weather

Indoor lighting conditions are strikingly different from solar irradiated environments both in light intensity and in emission spectra [12]. The disparity in light intensities is enormous: An illuminance of ~400 lux is expected in an office room (lux being the measurement unit for indoor light intensity), while the standard 1 sun AM1.5G irradiation (Standard Test Conditions, STC, 100 mW/cm^2) corresponds to ~10^5 lux [12,22]. Thus, performance under 1 sun cannot be indicative of indoor performance. For example, poly-Si (polycrystalline silicon), a cornerstone PV technology with good performance under solar irradiation, severely underperforms when placed under indoor light [12]. Instead, it is thought that amorphous thin films and nanomaterials are more suitable for diffuse incident light [23]. In fact, it has been confirmed that the efficiency of DSSCs increases, when the light intensity decreases under 20 mW/cm^2 [12,24]. This characteristic puts DSSCs in an advantageous position when working under weak solar light conditions (e.g. under cloud covered sky) and justifies their superiority versus OPVs and silicon cells [25,26] under indoor lighting. A lot of efforts have been devoted for the development of efficient components (electrodes, dyes, electrolytes, redox couples) and there has been increased interest in the research community towards optimizing DSSCs for indoor conditions. Freitag et al. (2017) [27], prepared a copper redox-DSSC co-sensitized with the highly performing XY1/D35 dyes that achieved 28.9% efficiency under 1000 lux of fluorescent light,

outperforming GaAs cells. Power generation of this magnitude was considered sufficient for the autonomous operation of a range of electronic devices operating indoors. In another of their works, for the powering of autonomous Internet of Things (IoT) devices -with machine learning capability- under ambient light, Michaels et al (2020) [28] prepared copper electrolyte based DSSCs through co-sensitization (XY1/L1), reaching 34% efficiency under 1000 lux of fluorescent light.

In the work of Yiming Cao et al (2018) [29] DSSC configurations, with the Y123/XY1b dye combination and copper electrolytes, were prepared and characterized under 1 sun and under indoor fluorescent light. The "1 sun" version of their DSSCs had the required redox species (Cu(II)) concentrations for sufficient mass transport, while the "indoor performing" version of their cells was prepared with significantly lowered redox species concentrations, in order to reduce recombination. A 2.8 cm^2 cell achieved 31.8% efficiency under 1000 lux fluorescent light (outperforming reported silicon, GaAs, OPV and perovskite cells). As for advances concerning the simpler robust [I^-/I_3^- redox - Ru dye] DSSC configuration, Rossi et al.(2015) [4] customized a N719-DSSC with a low I_2 content I^-/I_3^- electrolyte, thereby preparing an indoor optimized DSSC with an efficiency of 12.4% under 200 lux fluorescent light, the highest reported efficiency for I^-/I_3^- DSSCs under fluorescent light. Their customized device outperformed other tested PV technologies such as a-Si and p-Si. As expected, though their optimization strategy allowed for a highly performing indoor DSSC, the same modifications led to a decrease in performance under 1 sun (STC).

In the area of industrial products, as mentioned before BIPV/BAPV/PIPV benefit greatly from DSSC technology under indoor environments. An ever-increasing number of companies have turned their sights on the potential for indoor operating DSSCs [20,30,31], such as H.Glass [32], a Switzerland based manufacturer of glass-sealed DSSC solar panels for glass facades and building materials, with applications in indoor and outdoor environments or Fujikura, with DSSC modules customized for performance under specific light intensity conditions [14]. For Sweden-based Exeger [33], one of the areas of interest is the powering of electronic devices with natural and artificial light by solar cell integration, turning devices such as wearable electronics, tablets and e-readers into self-powered devices. In the area of BIPV, their goal is for

one square meter of façade to power one square meter of office space. Their solar cells are purported to take advantage of even diffuse and indoor light in order to produce electricity “from dawn until dusk”.

GCELL [30]’s lightweight DSSCs, designed for indoor energy harvesting product applications, are attuned to the 50-2000 lux lighting intensity range. Their cells are reported to generate a power density of 4-7 $\mu W/cm^2$ at 200 lux, allowing for indoor powered sensors, e-readers other applications. In 2016, GCell introduced the world’s first indoor solar powered iBeacon, which uses renewable energy to enable broadcasting. Furthermore, their solar cells have been used as part of a hotel’s large scale indoor solar system [34] for the powering of motorized blinds. 3GSolar [25], another provider of DSSC for electronic devices, has set a goal of replacing finite power sources in electronic devices with integrated miniature PV cells that harness energy from indoor or outdoor environment and achieve wireless and maintenance-free operation for the lifetime of the device (more than ten years). In low light conditions (under 2700k LED, 1000 lux), 3GSolar cells can reach ~16% efficiency. One such product is their Bluetooth sensor [35], able to operate under light intensities of over 100 lux.

4.1 “Panillumination” operation: adaptability to different lighting conditions

From the above cases, the superiority of DSSCs when compared to other PV technologies under indoor light sources, is especially evident. What is also evident, however, is the “fork” in optimization strategies when considering outdoor or indoor DSSC operation conditions. Optimizing a PV device for indoor environments usually detracts from its 1 sun performance [12], which is why specific operation environment designations are seen, even in industrial products [20]. Many past studies and industrial products present DSSCs singularly optimized for either high or low intensity operation conditions, because of the trade-off between indoor/outdoor performance optimization. The adaptability of DSSC can be further enhanced and it is crucial for them to be able to maintain their performance when the nature of the incident light changes, with respect to the intensity or emission spectrum.

The disparity between lab testing conditions and real life operation conditions is known for energy systems [36–38]. Under realistic operation conditions, the performance of a PV device [21] is not expected to remain identical to the performance evaluated under ideal lab conditions due to changes in light intensity and other factors concerning the surrounding environment [12] (e.g. daily cycle). Especially for handheld PIPV devices such as tablets, for which the operation environment is expected to change often (e.g. from outdoors to indoors), a DSSC optimized singularly for a specific lighting environment will not sufficiently cover energy needs (due to decreased performance during operation under lighting conditions different from the initially targeted ones). Thus, the perspective of a single DSSC maintaining performance even when the lighting conditions radically change must be adopted during optimization.

As the electrolyte is one of the key parameters that defines the final DSSC's optimization goal, focus should be placed on its proper formulation for maximum DSSC operational flexibility. The most common DSSC configuration utilizes a (dye-sensitized) mesoporous TiO_2 thin film as the semiconductor and a redox electrolyte (based on copper, cobalt or I^-/I_3^- shuttles, with differences in molecule size, charge, redox potential, etc that strongly affect the device performance) as the medium. There are factors (such as transparency) that depend on the concentration of redox species in the electrolyte, with the most significant being the mass transport of the redox species and the prominence of recombination during operation. Device function under high solar light intensities usually requires high concentrations of redox species [12,39] for sufficient dye regeneration, while, for operation under indoor light sources, lower concentrations are needed to prevent negative effects such as the recombination of electrons [40]. Thus, a finely tuned formulation must be achieved in DSSCs, in order to enhance indoor operation without impairing the function under higher intensity light.

Furthermore, the sensitizer is another key parameter in DSSCs that not only affects the device's response to a light source, but also its interfacial charge transfer behavior. Conscious study must be performed for the proper selection of a dye that both captures the incident light properly but also assures desirable behaviors at the interface. For this purpose, both the sensitizer's absorption profile (and its matching

with different indoor/outdoor light sources) and its effects on the electrochemical properties of the DSSC (e.g. recombination resistance), must be investigated in each case. By fine-tuning each separate component of a DSSC, a universal "pan-illumination" function can be achieved, leading to good performance under a wide range of different lighting conditions, a requirement for modern BIPV/BAPV and PIPV applications.

5. Electrolytes for indoor DSSCs

One of the most important parameters that determine whether optimization will be aimed towards indoor or outdoor DSSC operation is the composition of the electrolyte, specifically the concentration of the redox species in the solution. The combination of I^-/I_3^- electrolytes with ruthenium-based dyes is one of the oldest, most studied and straightforward configurations for DSSC (with low cost, readily available components) [41]. Triiodide concentration in the electrolyte is a key factor for indoor/outdoor optimization, as an excessive quantity leads to significant electron recombination [40] (along with Jsc and Voc losses [42,43]) and competitive optical absorption near the 450 nm wavelength [12] (especially significant for fluorescent lamps [11]), while an inadequate concentration leads to mass transport problems and Jsc [44] and FF [45] losses. Under low intensity light conditions, the requirements for sufficient redox species diffusion [29] (for fast dye regeneration) are less demanding, due to the lower number of oxidized sensitizer molecules [46], making low redox species concentrations suitable for indoor operation, while higher concentrations are usually needed for the more demanding outdoor operation (Fig 5). Thus, there is a need for an electrolyte formulation for "pan-illumination" performance [47], where the low redox species concentration doesn't impair solar operation, in order to achieve universal operation under multiple lighting conditions.

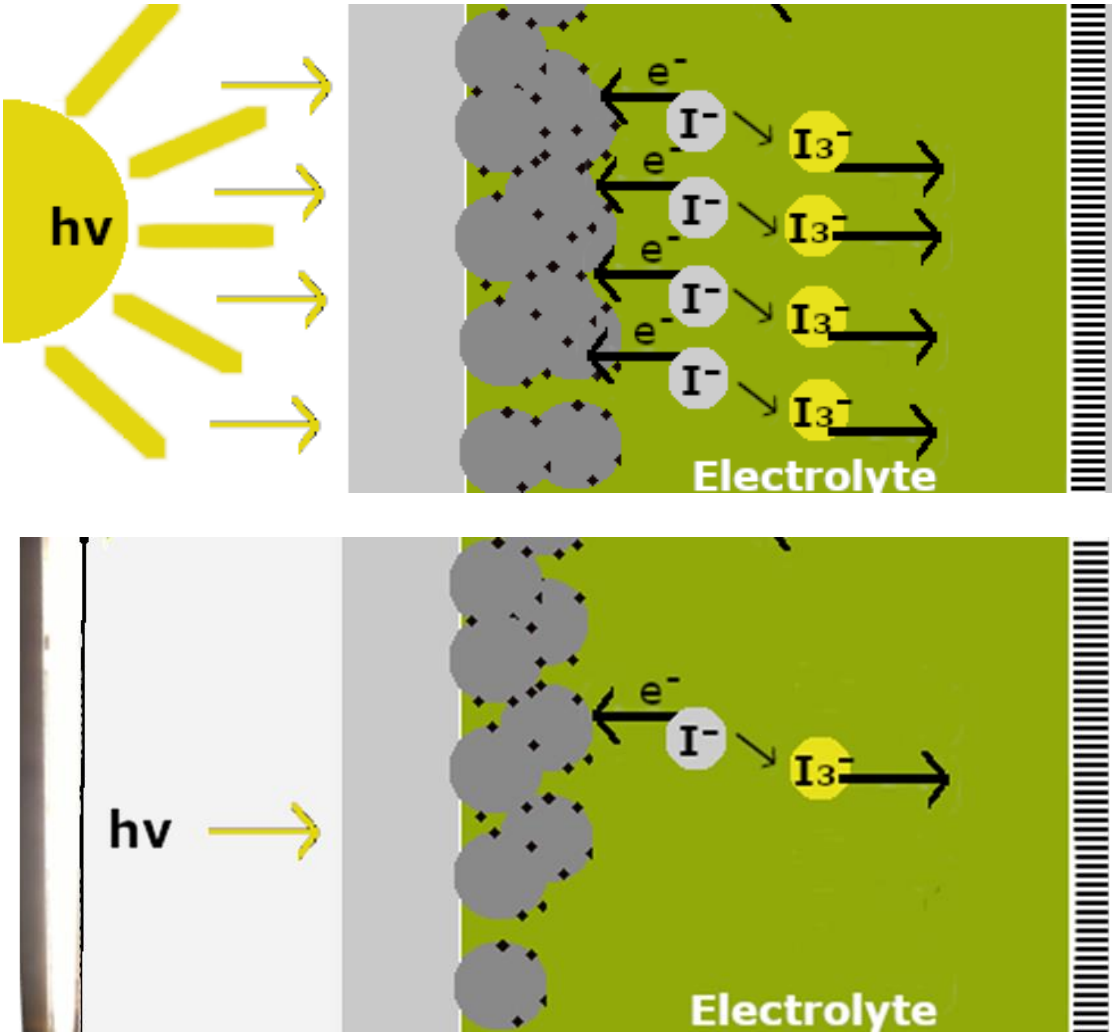

Fig 5. Depiction of different needs of dye regeneration by the electrolyte under solar (top) versus under indoor (bottom) light sources: The significant difference in the number of emitted photons (yellow arrows) and oxidized dye molecules, creates different needs for redox species concentration.

Redox media with high transparency and low viscosity are able to inhibit competitive light absorption and ensure high triiodide diffusion coefficients (thus preventing photocurrent loss) [45,48], respectively. Furthermore, Ionic Liquids (ILs) based on the imidazolium cation [49–51] are often suggested as the iodide source in the electrolyte. While ILs present great stability [49] and high ionic conductivity [50], they have high viscosity that leads to slow triiodide diffusion [52,53] (and decreased performance [54]), when they are used instead of organic solvents. ILs have been extensively studied in the literature [55–59]: In the work of Stergiopoulos et al. (2013), on solvent-free ionic liquid-based redox electrolytes [54], a high iodine concentration

(0.2 M) electrolyte blend with an IL based on 1,3-Dimethylimidazolium iodide (DMII) led to ~5% power conversion efficiency (PCE) under both 1 sun and 0.1 sun conditions. Moreover, Bidikoudi *et al*. developed innovative redox electrolytes for DSSCs using binary mixtures of 1-methyl-3-propylimidazolium iodide (MPII) with 1-alkyl-methylimidazolium tricyanomethanide (CnmimTCM, n = 2, 4, 6, 8) ionic liquids (ILs) to lower the high viscosity of MPII. The authors confirmed a systematic dependence of the cell photovoltaic performance on the alkyl chain length of CnmimTCM. The maximum power conversion efficiency reached 5 and 6.5% under 1 and 0.1 sun AM 1.5 G illumination, respectively, for the ionic liquid with the shortest alkyl chain [58]. In addition, the same group prepared composite redox electrolytes by blending a standard low viscosity ionic liquid solvent (EMimDCA, 1-ethyl-3-methylimidazolium dicyanamide) with various iodide-based ionic liquids based on the methylimidazolium cation [50]. The novel electrolytes based on the [CnC1im]IEMimDCA double salt ILs showed low viscosity and a high diffusion coefficient of triiodides. Under 1 sun illumination, the highest PCE (5.5%) was attained with DSSCs using the EMimDCA–DMII mixture and the device performance increased up to 6.5%, when the cells were illuminated by 0.1 sun. The formation of imidazolium IL mixtures with other ILs can lead to a viscosity decrease [60–63] and, for the aforementioned DMII, the promising results of its mixtures with lower viscosity agents (such as another IL or an organic solvent) have been highlighted in past research works [64–66].

One additional parameter that affects the DSSC performance is the presence of additives in the electrolyte. Concerning this matter, 4-tert-butylpyridine (TBP) [67,68] and N-methylbenzimidazole (NMBI) [42] are often used for Voc enhancement, while guanidinium thiocyanate (GuCNS) has been thought to improve both Jsc [69] and Voc [42], while alleviating the negative consequences arising from the former additives (negative TiO_2 CB edge shift and Jsc loss), thus encouraging the use of GuCNS with either TBP or NMBI in an electrolyte solution. The adsorption of these additives onto the photoelectrode/electrolyte interface, inhibits electron to triiodide recombination. While TBP and NMBI function in a similar way in a DSSC electrolyte, there is a significant difference in the optimum iodine (I_2) concentration needed in each case. TBP has been found to be far more appropriate for electrolytes

with low I_2 concentration [42], as similar PCEs have been obtained for optimum DSSC test configurations using 0.02 M [I_2]-TBP and 0.08 M [I_2]-NMBI electrolytes.

Concerning stability, under indoor light conditions, the incident light is not expected to have a significant impact on the device's temperature during operation, due to the low intensity of common artificial light sources. Under sunlight, however, the much higher intensity of solar light is expected to significantly raise the temperature of the device after prolonged operation, which can impact its overall properties. Especially in liquid-based DSSCs, there is concern for the evaporation of necessary components in the electrolyte (such as the solvent). Thus, while indoor lighting conditions are less demanding in this regard, for broad "panillumination" operation, stability is a serious concern and necessitates techniques such as sealing or the use of less volatile (or solid) components for the electrolyte formulation.

In a recent indoor operating N719-DSSC optimization work, Rossi et al (2015) [12] tailored their I^-/I_3^- electrolyte specifically for indoor conditions. As a result, under fluorescent light of 200 lux intensity, a champion DSSC presented the highest efficiency (12.4% PCE or 8 $\mu W/cm^2$ power density) among the tested PV devices (including a-Si and p-Si devices). However, their electrolyte, despite the increased indoor efficiency through its low I_2 content, led to decreased performance under 1 sun illumination, especially evident in the cells' FF. This highlights the importance of an electrolyte formulation that can perform well in either of the lighting conditions.

6. Sensitizers for indoor DSSCs

In a DSSC, the sensitizer is anchored onto the semiconductor layer of the working electrode, from where it can absorb the incident light, and thus generate electrons after oxidation. Light emitted in wavelengths where the dye absorbs strongly, lead to more electron (and current) generation, while the energy of light emitted in wavelengths that are not significant in the dye's absorbance spectrum largely goes to waste. These effects are evident in the Jsc of the PV device. Common lamps for indoor environments present emission spectra mostly active in the visible wavelength range [11], contrary to sunlight (e.g. with its strong infrared emissions). Due to the emission profile of common indoor light sources, the wavelength region around

550nm is especially significant for indoor operating PV devices. Even industrial products can be tailored to this specification, such as the indoor operating DSSCs produced by GCell, which present the highest absorbance in the range of 500 to 550 nm [70].

The two most prominent categories of dyes are metal complex sensitizers and organic (metal-free) sensitizers. Ruthenium metal complex dyes (Ru-dyes) are some of the oldest employed sensitizers in DSSCs, allowing for very good stability [71]. However, Ruthenium-based dyes have the disadvantages of the high cost and rarity of the required metal and their often complicated synthesis and purification [72]. Thus, organic (metal-free) dyes have been suggested as an alternative for DSSC systems [73]**.** The most popular metal-free dye class is the donor-(π-linker)-acceptor ("D-π-A") class, where a conjugated π-system connects the electron-deficient acceptor with the donor component. This design allows for the individual modification of each component and thus, tuning of a dye's spectroscopic and electronic characteristics becomes possible [72]. The higher extinction coefficients and simplicity of synthesis, found in organic dyes in comparison to Ru dyes, has led to their wide adoption in DSSCs [74]. For this dissertation, four dyes with different light absorption profiles spanning the visible wavelength region, where indoor fluorescent lamps emit, were studied:

N719

Ru-dye DSSCs, introduced back in 1991, are one of the first DSSC configurations. The initially complicated dye structure was soon simplified (going from three Ru metal centers to only one) with the N3 Ru dye [75], which then evolved into the N719 dye **(bis(tetrabutylammonium)-cis-di(thiocyanato)-N,N′-bis(4-carboxylato-4′-carboxylic acid-2,2′-bipyridine)ruthenium(II))** [73]**.** The amphiphilic spherical N719 dye, besides being one of the most common high performance dyes, has a well-fitting absorption spectrum to the fluorescent light's emission peaks (λmax at ~535 nm with an ε ~1.47 x 10^4 $M^{-1}cm^{-1}$ in EtOH [71]), makes it especially suitable for indoor DSSC operating under such light sources [24].

D35

Ru-dyes such as N719 [71] or Z907 [76] were exceedingly popular for a while but ruthenium's high cost resulted in increased research into Ru-free dyes [73]**.** This led to the metal free "D-π-A" dyes such as D35, with an absorption maximum around 450 nm (in acetonitrile) [77]. The Y-shaped D35 organic dye **(((E)-3-(5-(4-(bis(2',4'-dibutoxy-[1,1'-biphenyl]-4-yl)amino)phenyl)thiophen-2-yl)-2-cyanoacrylic acid)** [78]), is known for its effective suppression of semiconductor/electrolyte recombination. One of its more serious shortcomings, however, is its narrow spectrum of absorption (closer to the UV region) which limits the generated current [72].

LEG4

As a way to improve on D35's absorption in the visible range, the modifications of Gabrielsson et al (2013) [72] on the π-linker component eventually led to the introduction of the -also Y-shaped- LEG4 dye (**3-{6-{4-[bis(2',4'-dibutyloxybiphenyl-4-yl)amino-]phenyl}-4,4-dihexyl-cyclopenta-[2,1-b:3,4-b']dithiophene-2-yl}-2-cyanoacrylic acid**). The LEG series of dyes retained D35's donor fragment since it was considered to be key to D35 recombination suppressing behavior. LEG4 achieved expanded absorption towards higher wavelengths, centered around ~500 nm (in solution [79] or when adsorbed onto TiO_2 [80]**).** Compared to D35, LEG4's higher achieved photocurrents are attributed to both its higher extinction coefficient and its absorption spectrum (with its red shift) [74].

MK2

The MK2 dye (**2-Cyano-3-[5′′′-(9-ethyl-9H-carbazol-3-yl)-3′,3′′,3′′′,4-tetra-n-hexyl-[2,2′,5′,2′′,5′′,2′′′]-quater thiophen-5-yl] acrylic acid**), a part of the organic oligothiophene-based MK series with donor/acceptor units tethered by regioregular oligothiophene centers [81], is a long alkyl chain sensitizer designed in 2006 [82] with the aim of achieving longer electron lifetimes in TiO_2's CB (the presence of n-hexyl chains connected to thiophene groups leads to a retardation of charge recombination [83]), which presents strong absorption under 500 nm [82]. MK2 is one of the better MK dyes in DSSCs [83,84].

6.1 Orbital Energy Levels of the Sensitizers

Another significant factor for a sensitizer's good performance in DSSC is the position of their HOMO (Highest Occupied Molecular Orbital) and LUMO (Lowest Unoccupied Molecular Orbital) energy levels in relation to the I^-/I_3^- redox potential and the conduction band (CB) of the TiO_2 (photoanode). A higher energy LUMO level than TiO_2's CB is needed for injection of electrons into the photoanode, while a lower energy HOMO level than the electrolyte's redox potential is required for electron injection into the oxidized sensitizer (regeneration) [66]. In Fig. 6, a schematic representation of reported values for the HOMO (ground state)/LUMO (excited state) energy levels of the selected dyes is presented in comparison to the redox level of a I^-/I_3^- electrolyte and the CB of TiO_2 [85–87]. A much higher energy (much more negative) LUMO level can impair performance (higher losses in sensitization driving force) and, often, sensitizers with LUMO levels closer to TiO_2's CB level are preferred [65,66]. In Fig. 6, while the HOMO levels appear similar between dyes, N719's closer-to-TiO_2 CB LUMO level could signify a reduction of such losses.

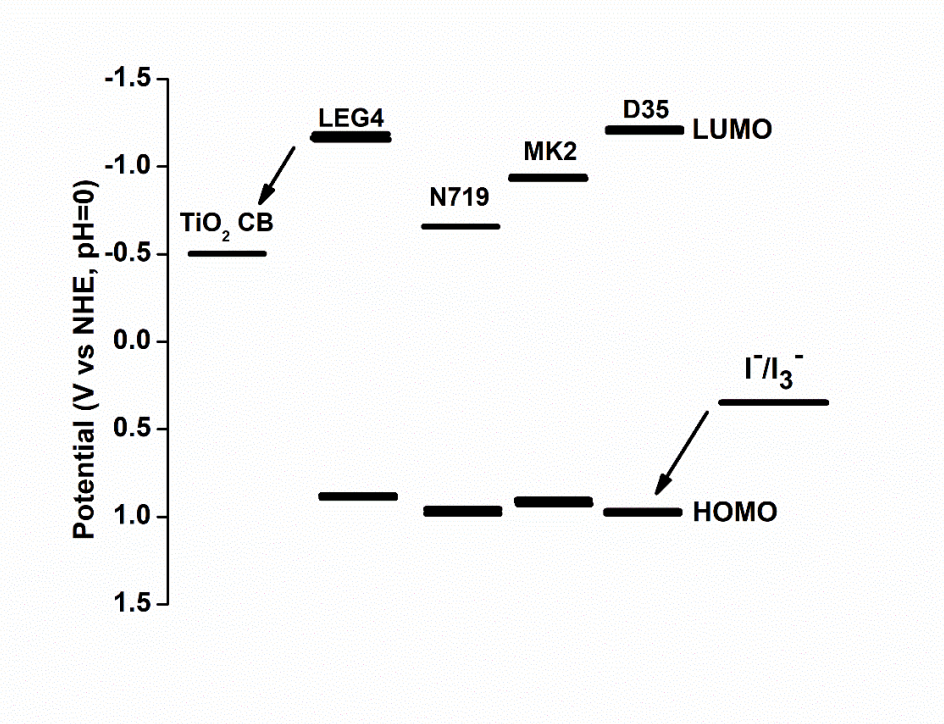

Fig. 6 HOMO and LUMO energy levels of sensitizers in comparison with the redox level of the I^-/I_3^- electrolyte and TiO_2's conduction band.

7. Purpose of this work

The main purpose of this dissertation is the optimization of such photoelectrochemical cells for their good operation under both low intensity visible artificial light and high intensity solar light. The low intensity visible light sources were artificial tube lights and intensity levels between 100-1000 lux were employed for the evaluation of solar cells, during low intensity visible light performance characterization. The aim was to construct photovoltaic devices that maintain their good performance when irradiated by this type of artificial light source, without jeopardizing their performance under solar light.

The 2nd and 3rd chapter cover the optimization of DSSC components for efficient energy production under both simulated solar light of high intensity and artificial low intensity indoor fluorescent light. This dual aim, coined "panillumination" as it signifies the ideal goal of a cell that operate well under all possible types of illumination, is achieved by careful tailoring of the main components of the cells. The 2nd chapter focuses on the I^-/I_3^- electrolyte as the target component for optimization and its constitution is carefully tailored to cover the radically different requirements of both high and low intensity light. The 3rd chapter covers the optimization of the photoanode with a detailed characterization of the effects of different sensitizers on cell performance under solar and indoor light. In the 4^{rth} chapter, focus is shifted towards perovskites, with the structural investigation of a promising stable perovskite material, that leads to a stable alternative to the electrolyte presented in the 2nd chapter. As a result of the extensive study, an optimized cell configuration with good performance under both simulated solar and low power indoor artificial light is presented.

Bibliographic references for introductory chapter

[1] C.J. Traverse, R. Pandey, M.C. Barr, R.R. Lunt, Emergence of highly transparent photovoltaics for distributed applications, Nat. Energy. 2 (2017) 849–860. https://doi.org/10.1038/s41560-017-0016-9.

[2] Grand View Research, Dye Sensitized Solar Cell Market Analysis By Application (Portable Charging , BIPV / BAPV , Embedded Electronics , Outdoor Advertising , Automotive (AIPV)) And Segment Forecasts To 2022, (2016). https://www.grandviewresearch.com/industry-analysis/dye-sensitized-solar-cell-market.

[3] N.H. Reich, W.G.J.H.M. van Sark, W.C. Turkenburg, Charge yield potential of indoor-operated solar cells incorporated into Product Integrated Photovoltaic (PIPV), Renew. Energy. 36 (2011) 642–647. https://doi.org/10.1016/j.renene.2010.07.018.

[4] A. Hagfeldt, G. Boschloo, L. Sun, L. Kloo, H. Pettersson, Dye-sensitized solar cells, Chem. Rev. 110 (2010) 6595–6663. https://doi.org/10.1021/cr900356p.

[5] Z. Yu, N. Vlachopoulos, M. Gorlov, L. Kloo, Liquid electrolytes for dye-sensitized solar cells, Dalt. Trans. 40 (2011) 10289–10303. https://doi.org/10.1039/c1dt11023c.

[6] M.K. Nazeeruddin, E. Baranoff, M. Grätzel, Dye-sensitized solar cells: A brief overview, Sol. Energy. 85 (2011) 1172–1178. https://doi.org/10.1016/j.solener.2011.01.018.

[7] S.Y. Huang, G. Schlichthörl, A.J. Nozik, M. Grätzel, A.J. Frank, Charge recombination in dye-sensitized nanocrystalline TiO2 solar cells, J. Phys. Chem. B. 101 (1997) 2576–2582. https://doi.org/10.1021/jp962377q.

[8] M. Mazloum-Ardakani, R. Arazi, Improving the effective photovoltaic performance in dye-sensitized solar cells using an azobenzenecarboxylic acid-based system, Heliyon. 5 (2019). https://doi.org/10.1016/j.heliyon.2019.e01444.

[9] S. Ito, P. Liska, P. Comte, R. Charvet, P. Pechy, U. Bach, L. Schmidt-Mende, S.M. Zakeeruddin, A. Kay, M.K. Nazeeruddin, M. Grätzel, Control of dark current in photoelectrochemical (TiO2/I --I3-) and dye-sensitized solar cells, Chem. Commun. (2005) 4351–4353. https://doi.org/10.1039/b505718c.

[10] M. Grätzel, Perspectives for dye-sensitized nanocrystalline solar cells, Prog. Photovoltaics Res. Appl. 8 (2000) 171–185. https://doi.org/10.1002/(SICI)1099-159X(200001/02)8:1<171::AID-PIP300>3.0.CO;2-U.

[11] C.D. Elvidge, D.M. Keith, B.T. Tuttle, K.E. Baugh, Spectral identification of lighting type and character, Sensors. 10 (2010) 3961–3988. https://doi.org/10.3390/s100403961.

[12] F. De Rossi, T. Pontecorvo, T.M. Brown, Characterization of photovoltaic devices for indoor light harvesting and customization of flexible dye solar cells to deliver superior efficiency under artificial lighting, Appl. Energy. 156 (2015) 413–422. https://doi.org/10.1016/j.apenergy.2015.07.031.

[13] J. Goldstein, I. Yakupov, B. Breen, Development of large area photovoltaic dye cells at 3GSolar, Sol. Energy Mater. Sol. Cells. 94 (2010) 638–641. https://doi.org/10.1016/j.solmat.2009.11.019.

[14] Fujikura, https://www.fujikura.co.uk/products/energy-and-environment/dye-sensitized-solar-cell, (n.d.).

[15] F. Sauvage, S. Chhor, A. Marchioro, J.E. Moser, M. Graetzel, Butyronitrile-based electrolyte for dye-sensitized solar cells, J. Am. Chem. Soc. 133 (2011) 13103–13109. https://doi.org/10.1021/ja203480w.

[16] B. O'Regan, M. Grätzel, A low-cost, high-efficiency solar cell based on dye-sensitized colloidal TiO2 films, Nature. 353 (1991) 737–740. https://doi.org/10.1038/353737a0.

[17] A. Ghosh, P. Selvaraj, S. Sundaram, T.K. Mallick, The colour rendering index and correlated colour temperature of dye-sensitized solar cell for adaptive glazing application, Sol. Energy. 163 (2018) 537–544.

https://doi.org/10.1016/j.solener.2018.02.021.

[18] A. Roy, A. Ghosh, S. Bhandari, P. Selvaraj, S. Sundaram, T.K. Mallick, Color Comfort Evaluation of Dye-Sensitized Solar Cell (DSSC) Based Building-Integrated Photovoltaic (BIPV) Glazing after 2 Years of Ambient Exposure, J. Phys. Chem. C. 123 (2019) 23834–23837. https://doi.org/10.1021/acs.jpcc.9b05591.

[19] P. Selvaraj, A. Ghosh, T.K. Mallick, S. Sundaram, Investigation of semi-transparent dye-sensitized solar cells for fenestration integration, Renew. Energy. 141 (2019) 516–525. https://doi.org/10.1016/j.renene.2019.03.146.

[20] 3GSolar product page, (n.d.). https://www.3gsolar.com/products.

[21] M. Pierro, F. Bucci, C. Cornaro, Full characterization of photovoltaic modules in real operating conditions: Theoretical model, measurement method and results, Prog. Photovoltaics Res. Appl. 23 (2015) 443–461. https://doi.org/10.1002/pip.2450.

[22] E.E. Richman, Requirements for Lighting Levels, (n.d.). http://www.lumitronlighting.com/lighting_nowledge/LUX LEVEL_usace_Requirements for Lighting Levels.pdf.

[23] A. Sacco, L. Rolle, L. Scaltrito, E. Tresso, C.F. Pirri, Characterization of photovoltaic modules for low-power indoor application, Appl. Energy. 102 (2013) 1295–1302. https://doi.org/10.1016/j.apenergy.2012.07.001.

[24] N. Tanabe, Dye-Sensitized Solar Cell for Energy Harvesting Applications, Fujikura Tech. Rev. 42 (2013) 109–113.

[25] Technology presentation. https://www.3gsolar.com/technology, 3GSolar, n.d.

[26] N. Sridhar, D. Freeman, A study of Dye Sensitized Solar Cells under Indoor and Low Level Outdoor Lighting: Comparison to Organic and Inorganic Thin Film Solar Cells and Methods to Address Maximum Power Point Tracking, Conf. Proc. 26th EU-PVSEC. (2011) 232–236. https://doi.org/10.4229/26thEUPVSEC2011-1CO.10.5.

[27] M. Freitag, J. Teuscher, Y. Saygili, X. Zhang, F. Giordano, P. Liska, J. Hua, S.M. Zakeeruddin, J.E. Moser, M. Grätzel, A. Hagfeldt, Dye-sensitized solar cells for efficient power generation under ambient lighting, Nat. Photonics. 11 (2017) 372–378. https://doi.org/10.1038/nphoton.2017.60.

[28] H. Michaels, M. Rinderle, R. Freitag, I. Benesperi, T. Edvinsson, R. Socher, A. Gagliardi, M. Freitag, Dye-sensitized solar cells under ambient light powering machine learning: Towards autonomous smart sensors for the internet of things, Chem. Sci. 11 (2020) 2895–2906. https://doi.org/10.1039/c9sc06145b.

[29] Y. Cao, Y. Liu, S.M. Zakeeruddin, A. Hagfeldt, M. Grätzel, Direct Contact of Selective Charge Extraction Layers Enables High-Efficiency Molecular Photovoltaics, Joule. 2 (2018) 1108–1117. https://doi.org/10.1016/j.joule.2018.03.017.

[30] Solar cell description. Section: "Electrical performance". https://gcell.com/gcell-products/custom-solar-cell, GCell, n.d.

[31] Ricoh, https://www.ricoh.com/technology/tech/066_dssc, (n.d.).

[32] H.Glass, (n.d.). http://h.glass.

[33] Exeger, (n.d.). https://exeger.com/applications.

[34] Skyco Shading Systems with G24 cells, (n.d.). https://gcell.com/case-studies/solar-powered-motorized-blinds.

[35] Energy harvesting demonstration kit, E-Peas Semicond. 3Gsolar. (2018). https://80b98441-3a4b-4f9a-a051-806d1c76a712.filesusr.com/ugd/3aba0c_f3547ce174544136b0c65a40b6e1ff5e.pdf.

[36] C. Cornaro, L. Renzi, M. Pierro, A. Di Carlo, A. Guglielmotti, Thermal and electrical characterization of a semi-transparent dye-sensitized photovoltaic module under real operating conditions, Energies. 11 (2018). https://doi.org/10.3390/en11010155.

[37] G. V. Belessiotis, K.G. Papadokostaki, E.P. Favvas, E.K. Efthimiadou, S.

Karellas, Preparation and investigation of distinct and shape stable paraffin/SiO2 composite PCM nanospheres, Energy Convers. Manag. 168 (2018) 382–394. https://doi.org/10.1016/j.enconman.2018.04.059.

[38] N. Stathopoulos, G. Belessiotis, P. Oikonomou, E. Papanicolaou, Experimental investigation of thermal degradation of phase change materials for medium-temperature thermal energy storage and tightness during cycling inside metal spheres, J. Energy Storage. 31 (2020) 101618. https://doi.org/10.1016/j.est.2020.101618.

[39] M.I. Asghar, K. Miettunen, S. Mastroianni, J. Halme, H. Vahlman, P. Lund, In situ image processing method to investigate performance and stability of dye solar cells, Sol. Energy. 86 (2012) 331–338. https://doi.org/10.1016/j.solener.2011.10.006.

[40] H. Ohno, Electrochemical Aspects of Ionic Liquids, in: 2nd ed., John Wiley & Sons, Inc., 2011: pp. 150–151. https://doi.org/10.1002/0471762512.

[41] A. Sacco, Electrochemical impedance spectroscopy: Fundamentals and application in dye-sensitized solar cells, Renew. Sustain. Energy Rev. 79 (2017) 814–829. https://doi.org/10.1016/j.rser.2017.05.159.

[42] T. Stergiopoulos, E. Rozi, C.S. Karagianni, P. Falaras, Influence of electrolyte co-additives on the performance of dye-sensitized solar cells, Nanoscale Res. Lett. 6:307 (2011). https://doi.org/10.1186/1556-276X-6-307.

[43] M. Berginc, U.O. Krašovec, M. Topič, Evaluation of the recombination processes in DSSC by measuring the open circuit voltage over a wide illumination intensity range, Phys. Status Solidi Appl. Mater. Sci. 210 (2013) 1750–1757. https://doi.org/10.1002/pssa.201329044.

[44] S. Mastroianni, I. Asghar, K. Miettunen, J. Halme, A. Lanuti, T.M. Brown, P. Lund, Effect of electrolyte bleaching on the stability and performance of dye solar cells, Phys. Chem. Chem. Phys. 16 (2014) 6092–6100. https://doi.org/10.1039/c3cp55342f.

[45] D. Perganti, A.G. Kontos, T. Stergiopoulos, V. Likodimos, J. Farnell, D.

Milliken, H. Desilvestro, P. Falaras, Thermal Stressing of Dye Sensitized Solar Cells Employing Robust Redox Electrolytes, Electrochim. Acta. 179 (2015) 241–249. https://doi.org/10.1016/j.electacta.2015.03.206.

[46] C.J. Barbé, F. Arendse, P. Comte, M. Jirousek, F. Lenzmann, V. Shklover, M. Grätzel, Nanocrystalline titanium oxide electrodes for photovoltaic applications, J. Am. Ceram. Soc. 80 (1997) 3157–3171. https://doi.org/10.1111/j.1151-2916.1997.tb03245.x.

[47] G. V. Belessiotis, I. Ibrahim, C.S. Karagianni, P. Falaras, DSSCs for Indoor Environments: From Lab Scale Experiments to Real Life Applications, SVOA Mater. Sci. &Technology. 3 (2020) 01–05.

[48] M. Zistler, P. Wachter, C. Schreiner, H.J. Gores, Electrochemical measurement of triiodide diffusion coefficients in blends of ionic liquids: Results for improving a critical parameter of dye-sensitized solar cells, J. Mol. Liq. 156 (2010) 52–57. https://doi.org/10.1016/j.molliq.2010.04.021.

[49] P. Wang, S.M. Zakeeruddin, J.E. Moser, M. Grätzel, A new ionic liquid electrolyte enhances the conversion efficiency of dye-sensitized solar cells, J. Phys. Chem. B. 107 (2003) 13280–13285. https://doi.org/10.1021/jp0355399.

[50] M. Bidikoudi, L.F. Zubeir, P. Falaras, Low viscosity highly conductive ionic liquid blends for redox active electrolytes in efficient dye-sensitized solar cells, J. Mater. Chem. A. 2 (2014) 15326–15336. https://doi.org/10.1039/c4ta02529f.

[51] M. Gorlov, L. Kloo, Ionic liquid electrolytes for dye-sensitized solar cells, J. Chem. Soc. Dalt. Trans. (2008) 2655–2666. https://doi.org/10.1039/b716419j.

[52] S.M. Zakeeruddin, M. Grätzel, Solvent-free ionic liquid electrolytes for mesoscopic dye-sensitized solar cells, Adv. Funct. Mater. 19 (2009) 2187–2202. https://doi.org/10.1002/adfm.200900390.

[53] V. Armel, J.M. Pringle, M. Forsyth, D.R. MacFarlane, D.L. Officer, P. Wagner, Ionic liquid electrolyte porphyrin dye sensitised solar cells, Chem. Commun. 46 (2010) 3146–3148. https://doi.org/10.1039/b926087k.

[54] T. Stergiopoulos, M. Konstantakou, P. Falaras, Dye solar cells combining a TiO2 surface-blocking organic sensitizer and solvent-free ionic liquid-based redox electrolyte, RSC Adv. 3 (2013) 15014–15021. https://doi.org/10.1039/c3ra42506a.

[55] N. Papageorgiou, Y. Athanassov, M. Armand, P. Bonho𝓍te, H. Pettersson, A. Azam, M. Grätzel, The Performance and Stability of Ambient Temperature Molten Salts for Solar Cell Applications, J. Electrochem. Soc. 143 (1996) 3099–3108. https://doi.org/10.1149/1.1837171.

[56] P. Wang, S.M. Zakeeruddin, I. Exnar, M. Grätzel, High efficiency dye-sensitized nanocrystalline solar cells based on ionic liquid polymer gel electrolyte, Chem. Commun. (2002) 2972–2973. https://doi.org/10.1039/b209322g.

[57] P. Wang, S.M. Zakeeruddin, P. Comte, I. Exnar, M. Grätzel, Gelation of ionic liquid-based electrolytes with silica nanoparticles for quasi-solid-state dye-sensitized solar cells, J. Am. Chem. Soc. 125 (2003) 1166–1167. https://doi.org/10.1021/ja029294+.

[58] M. Bidikoudi, T. Stergiopoulos, V. Likodimos, G.E. Romanos, M. Francisco, B. Iliev, G. Adamová, T.J.S. Schubert, P. Falaras, Ionic liquid redox electrolytes based on binary mixtures of 1-alkyl-methylimidazolium tricyanomethanide with 1-methyl-3-propylimidazolium iodide and implication in dye-sensitized solar cells, J. Mater. Chem. A. 1 (2013) 10474–10486. https://doi.org/10.1039/c3ta00117b.

[59] M. Bidikoudi, D. Perganti, C.S. Karagianni, P. Falaras, Solidification of ionic liquid redox electrolytes using agarose biopolymer for highly performing dye-sensitized solar cells, Electrochim. Acta. 179 (2015) 228–236. https://doi.org/10.1016/j.electacta.2015.02.122.

[60] F. Hao, H. Lin, Y. Liu, G. Yang, G. Wang, J. Li, Evidence for enhancing charge collection efficiency with an alternative cost-effective binary ionic liquids electrolyte based dye-sensitized solar cells, Electrochim. Acta. 56 (2011) 5605–5610. https://doi.org/10.1016/j.electacta.2011.04.009.

[61] A. qiang Mo, D. peng Cao, W. yang Wang, X. yan Li, B. xiu Mi, Z. qiang Gao, Z. cheng Liang, Comprehensive study of efficient dye-sensitized solar cells based on the binary ionic liquid electrolyte by modifying with additives and iodine, Optoelectron. Lett. 13 (2017) 263–267. https://doi.org/10.1007/s11801-017-7088-4.

[62] D. Kuang, C. Klein, Z. Zhang, S. Ito, J.E. Moser, S.M. Zakeeruddin, M. Grätzel, Stable, high-efficiency ionic-liquid-based mesoscopic dye-sensitized solar cells, Small. 3 (2007) 2094–2102. https://doi.org/10.1002/smll.200700211.

[63] D. Kuang, P. Wang, S. Ito, S.M. Zakeeruddin, M. Grätzel, Stable mesoscopic dye-sensitized solar cells based on tetracyanoborate ionic liquid electrolyte, J. Am. Chem. Soc. 128 (2006) 7732–7733. https://doi.org/10.1021/ja061714y.

[64] A. Mishra, N. Pootrakulchote, M. Wang, S.J. Moon, S.M. Zakeeruddin, M. Grätzel, P. Bäuerle, A thiophene-based anchoring ligand and its heteroleptic Ru(II)-complex for efficient thin-film dye-sensitized solar cells, Adv. Funct. Mater. 21 (2011) 963–970. https://doi.org/10.1002/adfm.201001863.

[65] G. Konti, G.C. Vougioukalakis, M. Bidikoudi, A.G. Kontos, C. Methenitis, P. Falaras, A Ru(II) molecular antenna bearing a novel bipyridine-acrylonitrile ligand: Synthesis and application in dye solar cells, Polyhedron. 82 (2014) 12–18. https://doi.org/10.1016/j.poly.2014.04.031.

[66] A.N. Kabanakis, M. Bidikoudi, M.M. Elsenety, G.C. Vougioukalakis, P. Falaras, Synthesis of novel semi-squaraine derivatives and application in efficient dye-sensitized solar cells, Dye. Pigment. 165 (2019) 308–318. https://doi.org/10.1016/j.dyepig.2019.02.028.

[67] S. Nakade, T. Kanzaki, W. Kubo, T. Kitamura, Y. Wada, S. Yanagida, Role of electrolytes on charge recombination in dye-sensitized TiO 2 solar cell (1): The case of solar cells using the I -/I3- redox couple, J. Phys. Chem. B. 109 (2005) 3480–3487. https://doi.org/10.1021/jp0460036.

[68] G. Boschloo, L. Häggman, A. Hagfeldt, Quantification of the effect of 4-tert-

butylpyridine addition to I -/I3- redox electrolytes in dye-sensitized nanostructured TiO2 solar cells, J. Phys. Chem. B. 110 (2006) 13144–13150. https://doi.org/10.1021/jp0619641.

[69] C. Zhang, Y. Huang, Z. Huo, S. Chen, S. Dai, Photoelectrochemical effects of guanidinium thiocyanate on dye-sensitized solar cell performance and stability, J. Phys. Chem. C. 113 (2009) 21779–21783. https://doi.org/10.1021/jp909732f.

[70] https://gcell.com, GCell, (n.d.).

[71] M.K. Nazeeruddin, S.M. Zakeeruddin, R. Humphry-Baker, M. Jirousek, P. Liska, N. Vlachopoulos, V. Shklover, C.H. Fischer, M. Grätzel, Acid-base equilibria of (2,2′-bipyridyl-4,4′-dicarboxylic acid)ruthenium(II) complexes and the effect of protonation on charge-transfer sensitization of nanocrystalline titania, Inorg. Chem. 38 (1999) 6298–6305. https://doi.org/10.1021/ic990916a.

[72] E. Gabrielsson, H. Ellis, S. Feldt, H. Tian, G. Boschloo, A. Hagfeldt, L. Sun, Convergent/divergent synthesis of a linker-varied series of dyes for dye-sensitized solar cells based on the D35 donor, Adv. Energy Mater. 3 (2013) 1647–1656. https://doi.org/10.1002/aenm.201300367.

[73] S. Ito, Investigation of Dyes for Dye-Sensitized Solar Cells: Ruthenium-Complex Dyes, Metal-Free Dyes, Metal-Complex Porphyrin Dyes and Natural Dyes, Sol. Cells - Dye. Devices. (2011). https://doi.org/10.5772/19960.

[74] H. Ellis, S.K. Eriksson, S.M. Feldt, E. Gabrielsson, P.W. Lohse, R. Lindblad, L. Sun, H. Rensmo, G. Boschloo, A. Hagfeldt, Linker unit modification of triphenylamine-based organic dyes for efficient cobalt mediated dye-sensitized solar cells, J. Phys. Chem. C. 117 (2013) 21029–21036. https://doi.org/10.1021/jp403619c.

[75] R. Katoh, A. Furube, T. Yoshihara, K. Hara, G. Fujihashi, S. Takano, S. Murata, H. Arakawa, M. Tachiya, Efficiencies of Electron Injection from Excited N3 Dye into Nanocrystalline Semiconductor (ZrO2, TiO2, ZnO, Nb2O 5, SnO2, In2O3) Films, J. Phys. Chem. B. 108 (2004) 4818–4822. https://doi.org/10.1021/jp031260g.

[76] P. Wang, B. Wenger, R. Humphry-Baker, J.E. Moser, J. Teuscher, W. Kantlehner, J. Mezger, E. V. Stoyanov, S.M. Zakeeruddin, M. Grätzel, Charge separation and efficient light energy conversion in sensitized mesoscopic solar cells based on binary ionic liquids, J. Am. Chem. Soc. 127 (2005) 6850–6856. https://doi.org/10.1021/ja042232u.

[77] Q. Liu, X. Lin, L. Mi, N. Gao, P. Song, F. Ma, Y. Li, Characterizations of efficient charge transfer and photoelectric performance in the cosensitization of solar cells, Appl. Sci. 8 (2018). https://doi.org/10.3390/app8071122.

[78] V. Saavedra Becerril, E. Sundin, M. Mapar, M. Abrahamsson, Extending charge separation lifetime and distance in patterned dye-sensitized SnO2-TiO2 μm-thin films, Phys. Chem. Chem. Phys. 19 (2017) 22684–22690. https://doi.org/10.1039/c7cp04486k.

[79] Y. Li, Y. Lv, Y. Liu, H. Gao, Q. Shi, Y. Li, DFT and TD-DFT investigations of organic dye with different π-spacer used for solar cell, J. Mater. Sci. Mater. Electron. 28 (2017) 9642–9652. https://doi.org/10.1007/s10854-017-6714-z.

[80] W. Yang, M. Pazoki, A.I.K. Eriksson, Y. Hao, G. Boschloo, A key discovery at the TiO2/dye/electrolyte interface: slow local charge compensation and a reversible electric field, Phys. Chem. Chem. Phys. 17 (2015) 16744–16751. https://doi.org/10.1039/c5cp01274k.

[81] T. Dohi, N. Yamaoka, S. Nakamura, K. Sumida, K. Morimoto, Y. Kita, Efficient synthesis of a regioregular oligothiophene photovoltaic dye molecule, MK-2, and related compounds: A cooperative hypervalent iodine and metal-catalyzed synthetic route, Chem. - A Eur. J. 19 (2013) 2067–2075. https://doi.org/10.1002/chem.201203503.

[82] N. Koumura, Z.S. Wang, S. Mori, M. Miyashita, E. Suzuki, K. Hara, Alkyl-functionalized organic dyes for efficient molecular photovoltaics, J. Am. Chem. Soc. 128 (2006) 14256–14257. https://doi.org/10.1021/ja0645640.

[83] Z.S. Wang, N. Koumura, Y. Cui, M. Takahashi, H. Sekiguchi, A. Mori, T. Kubo, A. Furube, K. Hara, Hexylthiophene-functionalized carbazole dyes for

efficient molecular photovoltaics: Tuning of solar-cell performance by structural modification, Chem. Mater. 20 (2008) 3993–4003. https://doi.org/10.1021/cm8003276.

[84] N. Koumura, Z.S. Wang, M. Miyashita, Y. Uemura, H. Sekiguchi, Y. Cui, A. Mori, S. Mori, K. Hara, Substituted carbazole dyes for efficient molecular photovoltaics: Long electron lifetime and high open circuit voltage performance, J. Mater. Chem. 19 (2009) 4829–4836. https://doi.org/10.1039/b905831a.

[85] H. Tian, A. Soto, B. Xu, L. Sun, A. Hagfeldt, F. Fabregat-Santiago, I. Mora-Sero, Y.S. Kang, J. Bisquert, E.M. Barea, Effect of the chromophores structures on the performance of solid-state dye sensitized solar cells, Nano. 9 (2014). https://doi.org/10.1142/S1793292014400050.

[86] M.K. Kashif, J.C. Axelson, N.W. Duffy, C.M. Forsyth, C.J. Chang, J.R. Long, L. Spiccia, U. Bach, A new direction in dye-sensitized solar cells redox mediator development: In situ fine-tuning of the cobalt(II)/(III) redox potential through lewis base interactions, J. Am. Chem. Soc. 134 (2012) 16646–16653. https://doi.org/10.1021/ja305897k.

[87] I.R. Perera, A. Gupta, W. Xiang, T. Daeneke, U. Bach, R.A. Evans, C.A. Ohlin, L. Spiccia, Introducing manganese complexes as redox mediators for dye-sensitized solar cells, Phys. Chem. Chem. Phys. 16 (2014) 12021–12028. https://doi.org/10.1039/c3cp54894e.

Experimental Details

Chapter 1 – Materials and Methods

1.1 Materials

The materials used in this work are presented below: Acetonitrile (C_2H_3N HPLC Gradient grade. Fisher Chemical. Cas:75-05-8), Butyronitrile, 99% (C_4H_7N, Alfa Aesar, Cas: 109-74-0), 3-Methoxypropionitrile, (C_4H_7NO, 98% GC, Aldrich, Cas: 110-67-8), 1,3-Dimethylimidazolium iodide, 99%, (io-li-tec, IL-0199-HP-0100), Iodine (I_2, Fisher Chemical, Cas: 7553-56-2), 4-tert-Butylpyridine 96% (Aldrich, Cas:3978-81-2), Lithium iodide (LiI, Merck), Guanidinium thiocyanate (Sigma-Aldrich, Cas: 593-84-0), Tetrabutylammonium iodide (Merck), 1-Methylbenzimidazole 99% (Aldrich, Cas: 1632-83-3), Ethanol absolute (VWR chemicals CAS: 64-17-5), N719 dye (Rutheniun 535 Bis-TBA, Dyesol), TiO_2 pastes DSL 18NR-T and DSL 30-NRD (Dyesol), TEC7 3.2 mm fluorine doped tin oxide coated glass slide (Aldrich) and the dyes N719, D35 and LEG4 from Dyenamo AB.

1.2 DSSC preparation

A typical DSSC preparation method is described below: FTO glass is cleaned with detergent, EtOh and acetone in ultra-sonicator baths followed by submersion in a $TiCl_4$ solution for 1 hour at 70°C. A double layered TiO_2 semiconductor film consisting of either two transparent layers or a transparent layer and a scattering layer is prepared by doctor blading the pastes onto the glass followed by sintering the glass at 125 °C, 325 °C and 525 °C for 5, 15 and 30 min respectively in sequence. After cooling, another $TiCl_4$ solution treatment takes place. Sensitization is applied by dipping the working electrode in either a 0.2 mM organic dye (D35, MK-2, LEG4) acetonitrile:tert-butanol (1:1) solution or a 0.3 mM Ru dye (N719) ethanol solution for 40 hours. A drop of the optimized electrolyte consisting of 1,3-dimethylimidazolium iodide (1M), iodine (15 mM), guanidinium thiocyanate (0.1 M), 4-tertbutylpyridine (0.5 M) and lithium iodide (50 mM) in acetonitrile/butyronitrile (v:v 85:15), is sandwiched between the working electrode and the transparent Pt coated counter electrode.

1.3 Characterization methods

Cyclic voltammograms were acquired at room temperature with a two Pt electrode (symmetric) arrangement, without illumination, at a scan rate of 0.05 V/s. The IUPAC convention was used for the presentation of the cyclic voltammograms. UV–visible absorbance spectra were recorded through a 3010 Hitachi spectrophotometer (60 mm integrating sphere) and, unless specified, $BaSO_4$ pellets were used as reference. Concerning the dye solutions used for the acquisition of the dye absorption spectra, a quartz cuvette of 1 cm optical length was used with scan speed of 600 nm/min. A good evaluation method for the optical characteristics of dye-sensitized semiconductor films is the light harvesting efficiency (LHE) characterization, which characterizes the working electrode's capacity for absorbing light. Initially, the absorbance spectra of sensitized TiO_2 films was acquired, through the transformation of diffuse reflectance spectra via the Kubelka-Munk function F(R) [1] (plain TiO_2 was used as a baseline). The LHE was calculated using these absorbance values (A(λ)), through the following equation [2–4]: $LHE(\lambda) = 1 - 10^{-f(\lambda)} = 1 - 10^{-A(\lambda)}$, where $f(\lambda)$ is the oscillator strength value for the dyes, corresponding to absorption intensity.

All photovoltaic performance tests took place in lab conditions, using simulated solar and low power fluorescent light. For the DSSCs, a black mask was used to define the active cell area (0.152 cm^2) during illumination and an Autolab PG-STAT-30 potentiostat (Image 3) was used for current-voltage measurements during linear sweep voltammetry (LSV), for both STC and indoor illumination measurements. LSV was performed from -0.9 to 0 V (cell operating range for all types of illumination and in the dark, scan rate of 3-5 mV/s) and from -1.5 to 1.5 (forward and reverse bias conditions for limited-current density measurement at STC, scan rate of 20 mV/s [5]). Electrochemical Impedance tests (EIS) were conducted at dark conditions with an applied voltage value near the cells' Voc, through Autolab PG-STAT-30 potentiostat's built-in frequency response analyzer (FRA).

Image 3. The Autolab PG-STAT-30 potentiostat used for the characterizations of the solar cells.

Another significant characterization method is the measurement of the Incident Photon-to-Current Efficiency (IPCE), which evaluates the efficiency of current production (photon to electron conversion) of the DSSC device with respect to the wavelength of incident light. An Oriel 1/8 monochromator was used for the measurement of IPCE (Image 4), placed between the xenon lamp and the DSSC for the filtering of the lamp's incident light (by wavelength). A Thorlabs silicon photodiode used for calibration of the IPCE spectra and a 2nd degree Savitsky-Golay filter was also applied (as it is often used in the bibliography for IPCE plots [6]). It is important to note the relationship between LHE and IPCE characterizations. The LHE characterization evaluates the optical characteristics of the working electrode's film, the ability of the dye sensitized semiconductor to absorb light and, as such, is limited in its scope. The IPCE, on the other hand, characterizes the DSSC device as a whole, instead of a single component or property as in LHE characterization (which focuses on the optical properties of the working electrode). As such, several more factors are at play in the evaluation of IPCE, such as recombination phenomena, and that is the reason for potential differences between the two types of spectra. For example, while the LHE might accurately present a film's wide range of light absorption, the IPCE spectrum of the final cell might present low efficiencies in the conversion of light from this wavelength range to electrons due to parameters (e.g. interfacial resistances) introduced when integrating the film into the final cell.

Image 4. Monochromator setup used for the IPCE characterization of the solar cells.

1.3.1 Simulation of different lighting conditions: irradiance and illuminance

A Xe lamp with applied AM 1.5G and 400 nm (UV) cut off (Oriel) optical filters (Solar light), was used for solar light testing conditions (1 sun, irradiance of 100 mW/cm^2) by placing the DSSCs across it at a specific distance, held in place via the employed mask (Image 5). For lower solar light intensity, the same setup was used with the addition of a neutral density filter (0.1 sun, 10 mW/cm^2).

Image 5. Xenon lamp with (top) and without (bottom) neutral density filter, for the simulation of 1 sun (100 mW/cm$_2$) and 0.1 sun (10 mW/cm$_2$) of light intensity, respectively

For indoor light performance characterization an Osram 930 Warm White fluorescent lamp [7] was used (Image 6), a common light source for indoor performance evaluation [8]. While irradiance (mW/cm^2) is mostly used for the characterization of a solar simulator's irradiation, for the measurement of light intensity from indoor light sources, a commonly used unit is the lux (photometric unit of illuminance), which is representative of the perception of light intensity by human eyes. With irradiance all wavelengths have equal weight, while in the case of illuminance [9], weighting of each wavelength's power with respect to the human eye sensitivity takes place.

Image 6. The fluorescent lamp used for the simulation of indoor lighting environments.

For indoor characterization, the incident power density was controlled by changing the relative position-along a horizontal axis- between measured cell and light source and during measurement the room was kept completely dark aside from the light source, to avoid exterior light affecting the measurement. A conversion between lux and irradiance units is needed for cell efficiency calculations and one proposed method for acquiring a conversion relationship between them is to measure the incident illuminance and the incident irradiance from the lamp at a specific point and use the ratio between them as a conversion factor [10]. With the help of a luxmeter (MS6612, HYELEC), most often used for the illuminance appraisal, a point along an horizontal axis was defined for each of the studied illuminance levels (between 100 and 1000 lux) and a radiometer was used to measure the emitted irradiance from the lamp at these points, thereby creating a conversion relation between illuminance and irradiance for the lamp (Image 7).

Image 7. Establishment of indoor lighting characterization setup: A luxmeter (left) and a radiometer (right) were used at set distances away from the fluorescent lamp, in order to create an equivalence relationship between lux (luxmeter) and irradiance (radiometer)

Relative errors arising with incident light power measurement can reach totals of ±10% (and errors on PCE value calculation can reach ±16%, in relative terms) [10]. Also, for smaller devices (especially those with active areas smaller than the luxmeter's detector, like the cells in this work), the incident light power from fluorescent lamps has been considered to be uniform over the device's active area (with small loss of uniformity for larger area devices) [10]. An equivalence of 200 lux to 61.8 μW/cm^2, 500 lux to 160 μw/cm^2 and of 1000 lux to 300μW/cm^2 was established, which is in good agreement with similar works using fluorescent lamps as light sources [8,10]. Besides its use in research works, the light level of 200 lux is often used for indoor performance evaluation by the PV industry [11], as it is considered representative of most residential environments. Thus, the solar cell characterization in this work covered irradiance levels from less than 0.0618% (200 lux) to 100% of the characteristic 1 sun light intensity.

Bibliographic references for Chapter 1

[1] A.G. Kontos, T. Stergiopoulos, V. Likodimos, D. Milliken, H. Desilvesto, G. Tulloch, P. Falaras, Long-term thermal stability of liquid dye solar cells, J. Phys. Chem. C. 117 (2013) 8636–8646. https://doi.org/10.1021/jp400060d.

[2] W. Sang-aroon, S. Tontapha, V. Amornkitbamrung, Photovoltaic performance of natural dyes for dye-sensitized solar cells: A combined experimental and theoretical study, Dye. Sol. Cells Math. Model. Mater. Des. Optim. (2019) 203–229. https://doi.org/10.1016/B978-0-12-814541-8.00006-9.

[3] J. Duan, Q. Xiong, H. Wang, J. Zhang, J. Hu, ZnO nanostructures for efficient perovskite solar cells, J. Mater. Sci. Mater. Electron. 28 (2017) 60–66. https://doi.org/10.1007/s10854-016-5492-3.

[4] Q. Wu, J. Hou, H. Zhao, Z. Liu, X. Yue, S. Peng, H. Cao, Charge recombination control for high efficiency CdS/CdSe quantum dot co-sensitized solar cells with multi-ZnS layers, Dalt. Trans. 47 (2018) 2214–2221. https://doi.org/10.1039/c7dt04356b.

[5] D. Perganti, A.G. Kontos, T. Stergiopoulos, V. Likodimos, J. Farnell, D. Milliken, H. Desilvestro, P. Falaras, Thermal Stressing of Dye Sensitized Solar Cells Employing Robust Redox Electrolytes, Electrochim. Acta. 179 (2015) 241–249. https://doi.org/10.1016/j.electacta.2015.03.206.

[6] E. Gabrielsson, H. Ellis, S. Feldt, H. Tian, G. Boschloo, A. Hagfeldt, L. Sun, Convergent/divergent synthesis of a linker-varied series of dyes for dye-sensitized solar cells based on the D35 donor, Adv. Energy Mater. 3 (2013) 1647–1656. https://doi.org/10.1002/aenm.201300367.

[7] Osram, L 18 W/930 data page, (n.d.). https://www.osram.com/ecat/LUMILUX DE LUXE T8-Fluorescent lamps T8-Fluorescent lamps-Lamps-Digital Systems/com/en/GPS01_1027895/PP_EUROPE_Europe_eCat/ZMP_60463/.

[8] Y. Cao, Y. Liu, S.M. Zakeeruddin, A. Hagfeldt, M. Grätzel, Direct Contact of Selective Charge Extraction Layers Enables High-Efficiency Molecular Photovoltaics, Joule. 2 (2018) 1108–1117.

https://doi.org/10.1016/j.joule.2018.03.017.

[9] N. Sridhar, D. Freeman, A study of Dye Sensitized Solar Cells under Indoor and Low Level Outdoor Lighting: Comparison to Organic and Inorganic Thin Film Solar Cells and Methods to Address Maximum Power Point Tracking, Conf. Proc. 26th EU-PVSEC. (2011) 232–236. https://doi.org/10.4229/26thEUPVSEC2011-1CO.10.5.

[10] F. De Rossi, T. Pontecorvo, T.M. Brown, Characterization of photovoltaic devices for indoor light harvesting and customization of flexible dye solar cells to deliver superior efficiency under artificial lighting, Appl. Energy. 156 (2015) 413–422. https://doi.org/10.1016/j.apenergy.2015.07.031.

[11] https://gcell.com, GCell, (n.d.).

Results and Discussion

Chapter 2 - Parameter of Electrolyte

2.1 Formulation of an electrolyte for "panillumination" DSSCs

In this chapter, building on previous findings concerning I^-/I_3^- electrolytes, ILs, redox media and additives, the formulation of an electrolyte solution for well performing DSSCs under both indoor and outdoor lighting conditions is presented: a "pan-illumination" electrolyte comprised of low concentration iodine along with an IL as the iodide source, mixed in a transparent low viscosity solution with the most suitable additives. The functional electrolyte ("A") was designed in order to reach high indoor efficiency values, while preventing the performance downgrade when under 1 sun [1]. This formulation, was tailored for electrolyte component synergy, by employing the DMII ionic liquid as the iodide source, a transparent low viscosity acetonitrile/butyronitrile (ACN/BN) solution as the redox medium and a low I_2 concentration along with the TBP additive. For low intensity lighting conditions, the low I_2 concentration (and resulting low I_3^- concentrations) ensures sufficient diffusion and dye regeneration while preventing significant recombination and absorbance around the significant 436 nm wavelength (due to triiodide). The almost transparent ACN/BN solvent ensures low viscosity (despite the included IL), high redox species diffusion and negligent light absorbance. For high intensity lighting conditions, the negative effects of the low I_3^- concentration on diffusion and regeneration are alleviated through the enhanced mass transport by the low viscosity ACN/BN solvent, the effect of the TBP additive (most appropriate for this low triiodide concentration) and the high ionic conductivity properties of the DMII IL.

2.2 Optimization method

As for the electrolyte formulation used in this work, the iodine concentration, additives and solvent mixture are especially significant for panillumination purposes. A lower iodine concentration (< 20 mM) is a good starting point for the dual-focused optimization as it assures good performance under low intensity light (as explained above), leaving proper solar light operation as the remaining goal. Concerning additives, while NMBI has better synergy with high iodine concentrations, TBP is

better suited for low iodine content. Thus, a combination of TBP with iodine concentrations of < 20mM is proper for operation under 1 sun irradiation. The addition of Guanidinium thiocyanate (GuNCS) and lithium iodide (LiI), further improves the performance. As for the solvent mixture, butyronitrile is an optimum choice as a co-solvent for acetonitrile, surpassing even valeronitrile.

In summary, The optimized "pan-illumination" electrolyte (Electrolyte "A") was prepared by dissolving iodine (15 mM), 1,3-dimethylimidazolium iodide (1M), 4-tertbutylpyridine (0.5 M), guanidinium thiocyanate (0.1 M) and lithium iodide (50 mM) in a mixture of acetonitrile and butyronitrile (vol. ratio of 85:15). For comparison, a reference electrolyte (Electrolyte "ref") proposed by the aforementioned De Rossi et al. [1], was used: In order to prepare the best reported I^-/I_3^- electrolyte for DSSC under 200 lux of fluorescent light: 0.7 M of tetrabutylammonium iodide (TBAI, iodide source), 0.15 M of N-methylbenzimidazole (NMBI) and 0.15 M of guanidinium thiocyanate (GuNCS) were mixed in a 3-methoxy-propionitrile (MPN) solvent with 8 mM of iodine. The above formulations are summarized in the table below.

Table 2.1 Panillumination electrolyte formulation

Role	Electrolyte component name (concentration)		
	Reference electrolyte	Optimized electrolyte	Comments
Iodide Source	TBAI (0.7 M)	DMII (1 M)	DMII has proven its superiority in comparative evaluations of methylimidazolium cation ILs
Additive #1	NMBI (0.15 M)	TBP (0.5 M)	TBP is the optimum choice for low I_2 concentrations
Additive #2	GuCNS (0.15 M)	GuCNS (0.1 M)	
Additive #3	-	LiI (50 mM)	
Solvent	MPN	ACN:BN (85:15)	The combined characteristics of the low viscosity ACN/BN mixture assure great electrolyte ion mobility in all tested light conditions. In the reference MPN-based electrolyte, DSSCs show severely impaired triiodide diffusion at high light intensities.
Iodine content	I_2 (8 mM)	I_2 (15 mM)	Optimal I_2 concentration: low enough for good indoor illumination performance but high enough for good electrolyte ion mobility under 1 sun.

For the DSSCs' construction, the TiO_2 electrodes [2] were sensitized through immersion in a 0.3 mM N719 dye solution (in ethanol) for 24 hours. A drop of electrolyte was placed between the photoelectrode and a Pt counter electrode and the cells were not encapsulated [3–5].

2.3. Characterization and application

2.3.1 Electrolyte characterization

To elucidate the critical properties of the prepared electrolyte solutions, they were characterized with voltammetric and optical methods. Cyclic voltammetry was employed [10], in order to investigate two of the most important electrolyte properties: chemical stability and diffusion characteristics. The cyclic voltammograms for the "A" and reference electrolytes, using a symmetric arrangement of two Pt electrodes, are reported in Fig. 2.1.

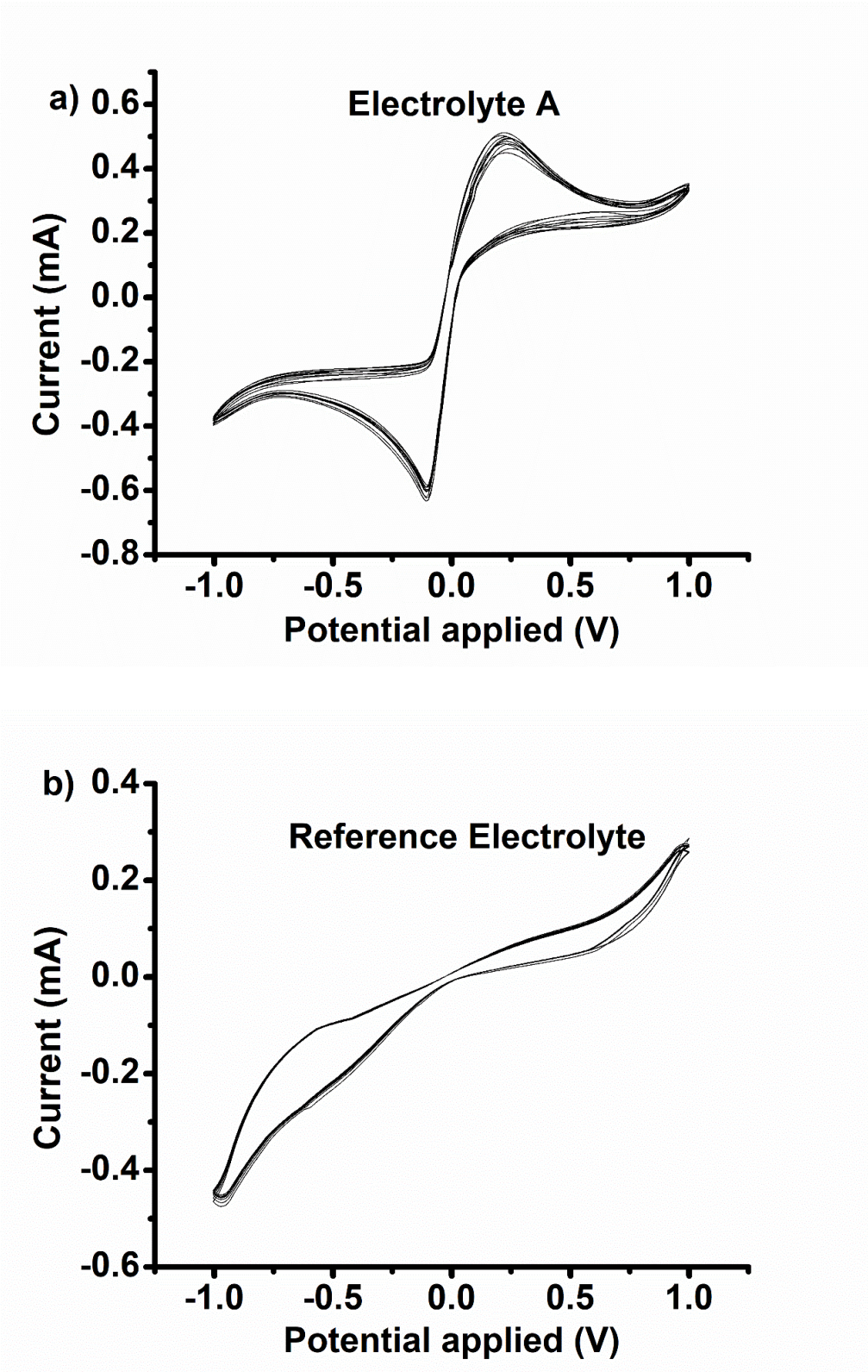

Fig. 2.1 *Cyclic voltammograms of "A" (a) and "reference" (b) electrolytes (20 cycles are displayed). WE:Pt, CE:Pt, Scan rate: 0.05 V/s. Top part represents oxidation, bottom part represents reduction*

For the optimized electrolyte ("A"), well-defined anodic/cathodic waves (representing the oxidation/reduction of the active species) were observed. The distance between anodic and cathodic peak currents (peak-to-peak separation) is related to the diffusion of the redox active species from and to the electrode [11]. This parameter accounts for the electrochemical reversibility and its relatively high value (ΔE_p=0.35 V) is probably due to the low concentration of iodine in the electrolyte solution. In addition, the species seem stable after reduction and subsequent re-oxidization [11] and good chemical reversibility is evident due to the (absolute) peak current ratio (cathodic to anodic, Ip_c/Ip_a), which is close to unit. On the contrary, this is not the case of the reference electrolyte, where it is difficult to distinguish clear waves and determine exact values for peak currents and the corresponding peak potentials. However, it is evident that the ΔEp in the reference electrolyte is significantly large, which can be a sign of sluggish electron transfer reactions [11,12] and justifies the preferential application of the optimized electrolyte "A" in electrochemical devices.

Another significant feature in the cyclic voltammograms concerns the high current values (in both anodic and cathodic domains) registered for electrolyte "A". Solvent viscosity should be taken into account in order to understand the above behavior, as the current can be significantly affected by the mass transport of the species in the electrolyte solution [13,14]. It is important to note that there is a large excess of I^- in the electrolyte and thus, triiodide (formed by iodine addition to the iodide source [15]) is considered to be the diffusion limiting species, with its concentration being equal to that of iodine [1,16]. The optimized electrolyte is based on acetonitrile (ACN), a low viscosity (0.33 mPa*s) solvent with excellent chemical stability [17]. In the indoor I^-/I_3^- DSSC work in which the reference electrolyte was proposed [1], 3-methoxypropionitrile (MPN), a common solvent (with a viscosity of 2.5 mPa*s [17]) was used. In ACN the triiodide's diffusion is significantly higher [18] and the diffusion coefficient of I^- has been reported to be as high as $3.2x10^{-5}$ cm^2s^{-1} [19]. Thus, low viscosity can lead to enhanced mass transport [19] and to the increased current values observed for the ACN-based electrolyte.

For all of these reasons, ACN solvent is an ideal candidate for the optimized electrolyte with low I_2 concentration. Furthermore, electrolyte "A" uses a mixture of

acetonitrile (ACN) and butyronitrile (BN), a higher boiling point solvent. Sauvage et al. reported that butyronitrile-based electrolytes allow for high efficiency DSSCs, while also exhibiting excellent stability. In fact, when compared to MPN's case, the BN-based electrolyte showed improved triiodide diffusion (enhanced mass transport due to BN-electrolyte's lower viscosity) and the BN-DSSCs showed higher efficiency and stability [20]. Thus, in electrolyte "A", the mixing of DMII with low viscosity organic solvents (ACN and BN) allows the utilization of the IL's advantages while preventing significant electrolyte viscosity increase, thereby ensuring good triiodide diffusion in spite of the low I_2 content.

UV-Vis spectrometry was also used for electrolyte characterization. Initially, the corresponding solvents were examined (Fig. 2.2a): The ACN/BN mixture shows no absorption (transparent) as expected. As for the electrolytes themselves, in the case of the MPN-based reference electrolyte, there is an intense and broad absorption band (Fig. 2.2b) attributed to the behavior of the MPN solvent. As for the ACN/BN based electrolyte "A", the absorbance (Fig. 2.3) is mostly negligent with only a very small absorption peak centered at 365 nm, mainly due to the (low) iodine content. An absorption tail which extends into the visible range can be observed, characteristic of the higher charge multiplates of iodine (triiodide and higher) [2,21].

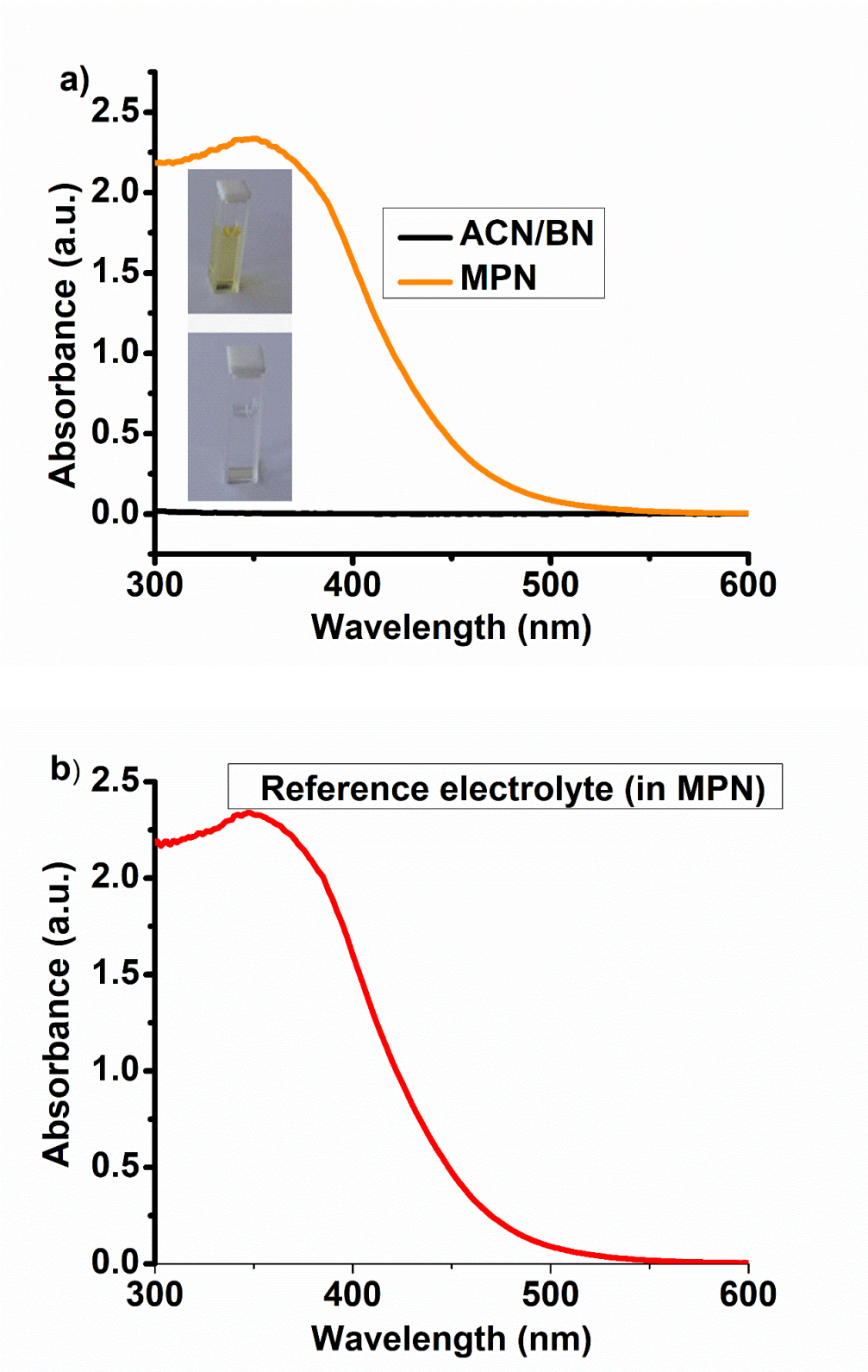

Fig. 2.2 *Absorbance spectra of a) MPN (yellow) and ACN/BN (clear) b) reference electrolyte: solution was diluted in its respective solvent (1:1000 ratio) to avoid issues of signal saturation.*

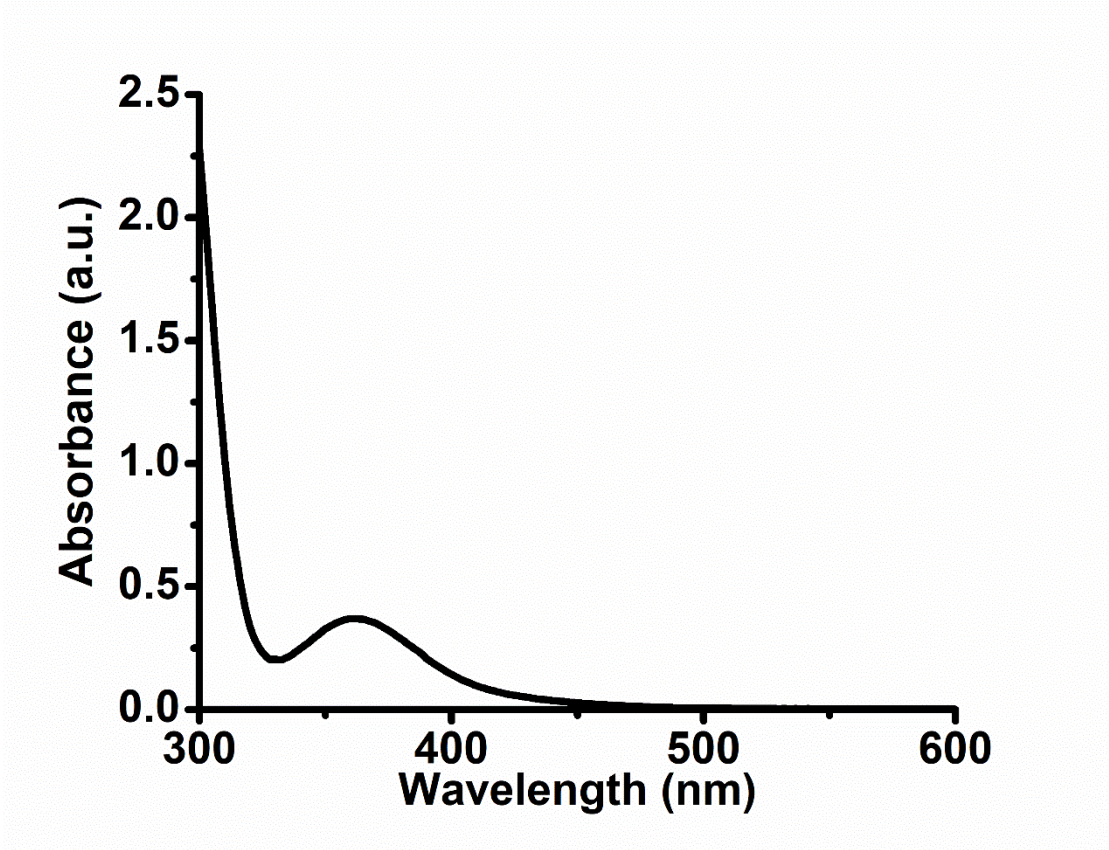

Fig. 2.3. *UV-Vis spectra of electrolyte "A". The solution was diluted in its respective solvent (1:1000 ratio) to avoid issues of signal saturation.*

2.3.2 DSSC performance dependence on illumination type and light intensity

The optimized electrolyte ("A") and the reference electrolyte were incorporated in DSSC devices and their performance was evaluated under different illumination conditions and irradiance levels. For indoor performance evaluation a fluorescent light source at 200 lux was employed, a low intensity illuminance level often used in related studies and in the PV industry [9], as it is thought to accurately represent residential lighting conditions. For high and low power solar light, the 1 sun and 0.1 sun (100 mW/cm^2 and 10 mW/cm^2 light intensity) conditions were considered to be representative. Thus, the light irradiance levels employed for DSSC performance evaluation range from 0.0618% (200 lux) of STC light intensity to 100% (full 1 sun). The J-V curves (plots of photocurrent density vs applied voltage) for the cells with electrolyte "A" and with the reference electrolyte for each lighting type are presented at Fig. 2.4 (a-c) and Figure 2.5 (a-c), and, from the corresponding analysis, the

average values (of 3 different cells) of the obtained photovoltaic parameters are summarized in Table 2.2. As expected, the resulting PCEs are significantly higher under indoor lighting than under 1 sun illumination conditions, since DSSC efficiency is known to increase when switching from sunlight to indoor lighting conditions, even for devices designed for STC operation [1].

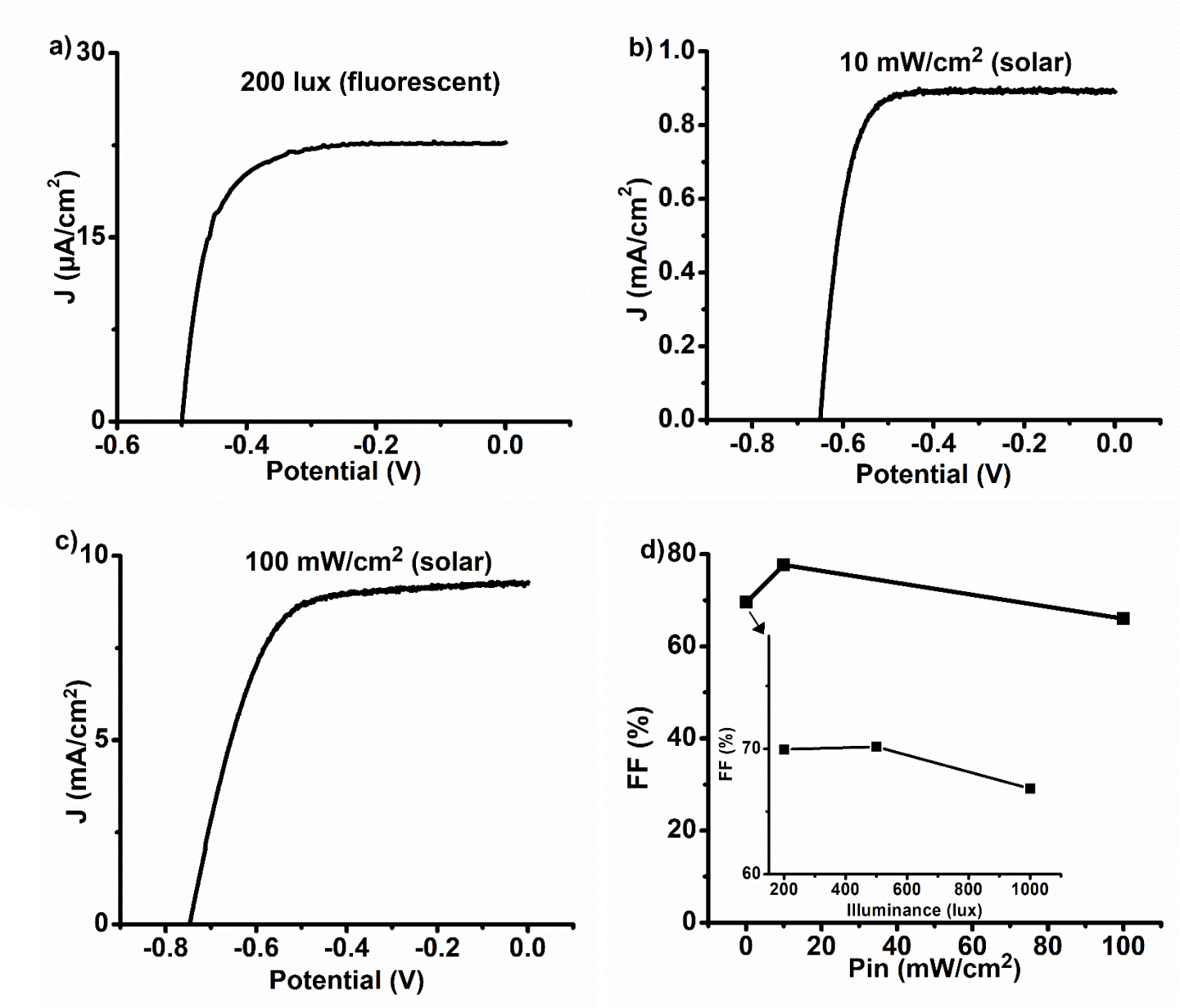

Fig. 2.4 *J-V curves for cells using electrolyte "A", under lighting conditions of a) 200 lux of fluorescent lighting, b) 0.1 sun and c) 1 sun, along with d) trends of FF value for all tested light levels (inset presents FF value for all illuminance/lux levels, with the arrow indicating the corresponding irradiance region for these low intensity levels)*

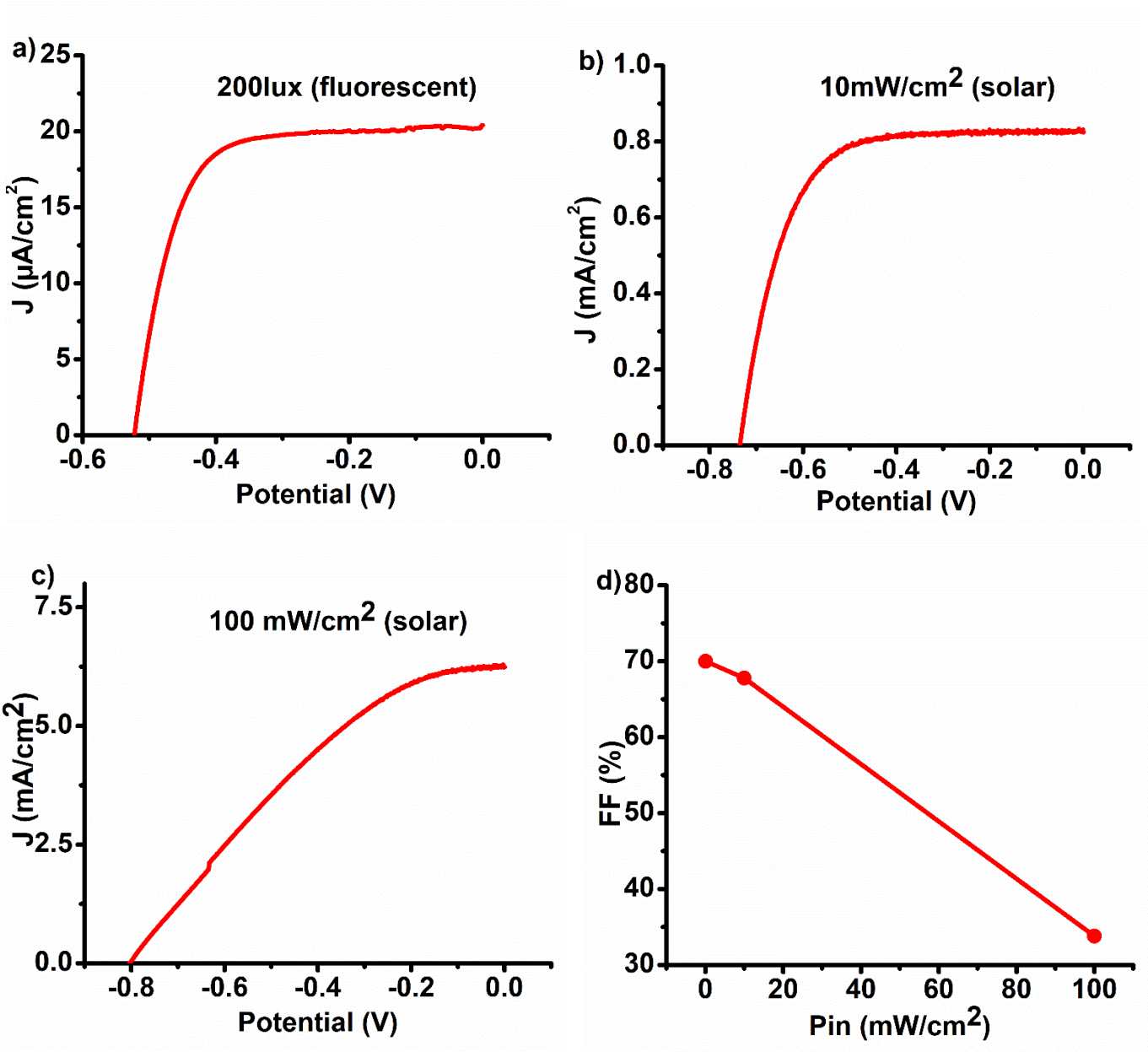

Fig 2.5 *J-V curves for cells based on the reference electrolyte, under lighting conditions of a) 200 lux of fluorescent lighting, b) 0.1 sun and c) 1 sun, along with d) trends of FF value for all tested light levels*

Table 2.2 *Characteristic PV parameter values for DSSCs with electrolyte "A" and reference electrolyte, under different illumination conditions*

Lighting conditions	**Electrolyte used**	**J_{sc} (mA/cm^2)**	**V_{oc} (mV)**	**FF (%)**	**PCE (%)**
200 lux fluorescent light (61.8 μW/cm^2)	"A"	0.021	481	69.6	11.56
	Reference	0.019	522	70	11.78
0.1 sun solar sim. light (10 mW/cm^2)	"A"	0.89	650	77.7	4.5
	Reference	0.83	735	67.8	4.13
1 sun solar sim. light (100 mW/cm^2)	"A"	9.4	763	66	4.75
	Reference	6.58	814	33.8	1.81

Under 200 lux fluorescent lighting conditions, both cell types present similar performance (PCE ~11.5%) with no significant difference in fill factor (FF). The J_{sc} and V_{oc} values, however, are of interest. In regards to the generated photocurrent, the cells incorporating the optimized electrolyte "A" show high photocurrent density, possibly due to transparent nature of their electrolyte which ensures negligent incident photon capture under 500 nm, an important area for fluorescent light. It can be hypothesized that this is not the case for the colored electrolyte in the reference cells, as its significant absorption in the wavelength area bellow 500 nm is expected to have led to Jsc decrease [15]. It is important to notice that a significant emission line of fluorescent lamps is located at 436 nm [22]. The close-to-transparent nature of the "A" solution ensures that no competitive absorption will take place between electrolyte and dye, thus avoiding significant photocurrent losses, especially during operation under indoor fluorescent light. As for the voltage, for "A" electrolyte cells, the relatively low V_{oc} values possibly result from a lower resistance to recombination by their less viscous solvent which does not significantly inhibit triiodide access at the electrode/electrolyte interface. In the case of reference electrolyte, a potentially mass transport-impaired diffusion (due to its high viscosity) does not seem to significantly detract from its performance (the regeneration requirements are less strict under low intensity light).

Under 0.1 sun lighting conditions, once again, the cells efficiencies do not differ significantly. However, a clear sign of superior performance concerns the fill factor, which is significantly higher for the cells using electrolyte "A". This is even more obvious when going to full 1 sun lighting conditions, where the fill factor value for cells with reference electrolyte is halved, severely impacting their efficiency. On the contrary, for cells based on electrolyte "A", the result of the synergetic strategy leads to high short circuit photocurrent, as expected [23], and to a fill factor that ensures a ~2.5 times higher PCE under 1 sun. The ACN/BN solvent-TBP additive synergy with the low I_3^- concentrations, ensures a performance that is stable between lighting types and intensity levels, evident by the constantly high FF retained between them. An electrolyte formulation containing twice the I_2 content found in the "A" samples was also evaluated, through its performance in DSSCs. Under 1 sun, the corresponding cells also showed a higher performance (Table 2.3) than those containing the reference electrolyte but they did not reach the PCEs obtained in the case of electrolyte "A", possibly due to the increased triiodide content's enhanced recombination activity, further highlighting the importance of a finely tailored electrolyte component synergy.

Table 2.3 *Photovoltaic parameters for cells with different iodine concentrations in their ACN/BN-based electrolyte.*

iodine concentration	Lighting conditions	PCE (%)	Jsc (mA/cm^2)	Voc (mV)	FF (%)
15 mM (electrolyte "A ")	1sun	4.75	9.4	763	66
30 mM		3.49	7.22	746	64.8
15 mM (electrolyte "A")	200 lux	11.56	0.021	481	69.6
30 mM		9.48	0.0187	475	67.1

It is common for devices designed solely for indoor lighting conditions, to have much less FF when evaluated under STC [1]. Furthermore, when replacing the electrolyte solvent with a more viscous one (such as ACN with MPN [24]), a significant drop is expected for the FF value [2,21] along with decreased electrical parameters and efficiency. Additionally, a smaller than expected J_{sc} at higher incident light intensities could signify triiodide mass transport or dye regeneration limitations, during increased electron injection activity within the photoanode [21]. The significantly

increased needs for redox species diffusion and regeneration for the much greater number of active dye molecules (due to the incident light intensity increase, under 1 sun), imposes requirements for mass transport in the electrolyte that the "pan-illumination" electrolyte formulation was able to sufficiently cover. On the contrary, the high viscosity of MPN along with the very small concentration of I_3^- (and, thus, small concentration gradient, which drives diffusion) in the NMBI-based reference electrolyte formulation, leads to severe mass transport problems, reflected in low J_{sc} and efficiency. It is interesting to note that only the performance under high intensity solar illumination is affected by the small triiodide concentration. Kontos et al 2013 [21] observed that, in the case of MPN-solvent DSSCs under 1 sun illumination, while the total effect of triiodide depletion was considered detrimental for the cell performance, it was much less significant under low solar light illumination.

In well performing DSSCs with sufficient I_3^- diffusion and charge transport ability, the J_{sc} is known to linearly increase with light intensity [15]. In Fig. 2.6 the plots of the cells' generated photocurrent and power density in relation to the incident light irradiance (200lux, 0.1 sun and 1 sun) are shown for the "A" electrolyte. Linear fitting was applied on all plots in order to determine the adjusted R^2 (coefficient of determination) value and, thus, evaluate their linearity.

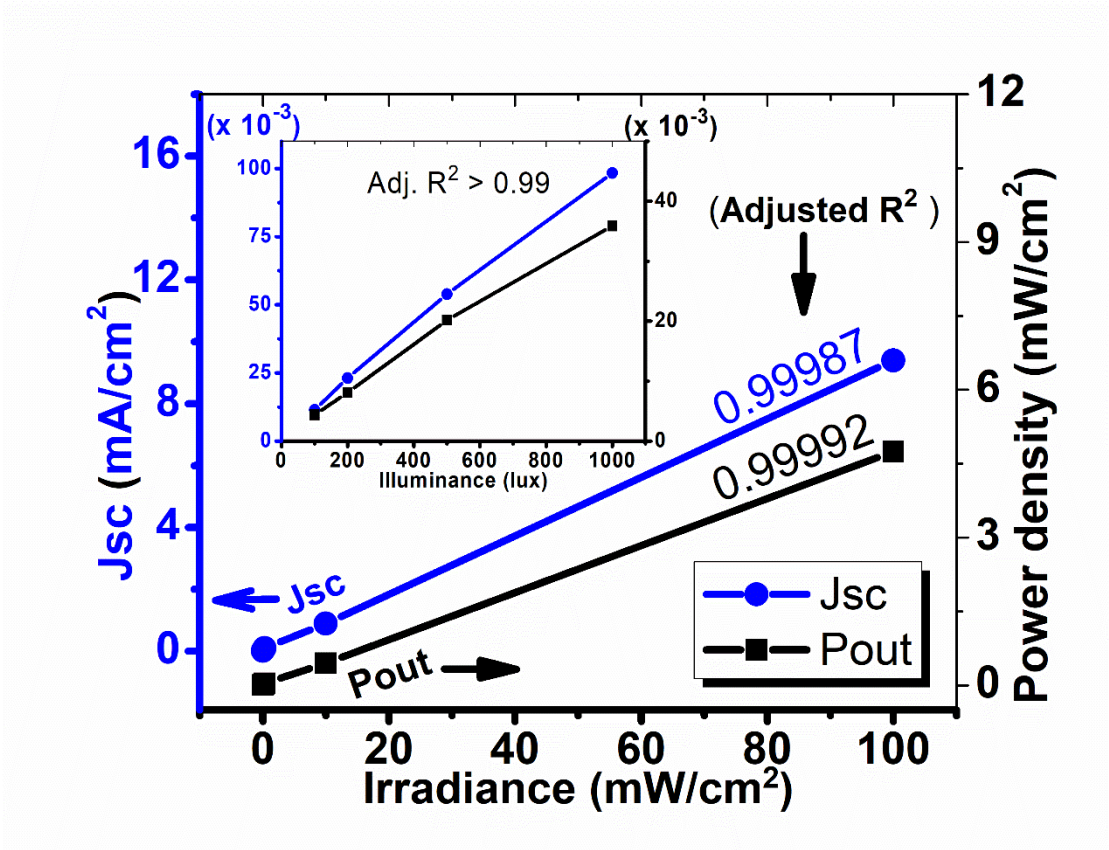

Fig. 2.6 *Photovoltaic parameters of cells using electrolyte "A", under different light intensity levels. Adjacent to each plot are the adjusted values for* R^2*, regarding the quality of the linear fit for each plot. The respective parameters for 100-1000 lux are shown in the upper left inset.*

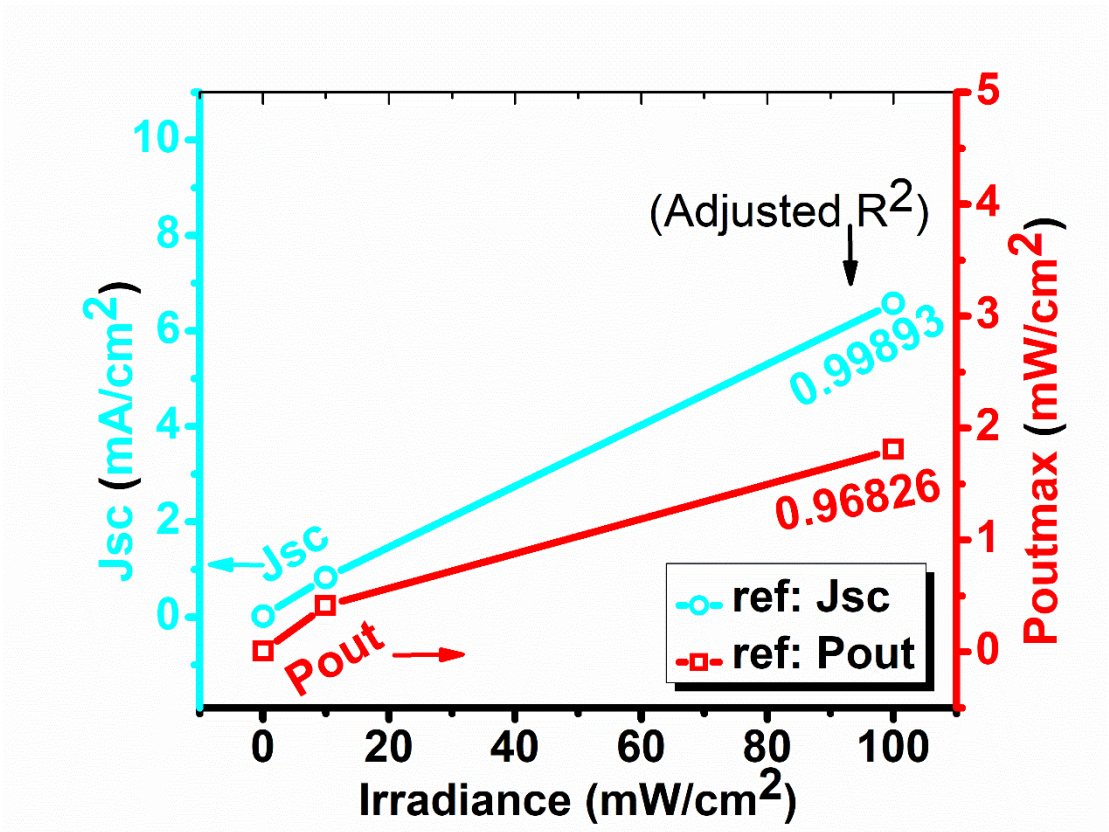

Fig. 2.7 *Photovoltaic parameters of cells based on the reference electrolyte, under different light intensity levels. Adjacent to each plot are the adjusted values for R^2, regarding the quality of the linear fit for each plot.*

For cells based on electrolyte "A", near perfect linearity is evident for both measured parameters, while devices using the reference electrolyte (Fig. 2.7) present less ideal linearity in the case of J_{sc} and a great deviation in the case of the generated power density with the cause being, as expected, the problematic performance under higher light intensity.

Table 2.4 *Characteristic PV values of cells with electrolyte "A" under fluorescent lighting*

Illuminance (lux)	**PCE (%)**	**Jsc ($\mu A/cm^2$)**	**Voc (mV)**	**Poutmax ($\mu W/cm^2$)**	**FF (%)**
100	14.21	11.44	494.00	4.39	77.68
200	13.07	23.10	500.00	8.08	69.96
500	12.61	53.93	533.00	20.17	70.17
1000	11.96	98.36	546.00	35.89	66.83

The performance of the cells with electrolyte “A” between 100 and 1000 lux of fluorescent lighting (Fig. 2.6 inset, Table 2.4) was also characterized, as this range covers a wide array of real-life illuminance conditions [25]. A near perfect linearity of photogenerated current and maximum output power with illuminance level is evident from the inset graph. This proportionality is a characteristic feature of a well performing indoor optimized DSSC [1].

2.3.3 Effects of electrolyte formulation on fundamental DSSC parameters

A good match between a device’s spectral response and the emission spectra of indoor lighting sources is necessary for good performance under these conditions [1]. The spectral responsiveness of the cells with electrolyte “A” through analysis of the action spectrum was studied and shown in Fig. 2.8. The incident photon to current efficiency (IPCE) covers the fluorescent lamp’s emission lines very well with a maximum quantum yield (collected electrons to absorbed photons ratio) of about 60% at 520 nm, and thus, shows proper utilization of incident light from both solar and indoor fluorescent lighting sources. The good fit of the IPCE to the indoor lamp’s emission was achieved not only due to the choice of dye but also because of the transparent nature of the electrolyte. Additionally, the significantly low I_3^- species concentration results in suppressed competitive light absorption from the electrolyte in the region near 450nm, thus permitting enhanced photon absorption by the dye and generating higher photocurrent [1,15]. This is especially evident in the photocurrent values of the cells with electrolyte “A” under indoor light, as the fluorescent lamp emits strongly close to this wavelength [6,22].

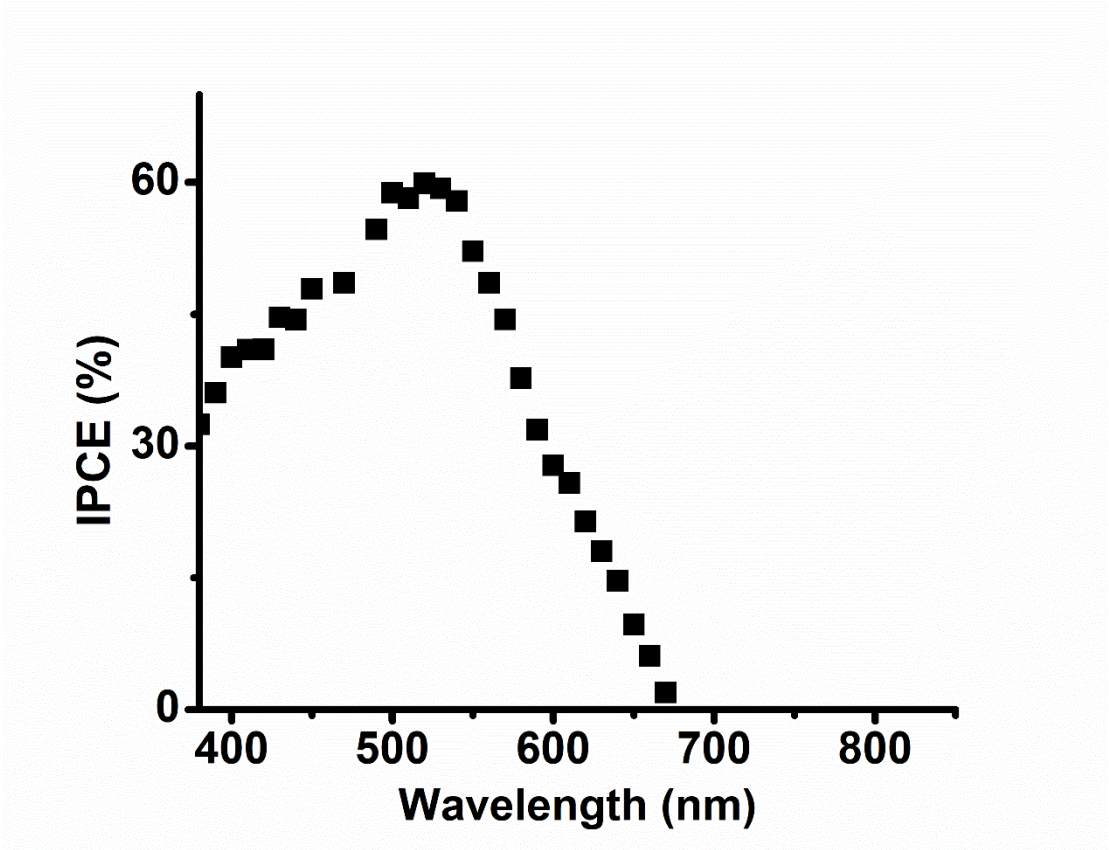

Fig. 2.8 *IPCE spectrum of the optimized cells using the optimized electrolyte "A"*

In order to further investigate the effects of the electrolyte formulation on the cells operation, detailed analysis using Electrochemical Impedance Spectroscopy (EIS) was performed. The EIS spectra (Nyquist plots) for the cells with the electrolyte "A" and those using the reference electrolyte are shown in Fig. 2.9 and Fig. 2.10, respectively, with the resulting area-normalized resistances shown in Table 2.5.

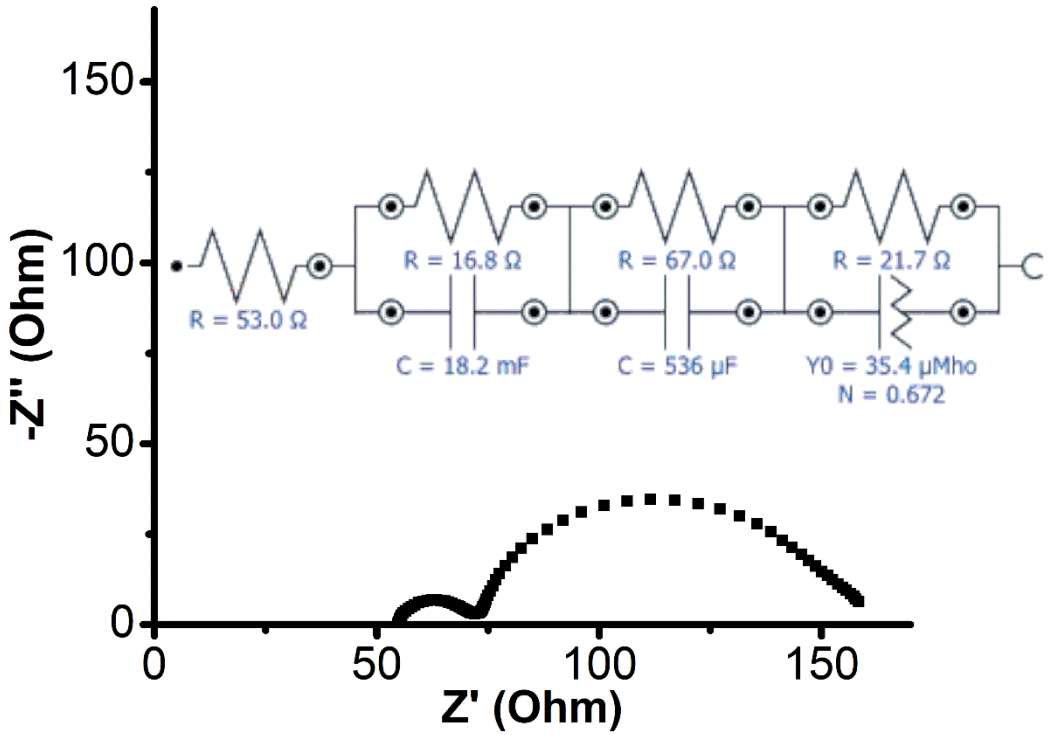

Fig. 2.9. *Electrochemical Impedance spectrum (Nyquist plot) of cells with electrolyte "A" recorded in the dark near* V_{oc}

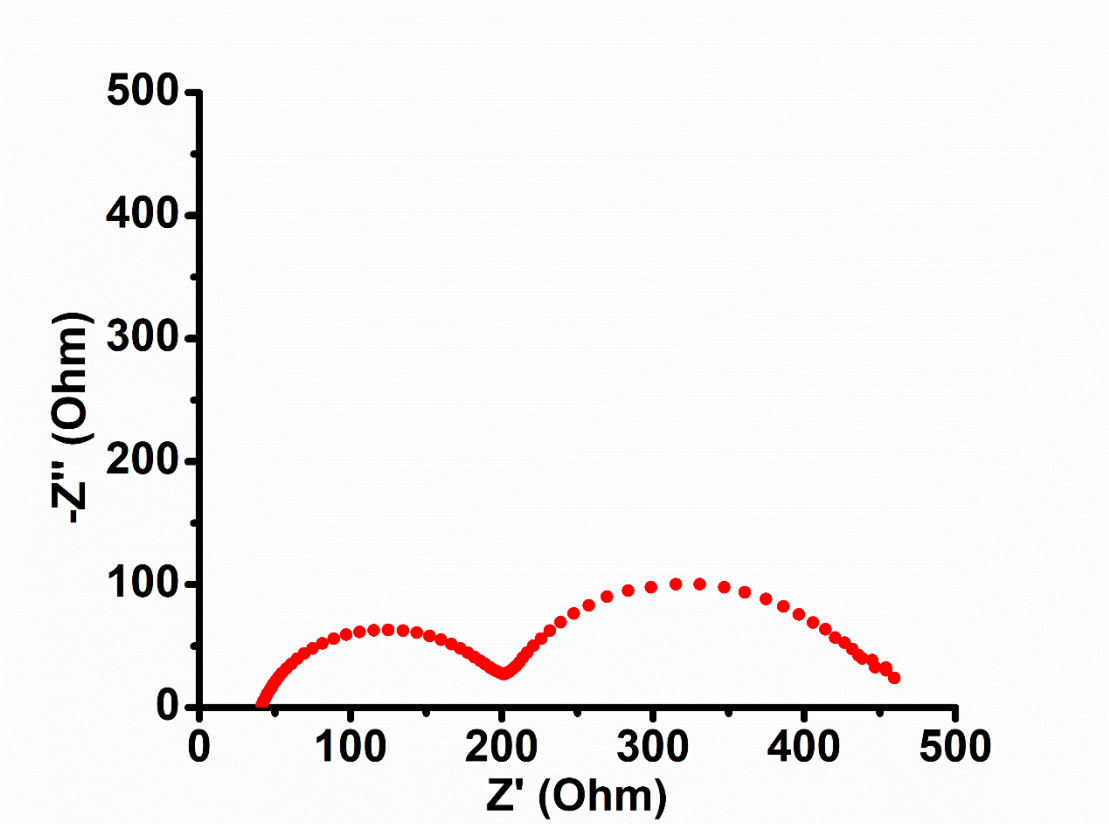

Fig. 2.10 *Electrochemical Impedance spectrum (Nyquist plot) of a cell with the reference electrolyte recorded in the dark near Voc.*

Table 2.5 *Area-normalized electrochemical resistances in the tested cells*

DSSC electrolyte	Resistances (Ohm*cm^2)		
	R_{ct}	R_{rec}	R_{dif}
"A"	2.55	10.18	3.30
Reference	25.99	28.42	8.91

Three semi to quasi-semicircles were observed and were fitted according to a model established in the literature [2,26]. The equivalent circuit represents: a) the leftmost semicircle, the charge transfer resistance at the electrolyte/counter electrode interface (R_{ce}), b) the middle semicircle, the TiO_2/electrolyte recombination resistance (R_{rec}) and c) the rightmost semicircle, the diffusion resistance in the electrolyte (R_{dif}). For better fitting, one of the capacitances was replaced with a constant phase element (CPE) [21], as its use is suggested (instead of the ideal capacitance) for rough electrode surfaces [16,18].

The series resistance (Rs) is dependent upon factors such as the glass substrate resistance and the wiring and is not of interest for the present study. The R_{rec}, R_{ce} and R_{dif} resistances are determinant parameters for the fill factor value of a DSSC [5,27]. The cells with electrolyte "A" exhibit relatively low R_{ce} and R_{dif} values [2] -despite the electrolyte's low triiodide content [21]- allowing for good transport of electrons through the C.E./electrolyte interface and fast redox species diffusion, respectively. Increased diffusion of triiodide (low R_{dif}) leads to the superior FF values [2,27], while the R_{rec} value is sufficiently high to ensure low recombination rates [28]. It is evident that the low triiodide content in the solution does not significantly impair the cell's operation, as the synergetic relationship achieved in the electrolyte formulation "A" allows for good ion diffusion and charge transport, despite the low concentration of triiodide. In turn, such a low concentration allows for suppressed recombination (and is aided in this goal by the TBP additive).

When using the reference electrolyte, all resistances show significantly high values, possibly due to the increased difficulty during mass (and charge) transport. A lower iodine concentration, especially in the viscous MPN electrolyte, is expected to result in higher R_{rec} [2,24], through which the solar cells with the reference electrolyte achieve great suppression of charge recombination, leading to increased Voc [15,29]. In fact, as Voc values depend on the difference between the TiO_2 electrode electrons' Fermi levels and the redox potential, an electron density increase in the TiO_2 film-due to longer recombination lifetimes- would cause a Fermi level increase and, thus, a Voc increase [15]. The downside of the reference electrolyte is far greater though, as the diffusion resistance also increases greatly. Most probably, the increase of R_{dif} (and R_{ce}) and its negative impact on the FF value, led to the general performance downgrade under 1 sun in cells with the reference electrolyte (Table 2.2) [2].

As mentioned before, in the case of "A" electrolyte, the diffusion limiting species is considered to be triiodide and in the respective cells, the low I_3^- concentration alone could lead to mass transport and current limitations [27] and the effect is expected to be exacerbated by higher viscosity [28]. In order to better understand the significance of the redox species diffusion in the electrolyte, photocurrents were recorded through

both forward and reverse bias regions (between -1.5 and 1.5 V) under 1 sun using linear sweep voltammetry [30,31], and the results are presented in Fig. 2.11 and Fig. 2.12. In the reverse bias region the saturated diffusion limited current (due to triiodide depletion at the CE) for the cells can be observed [21,31], for which a significantly high value is required for good DSSC operation [2]. Following the literature, a limited current value of more than double the value of the short circuit current is a good indicator of the photocurrent not being significantly affected [32]. In fact, for the cells using the optimized electrolyte "A", under 1 sun irradiation the diffusion limited current is more than 5 times larger than the short circuit photocurrent, indicating that ionic transport in the electrolyte does not limit the device performance, despite the low triiodide concentration [2]. On the other hand, for cells employing the reference electrolyte (Fig. 2.12a), the diffusion limited current is barely larger than its short circuit current, a clear indication of the limiting effects that diffusion imposes on the photogenerated current under 1 sun [21]. It is worth mentioning that this problem does not appear when these cells (with the reference electrolyte) are operating under 0.1 sun irradiation: Under 0.1 sun, the diffusion limited current is almost 3 times larger than the short circuit current (Fig. 2.12b). In fact, at such a low intensity irradiance, diffusion limitations on the current are not expected, with recombination being the main problem for J_{sc} [33]. These findings further validate the hypothesis that under the lower light intensities, diffusion of triiodides in the electrolyte is adequate in either electrolyte formulation for good performance, while for higher intensities (and corresponding increased diffusion requirements), the poor mass transport kinetics for the reference electrolyte significantly impair DSSC operation. Finally, the optimized electrolyte formulation ("A"), allows for unimpeded DSSC operation with no current limitation in the cell's operating range, under even the most demanding light intensity conditions.

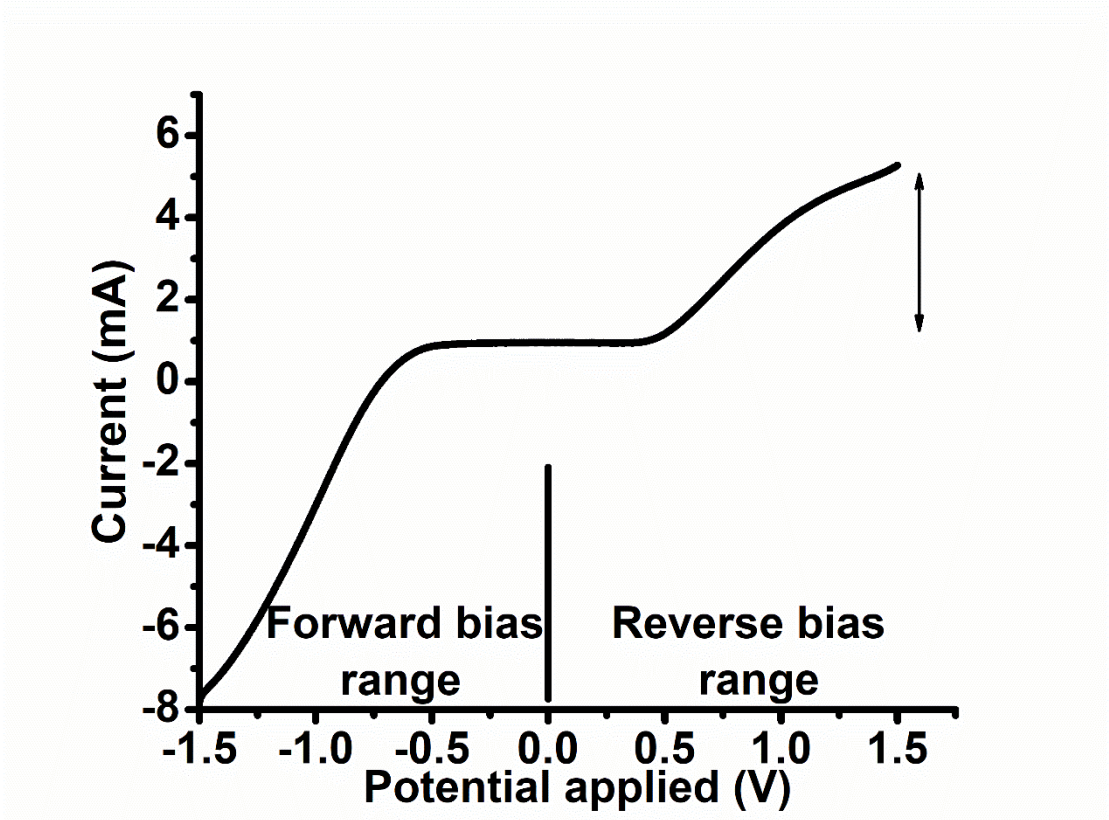

Fig. 2.11 *LSV in forward and reverse voltage bias areas under 1 sun irradiation for the cells using the optimized electrolyte "A". The arrows define the difference between diffusion limited current and short circuit current.*

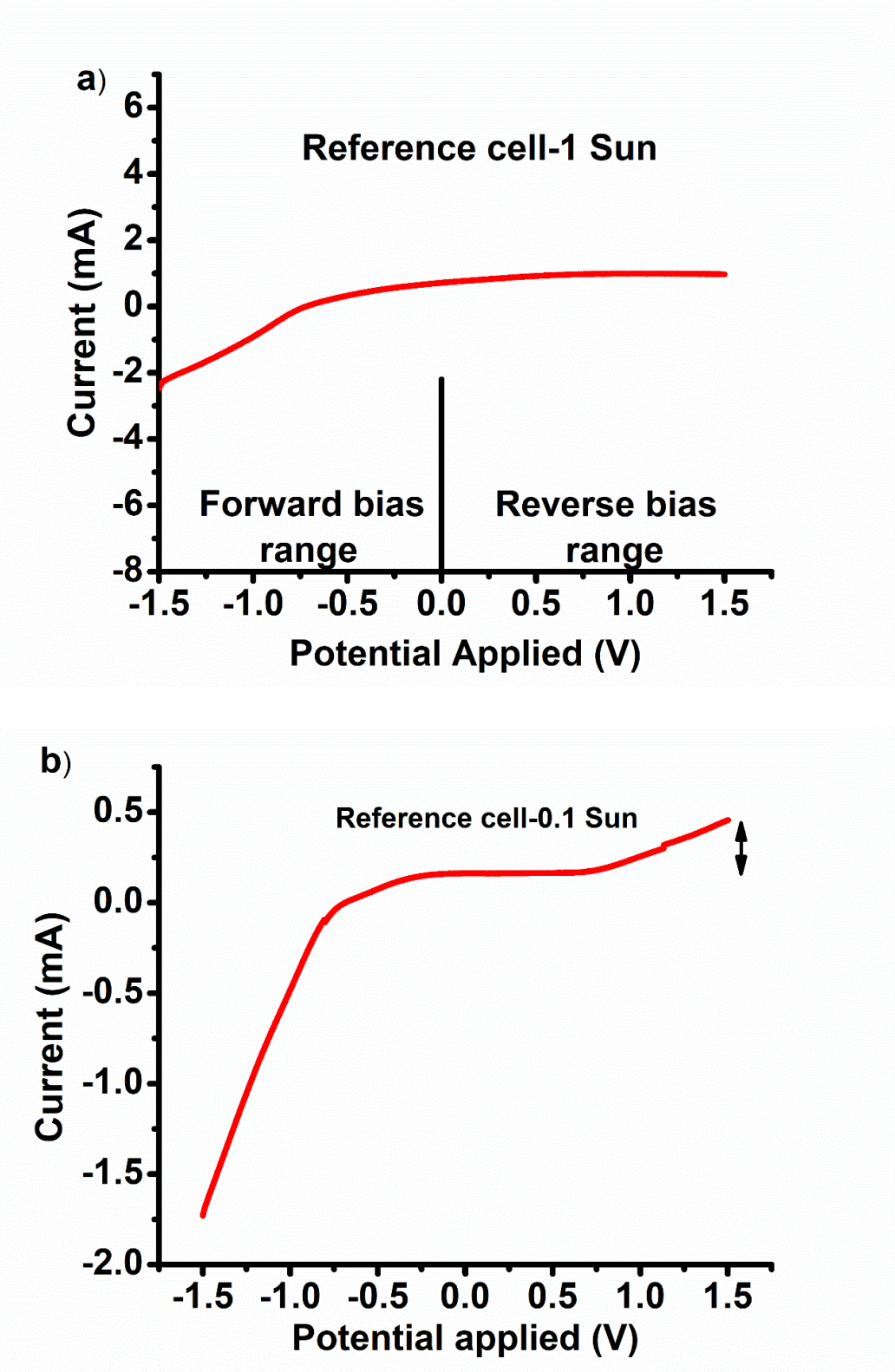

Fig. 2.12 *LSV in forward and reverse voltage bias areas under a) 1sun and b) 0.1 sun irradiation for a cell with the reference electrolyte. The arrows define the difference between diffusion limited current and short circuit current (where it exists).*

In summary, under indoor light a) the transparency of the electrolyte led to almost no competitive absorption (by the electrolyte) near the important 436 nm wavelength (enhanced Jsc), b) the low triiodide content assured adequately low recombination and c) the TBP additive, in good synergy with low I_2 concentrations, enhanced Voc. Under simulated sunlight, the good ion mobility, facilitated by the low solvent viscosity, allowed for sufficient triiodide diffusion (enhanced Jsc), with the low triiodide content and TBP having the same effect on recombination suppression and Voc enhancement in this case as well. Under all conditions, the fill factor of the device remained sufficiently high and its operation was unimpeded. For all the above reasons, the optimized electrolyte "A" allows for similar performance under indoor and low intensity solar lighting, while resulting in greatly superior performance during the much more demanding 1sun operation, in comparison with the literature data.

Bibliographic references for Chapter 2

[1] F. De Rossi, T. Pontecorvo, T.M. Brown, Characterization of photovoltaic devices for indoor light harvesting and customization of flexible dye solar cells to deliver superior efficiency under artificial lighting, Appl. Energy. 156 (2015) 413–422. https://doi.org/10.1016/j.apenergy.2015.07.031.

[2] D. Perganti, A.G. Kontos, T. Stergiopoulos, V. Likodimos, J. Farnell, D. Milliken, H. Desilvestro, P. Falaras, Thermal Stressing of Dye Sensitized Solar Cells Employing Robust Redox Electrolytes, Electrochim. Acta. 179 (2015) 241–249. https://doi.org/10.1016/j.electacta.2015.03.206.

[3] T. Stergiopoulos, E. Rozi, C.S. Karagianni, P. Falaras, Influence of electrolyte co-additives on the performance of dye-sensitized solar cells, Nanoscale Res. Lett. 6:307 (2011). https://doi.org/10.1186/1556-276X-6-307.

[4] T. Stergiopoulos, M. Konstantakou, P. Falaras, Dye solar cells combining a TiO2 surface-blocking organic sensitizer and solvent-free ionic liquid-based redox electrolyte, RSC Adv. 3 (2013) 15014–15021.

https://doi.org/10.1039/c3ra42506a.

[5] G. Konti, G.C. Vougioukalakis, M. Bidikoudi, A.G. Kontos, C. Methenitis, P. Falaras, A Ru(II) molecular antenna bearing a novel bipyridine-acrylonitrile ligand: Synthesis and application in dye solar cells, Polyhedron. 82 (2014) 12–18. https://doi.org/10.1016/j.poly.2014.04.031.

[6] Osram, L 18 W/930 data page, (n.d.). https://www.osram.com/ecat/LUMILUX DE LUXE T8-Fluorescent lamps T8-Fluorescent lamps-Lamps-Digital Systems/com/en/GPS01_1027895/PP_EUROPE_Europe_eCat/ZMP_60463/.

[7] Y. Cao, Y. Liu, S.M. Zakeeruddin, A. Hagfeldt, M. Grätzel, Direct Contact of Selective Charge Extraction Layers Enables High-Efficiency Molecular Photovoltaics, Joule. 2 (2018) 1108–1117. https://doi.org/10.1016/j.joule.2018.03.017.

[8] N. Sridhar, D. Freeman, A study of Dye Sensitized Solar Cells under Indoor and Low Level Outdoor Lighting: Comparison to Organic and Inorganic Thin Film Solar Cells and Methods to Address Maximum Power Point Tracking, Conf. Proc. 26th EU-PVSEC. (2011) 232–236. https://doi.org/10.4229/26thEUPVSEC2011-1CO.10.5.

[9] https://gcell.com, GCell, (n.d.).

[10] K. Izutsu, Electrochemistry in Nonaqueous Solutions, in: 2nd ed., Wiley-VCH, 2009: p. 136.

[11] N. Elgrishi, K.J. Rountree, B.D. McCarthy, E.S. Rountree, T.T. Eisenhart, J.L. Dempsey, A Practical Beginner's Guide to Cyclic Voltammetry, J. Chem. Educ. 95 (2018) 197–206. https://doi.org/10.1021/acs.jchemed.7b00361.

[12] K.R.J. Lovelock, F.N. Cowling, A.W. Taylor, P. Licence, D.A. Walsh, Effect of viscosity on steady-state voltammetry and scanning electrochemical microscopy in room temperature ionic liquids, J. Phys. Chem. B. 114 (2010) 4442–4450. https://doi.org/10.1021/jp912087n.

[13] N. Marinakis, M. Willgert, E.C. Constable, C.E. Housecroft, Optimization of

performance and long-term stability of p-type dye-sensitized solar cells with a cycloruthenated dye through electrolyte solvent tuning, Sustain. Energy Fuels. 1 (2017) 626–635. https://doi.org/10.1039/c7se00060j.

[14] C.L. Bentley, A.M. Bond, A.F. Hollenkamp, P.J. Mahon, J. Zhang, Electrode reaction and mass-transport mechanisms associated with the iodide/triiodide couple in the ionic liquid 1-ethyl-3-methylimidazolium bis(trifluoromethanesulfonyl)imide, J. Phys. Chem. C. 118 (2014) 22439–22449. https://doi.org/10.1021/jp506990e.

[15] W. Kubo, S. Kambe, S. Nakade, T. Kitamura, K. Hanabusa, Y. Wada, S. Yanagida, Photocurrent-determining processes in quasi-solid-state dye-sensitized solar cells using ionic gel electrolytes, J. Phys. Chem. B. 107 (2003) 4374–4381. https://doi.org/10.1021/jp034248x.

[16] M. Zistler, P. Wachter, P. Wasserscheid, D. Gerhard, A. Hinsch, R. Sastrawan, H.J. Gores, Comparison of electrochemical methods for triiodide diffusion coefficient measurements and observation of non-Stokesian diffusion behaviour in binary mixtures of two ionic liquids, Electrochim. Acta. 52 (2006) 161–169. https://doi.org/10.1016/j.electacta.2006.04.050.

[17] Z. Yu, N. Vlachopoulos, M. Gorlov, L. Kloo, Liquid electrolytes for dye-sensitized solar cells, Dalt. Trans. 40 (2011) 10289–10303. https://doi.org/10.1039/c1dt11023c.

[18] A. Hauch, A. Georg, Diffusion in the electrolyte and charge-transfer reaction at the platinum electrode in dye-sensitized solar cells, Electrochim. Acta. (2001) 3457–3466. https://doi.org/10.1016/S0013-4686(01)00540-0.

[19] A. Ejigu, K.R.J. Lovelock, P. Licence, D.A. Walsh, Iodide/triiodide electrochemistry in ionic liquids: Effect of viscosity on mass transport, voltammetry and scanning electrochemical microscopy, Electrochim. Acta. 56 (2011) 10313–10320. https://doi.org/10.1016/j.electacta.2011.03.108.

[20] F. Sauvage, S. Chhor, A. Marchioro, J.E. Moser, M. Graetzel, Butyronitrile-based electrolyte for dye-sensitized solar cells, J. Am. Chem. Soc. 133 (2011)

13103–13109. https://doi.org/10.1021/ja203480w.

[21] A.G. Kontos, T. Stergiopoulos, V. Likodimos, D. Milliken, H. Desilvesto, G. Tulloch, P. Falaras, Long-term thermal stability of liquid dye solar cells, J. Phys. Chem. C. 117 (2013) 8636–8646. https://doi.org/10.1021/jp400060d.

[22] C.D. Elvidge, D.M. Keith, B.T. Tuttle, K.E. Baugh, Spectral identification of lighting type and character, Sensors. 10 (2010) 3961–3988. https://doi.org/10.3390/s100403961.

[23] H. Matsumoto, T. Matsuda, Photoelectrochemical solar cells using ionic liquid as an involatile electrolyte, Electrochemistry. 70 (2002) 190. https://doi.org/10.5796/electrochemistry.70.190.

[24] C.-H. Yang, S.-H. Liao, Hydrothermal Processed TiO 2 Nanoparticles for Optimization in Dye-Sensitized Solar Cells Using Statistical Experimental Strategies , ECS Trans. 19 (2019) 3–20. https://doi.org/10.1149/1.3268158.

[25] E.E. Richman, Requirements for Lighting Levels, (n.d.). http://www.lumitronlighting.com/lighting_nowledge/LUX LEVEL_usace_Requirements for Lighting Levels.pdf.

[26] F. Fabregat-Santiago, G. Garcia-Belmonte, I. Mora-Seró, J. Bisquert, Characterization of nanostructured hybrid and organic solar cells by impedance spectroscopy, Phys. Chem. Chem. Phys. 13 (2011) 9083–9118. https://doi.org/10.1039/c0cp02249g.

[27] S. Mastroianni, I. Asghar, K. Miettunen, J. Halme, A. Lanuti, T.M. Brown, P. Lund, Effect of electrolyte bleaching on the stability and performance of dye solar cells, Phys. Chem. Chem. Phys. 16 (2014) 6092–6100. https://doi.org/10.1039/c3cp55342f.

[28] A.N. Kabanakis, M. Bidikoudi, M.M. Elsenety, G.C. Vougioukalakis, P. Falaras, Synthesis of novel semi-squaraine derivatives and application in efficient dye-sensitized solar cells, Dye. Pigment. 165 (2019) 308–318. https://doi.org/10.1016/j.dyepig.2019.02.028.

[29] M. Grätzel, Perspectives for dye-sensitized nanocrystalline solar cells, Prog. Photovoltaics Res. Appl. 8 (2000) 171–185. https://doi.org/10.1002/(SICI)1099-159X(200001/02)8:1<171::AID-PIP300>3.0.CO;2-U.

[30] A. Listorti, C. Creager, P. Sommeling, J. Kroon, E. Palomares, A. Fornelli, B. Breen, P.R.F. Barnes, J.R. Durrant, C. Law, B. O'Regan, The mechanism behind the beneficial effect of light soaking on injection efficiency and photocurrent in dye sensitized solar cells, Energy Environ. Sci. 4 (2011) 3494–3501. https://doi.org/10.1039/c1ee01443a.

[31] S. Mastroianni, A. Lembo, T.M. Brown, A. Reale, A. Di Carlo, Electrochemistry in reverse biased dye solar cells and dye/electrolyte degradation mechanisms, ChemPhysChem. 13 (2012) 2964–2975. https://doi.org/10.1002/cphc.201200229.

[32] M.I. Asghar, K. Miettunen, S. Mastroianni, J. Halme, H. Vahlman, P. Lund, In situ image processing method to investigate performance and stability of dye solar cells, Sol. Energy. 86 (2012) 331–338. https://doi.org/10.1016/j.solener.2011.10.006.

[33] M. Berginc, U. Opara Krašovec, M. Jankovec, M. Topič, The effect of temperature on the performance of dye-sensitized solar cells based on a propyl-methyl-imidazolium iodide electrolyte, Sol. Energy Mater. Sol. Cells. 91 (2007) 821–828. https://doi.org/10.1016/j.solmat.2007.02.001.

Chapter 3 - Parameter of Sensitizer

3.1 The effects of sensitizers under indoor light operation

As mentioned in the previous chapter, a common trend in indoor focused PV works is the decrease of the 1 sun PCE, the efficiency under simulated solar light, as a side effect of the singularly focused indoor optimization [1]. On the other hand, optimizing the 1 sun performance of PV can detract from indoor performance, thus, leading to either "outdoor" or "indoor" specialized devices and products [2,3]. As an equivalent goal to the single panchromatic dye pursuit [4], this focus is directed at the pursuit of single PV devices that are able to operate efficiently under all possible lighting conditions, no matter how radically different they may be from each other, aka "pan-illumination" devices [5].

The two most significant differences when going from 1 sun conditions to indoor lighting are found in the intensity and spectrum of the incident light [1]. Changes to light intensity and spectrum can also occur for sunlight for natural reasons e.g. weather shifts can lead to diffuse solar light with significant emission spectra differences when compared to direct solar light [6] (e.g. less photons from the infrared region when under diffuse light). Thus, these differences are key in formulating a proper "pan-illumination" optimization strategy. Regarding spectral agreement, a light source's spectrum, the distribution of its emission across wavelengths, is very significant when choosing an indoor operating PV device [7], with an optimum agreement between it and the PV device's absorbance spectrum suggested. While the solar light emission spectrum is broad, typical indoor fluorescent lamps are comprised of separate and distinct emission peaks [8] and, thus, while for 1 sun conditions, a broad visible light absorption spectrum is suggested for an absorber [9], for indoor light, the optimal requirements may be different and more specific.

Due to the radical difference in light intensity between indoor and outdoor light sources (and the smaller number of generated excitons under low intensity light), a crucial parameter for indoor optimization of DSSCs, is recombination [10,11], as the

cost of generated charge loss can be more severe under weak illumination conditions and recombination suppression is critical. Thus, as the next logical step, while using the optimized "pan-illumination" electrolyte presented in the previous chapter, the focus shifts on the effects of sensitizers in a solar cell's absorption spectrum and charge recombination behavior and the combined impact of these properties on the performance under both solar and indoor lighting.

In this chapter, a comparative evaluation of sensitizers in DSSCs under both solar and indoor light is presented. Several dyes with a variety of absorption profiles (spanning the entire visible region), were used in comparative tests performed in DSSCs under illumination from simulated solar light of different intensities (1 sun, 0.1 sun) and from indoor fluorescent light, with focus given on the effects of recombination and spectral agreement on the performance across the different light types and intensities.

3.2 Optical analysis of dyes

Each of the four dyes absorbs strongly within the visible part of the light spectrum but the difference lies in the specific position of their absorption peaks, which is of great importance for indoor light harvesting. Fluorescent lighting is one of the more common light sources for indoor environments [1] and a typical indoor fluorescent lamp's emission spectra is characterized by three main emission lines, with the two more prominent located at ~544 nm and ~611 nm and a significant third one at ~436 nm [6,8,18]. Concerning optical characterization, the dyes' normalized absorption spectra was obtained (for direct qualitive comparison between their absorption profiles), their extinction coefficients at their respective λmax and the absorption spectra of transparent TiO_2 films onto where the dyes have been adsorbed.

The normalized absorption spectra of all dyes (in acetonitrile/tert-butanol 1:1,v:v solutions) in relation to the main emission lines of the fluorescent light source can be seen in Fig. 3.1 and is in good agreement with bibliographic sources [19–22]. The emission spectrum of the fluorescent lamp is also presented (normalized to 0.6, instead of unity, for better visual clarity in the graphs). The respective molar extinction coefficients were calculated (using the calibration curve method [23–25]) and are presented in Table 3.1, with the values also in agreement with past works

[17,22,26,27]. The biggest extinction coefficient belongs to LEG4, more than 3 times the value for N719 (the smallest value), with MK-2 being a close second behind LEG4.

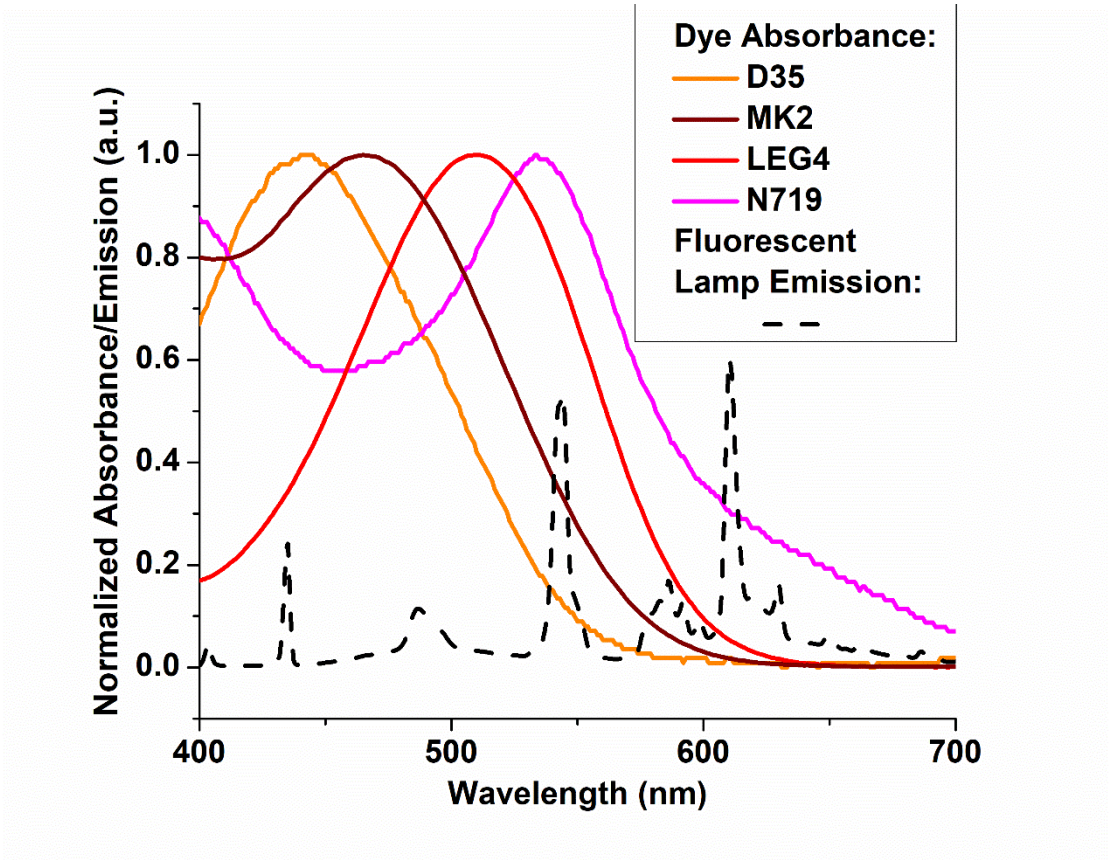

Figure 3.1. Normalized dye absorption spectra (in acetonitrile:tert-butanol 1:1) between 400 and 800 nm. The black dash curve represents the emission spectrum of the fluorescent light source.

Table 3.1 Absorbance maxima and extinction coefficients of different dyes dissolved in an acetonitrile:tertbutanol solvent (1:1)

Sensitizer	λmax (nm)	ε (M^{-1} cm^{-1})
D35	442	34000
MK2	465	39720
LEG4	510	45717
N719	533	13675

When the dyes are adsorbed onto transparent TiO_2 there are slight changes to their absorption profile. The absorption spectra of these dye/TiO_2 combinations, presented in Fig. 3.2, are in good agreement with bibliographic data [28–31]. The absorption peak blue shift of LEG4, when going from being dissolved in a solution to being adsorbed onto a mesoporous TiO_2 surface, has been attributed to the terminal carboxylic group's deprotonation [29]. For D35, it is evident that the spectra, in all cases, has poor coverage of the most important indoor emission wavelengths, only really covering the third emission peak (in order of importance) of the fluorescent lamp. MK-2 has a wider and more red shifted coverage, taking better advantage of the 544 nm peak but coming short on the 611 nm peak. For the LEG4 dye, the displaced spectra, when adsorbed onto TiO_2, renders its absorption profile similar to the one for MK-2. Finally, N719, covers the first two of three peaks sufficiently well.

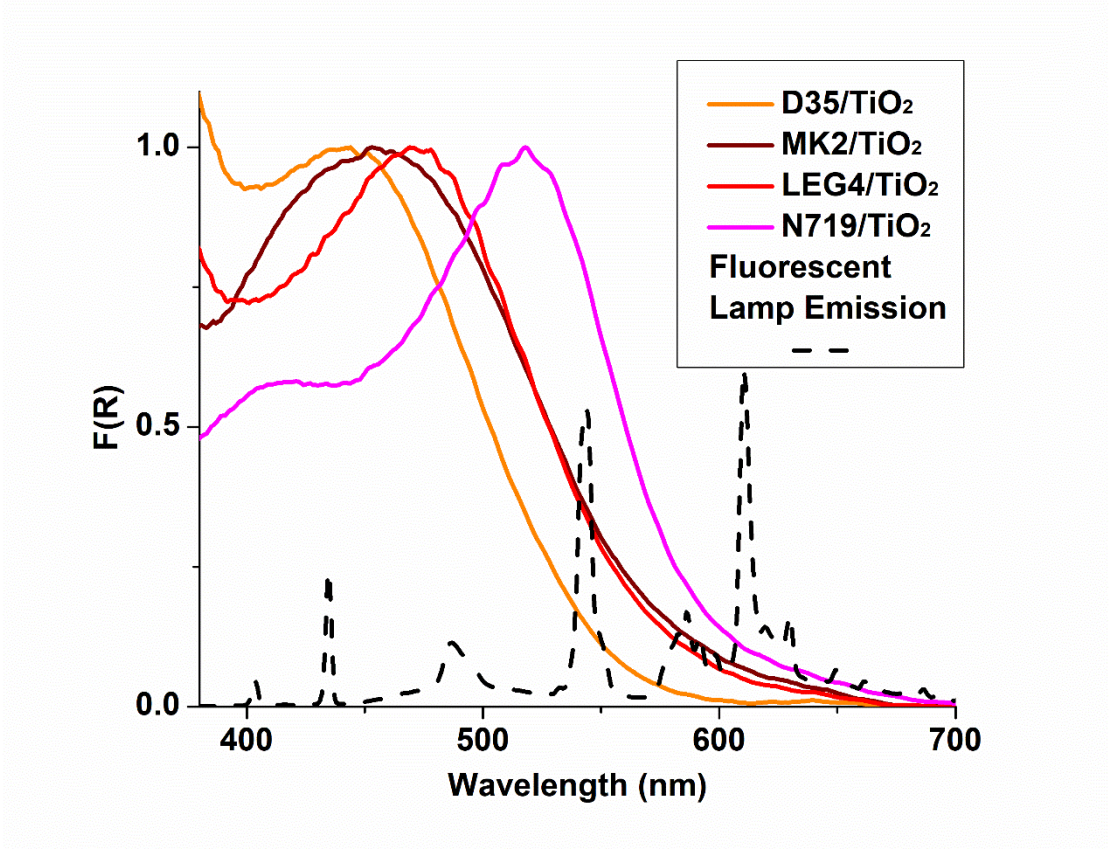

Fig. 3.2 Normalized absorption profile of the dyes adsorbed onto transparent TiO_2 in comparison the indoor fluorescent lamp's emission spectrum (arbitrary units for F(R))

In order to evaluate the light harvesting behavior of the dyes when adsorbed onto a semiconductor, the light harvesting efficiency (LHE) of dye-sensitized TiO_2 films was calculated (Fig. 3.3). It is evident that D35 presents the least appropriate matching with the fluorescent lamp spectrum among the selected dyes, while, again, MK2 has a better coverage and presents a very similar profile with LEG4. The superiority of N719 is evident, as it has the broadest coverage in the visible domain and presents the best match with the lamp emission spectrum.

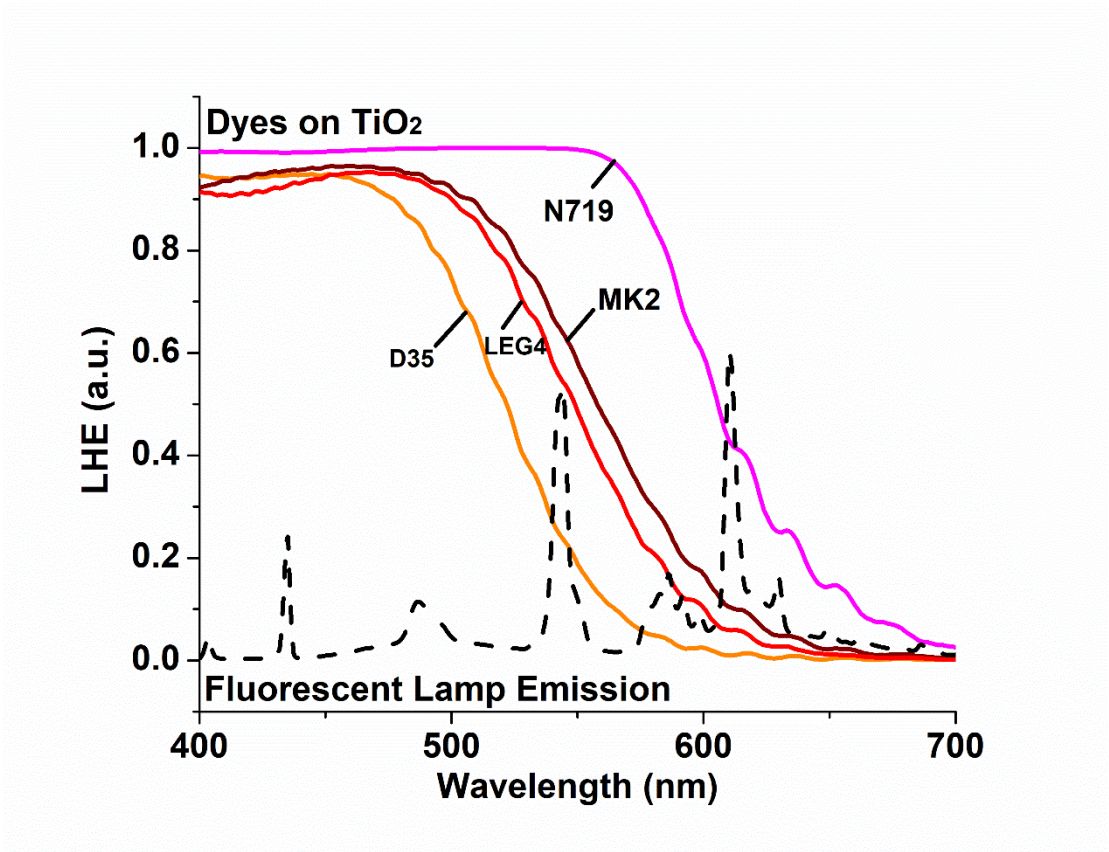

Fig. 3.3 Light harvesting efficiency of dyes adsorbed on TiO_2 films. The dash curve represents the emission spectrum of the fluorescent light source (normalized to 0.6 for visual clarity).

3.3 Photovoltaic performance evaluation

The aforementioned dyes were employed as sensitizers in DSSC operating under 1 sun, 0.1 sun and under 200 lux fluorescent light, in order to evaluate their performance during irradiation from (simulated) solar and indoor fluorescent sources. The J-V curves appear in Fig. 3.4 (a,b,c) and the respective photovoltaic parameters

are presented in Table 3.2. As expected, in all cases (Fig.3.4d), there is an increase in efficiency when going from 1 sun to indoor light conditions [1].

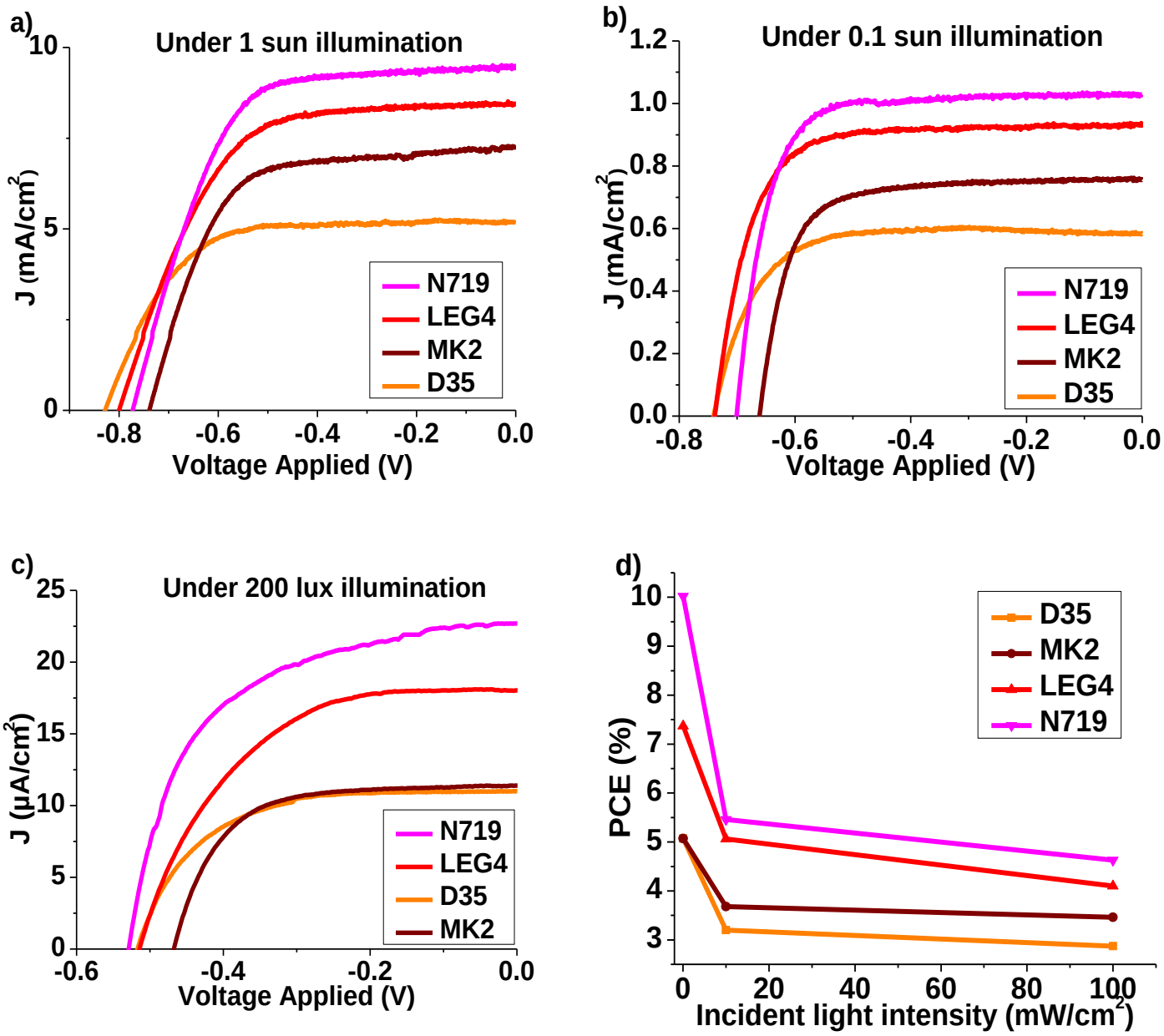

Figure 3.4. JV curves of the DSSCs with different dyes under a) 1 sun, b) 0.1 sun and c) 200 lux of fluorescent light along with d) trends of PCE between different light intensity levels

Table 3.2 Photovoltaic parameters of DSSCs with different dyes, tested under different lighting types and intensities

Dye	1 sun | 0.1 sun | 200lux*				
	Jsc (mA/cm^2)	**Voc (mV)**	**FF (%)**	**Pout$_{max}$ (mW/cm^2)**	**PCE (%)**
D35	5.18|0.58|0.011	830|740|520	66.8|74.6|60.3	2.87|0.32|0.00345	2.87|3.2|5.07
MK2	7.29|0.76|0.0114	740|662|470	64.1|73.4|64.4	3.46|0.368|0.00345	3.46|3.68|5.07
LEG4	8.44|0.93|0.018	800|738|514	60.7|73.7|54.2	4.1|0.506|0.00501	4.1|5.06|7.37
N719	9.5|1.03|0.0227	773|701|526	63.1|75.9|57	4.63|0.546|0.00681	4.63|5.46|10.02

*** (fluorescent lamp)**

A good proportionality for the values of generated current and power output with varying levels of input power, is a mark of a well optimized indoor DSSC [1]. The linearity tests for the generated current density (J_{sc}) and output power (P_{out}) between light intensity levels (Fig. 3.5) presents adjusted R^2 (coefficient of determination, for linear fitting) values over 0.999 for both parameters in all cases, indicating near perfect linearity, as expected due to the use of the well performing "pan-illumination" electrolyte: Regardless of the employed dye, the cells -using the same low I_2 content electrolyte under all tested lighting conditions- show no signs of performance impairment when going from indoor to 1 sun conditions.

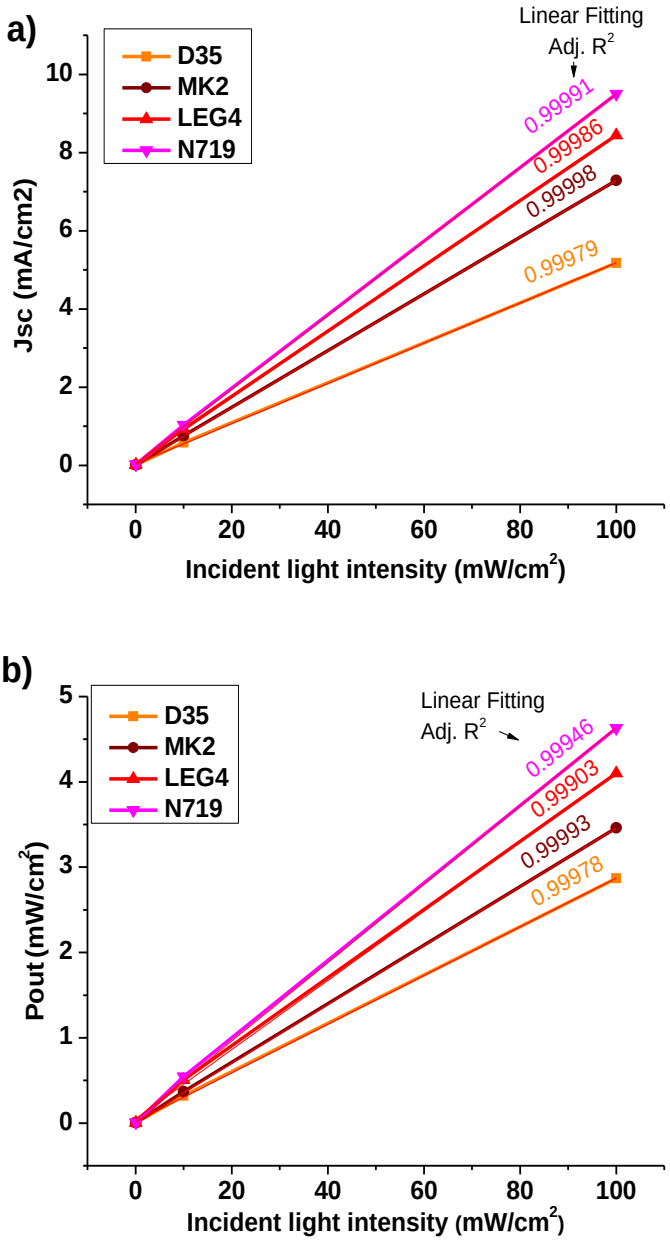

Fig. 3.5 Linearity tests for DSSCs using the tested sensitizers from 200 lux of fluorescent light (61.8μW/cm^2) to 1 sun solar simulated light (100 mW/cm^2), concerning Jsc (a) and Pout (b)

Concerning MK2 and LEG4, though the MK2 showed a slightly wider LHE spectrum than LEG4, it was not enough to overcome the performance of LEG4 under 1 sun and this inferiority is even more pronounced under indoor light, where MK2 performance falls further behind. Under 200 lux fluorescent light, N719 and LEG4 retain their

superior position. Concerning MK2 and D35, an interesting trend takes place when going from 1 sun to 200 lux: When going from higher to lower intensity solar illumination (1 to 0.1 sun), the percentile difference in efficiency and current between D35 and MK2 becomes smaller, as MK2's superiority over D35 starts to decrease, while D35 maintains the highest Voc. Finally, under 200 lux of fluorescent lighting D35 manages to reach MK2's efficiency (Fig. 3.4d). It can be theorized that the observed changes in cell performance when going from 1 sun to indoor light may be attributed to differences in the recombination suppression capability of each dye and this hypothesis will be further build upon in the electrochemical analysis. Thus, in order to elucidate upon the behaviors of the DSSCs under the different lighting conditions the cells were characterized through action spectra (Incident photon to current efficiency-IPCE) and Electrochemical Impedance spectroscopy (EIS)..

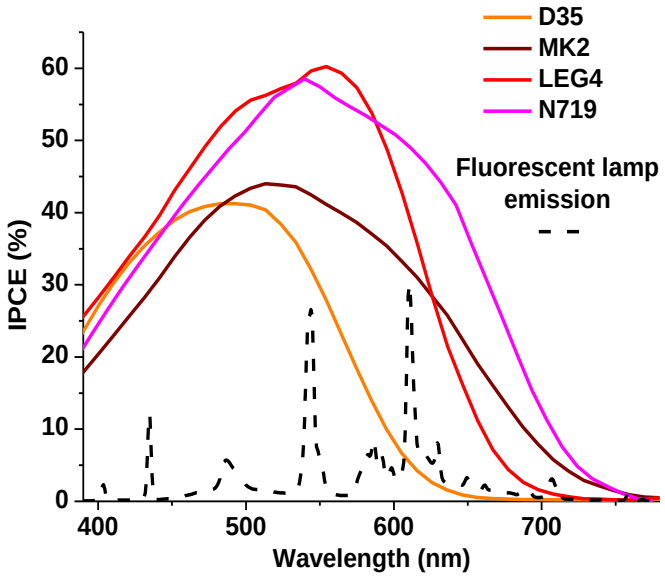

Figure 3.6 IPCE spectra of the tested cells with different sensitizers in comparison to the emission spectrum of the indoor lamp

In Fig. 3.6, the IPCE spectra of the tested DSSCs and the emission spectrum of the fluorescent lamp are presented. Due to the low triiodide concentration [1,32] and the choice of solvents (ACN/BN mixture), the almost transparent color of the tailored electrolyte ensures that no competitive absorption between dyes and electrolyte takes place in the wavelength region bellow 500 nm (a significant emission region for

fluorescent light sources [18]). Thus, more photons are available for capture by the chosen dyes (and more current is produced), which is especially important for the indoor performance of the cells. A well matched IPCE spectrum to the indoor light lamp's emission spectrum is expected for a well performing indoor PV device [1]: The proper choice of dye, along with the minimization of any competitive absorption by the electrolyte, allows for optimal light harvesting from the fluorescent lamp.

The IPCE spectra are in general agreement with the literature [17,30,33]. The values of integrated Jsc (over the whole studied wavelength region), calculated from the IPCE plots, are very similar to the values measured from the 1 sun experiments with differences being under 0.5 mA/cm^2 (Fig.3.7). The N719-cell, has the best coverage of the fluorescent lamp's emission lines. Centered around ~540nm [30], its IPCE maximum is properly placed to take full advantage of the indoor light source's emission, edging out LEG4's coverage at the highest 611 nm emission peak, and validating the superior current under these conditions. Its wider spectrum, also takes better advantage of the 1 sun emission spectrum, explaining the highest Jsc, observed in this case as well and making N719 the most optically fitting DSSC sensitizer for "pan-illumination" purposes, despite its low extinction coefficient. Compared to N719, LEG4's is close behind on the spectral coverage of the indoor and solar emission sources, as well as on its Jsc values. MK2 has a wider spectral coverage compared to LEG4, as seen in the LHE graph, but its IPCE values are lower, making it significantly less efficient in this case. The IPCE analysis characterizes the entirety of a DSSC and not just the light harvesting characteristics of a sensitized photoanode film (as in LHE), which is why there are more factors at play in this evaluation (such as recombination suppression properties). Regarding D35 and MK2, the MK2 spectrum is centered around higher wavelengths then D35 [17,33], and this dye is able to take better advantage of both the solar emission (wider spectrum) and the indoor fluorescent spectrum (better coverage). While the better spectral matching of MK2 can be partly responsible for its higher efficiency under solar irradiation, it is of interest that MK2 and D35 DSSCs have equal efficiency under indoor light. It can be hypothesized that the recombination suppression ability is a critical factor here.

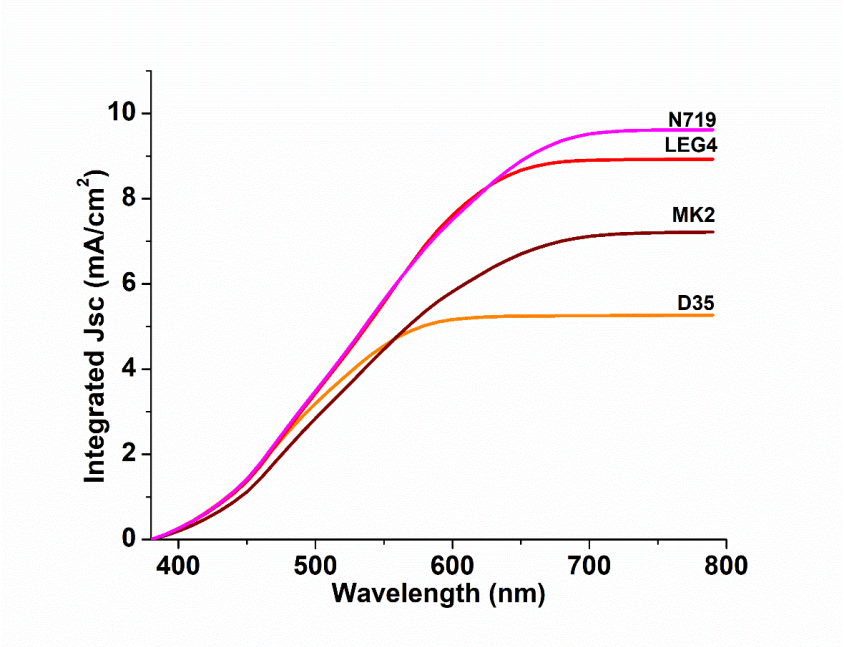

Fig. 3.7 Integrated current of each dye derived from the IPCE analysis

As mentioned before, the suppression of recombination is even more crucial for DSSCs operating under low power light [10], because, due to the smaller amount of photogenerated charge under these conditions, their loss to recombination can be more costly [34]. To elucidate upon the effects of recombination for the tested cells, EIS analysis was performed. The Nyquist spectra and derived resistances are presented in Fig. 3.8 and Table 3.3, respectively. The reason for R_{diff} overlapping with the middle R_{rec} resistance, in Fig 3.8, is the low viscosity of the electrolyte's solvent mixture and the short I^- diffusion length available due to the thin spacer in the cell [27].

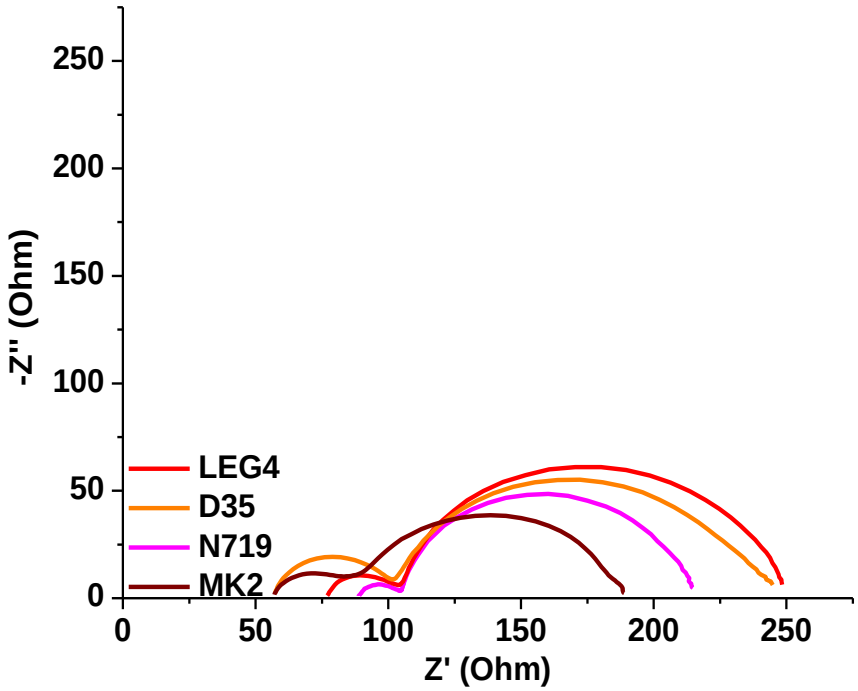

Figure 3.8. Nyquist plots for all tested DSSCs under dark near their Voc

Table 3.3 Derived area-normalized resistance values for the tested DSSCs by the impedance measurements

DSSC dye	Resistances (Ohm*cm^2)		
	Rct	Rrec	Rdif
D35	6.61	13.3	9.32
MK2	3.94	9.04	7.54
LEG4	4.24	12.9	9.45
N719	2.4	11.38	5.84

Though each dye has a significantly different structure, attention has been given in each case, so that can they can all suppress recombination phenomena to a degree with their tailored components and mechanisms. The bulky butoxy chains, in the case of the [D-π-A] structured D35 dye, provide insulation and inhibit {TiO_2-electrolyte} electron recombination [35,36], thus leading to high Voc values [37]. As the donor unit of D35 is largely responsible for its recombination suppression ability, this fragment was retained for its π-linker modified evolution, the LEG4 dye [17]. For the

MK2 dye, suppression of recombination is achieved via the n-hexyl chains (tethered to its thiophene groups) [26]. Finally, in the case of N719-sensitized DCCSs, factors such as the strong dye-TiO_2 binding and the metal-to-ligand charge transfer mechanism have been thought to facilitate electron injection (into TiO_2) at a much greater speed compared to recombination phenomena [38,39]. The highest recombination resistance is found for the D35-based cells, with LEG4 and N719 close behind and with MK2 having a significantly lower value. The lower R_{rec} in the case of MK2, is potentially the cause for the aforementioned relative impairment in the performance of the respective DSSC under indoor light. Though a potential superiority of MK2 over D35 and LEG4 could have been expected under all tested light sources due to MK2's optical characteristics, its apparent performance impairment was likely caused by its increased recombination, especially under low intensity fluorescent light.

Therefore, it can be concluded that there are two significant requirements for a solar cell absorber for both solar and indoor environments. The ideal absorber should exhibit proper spectral overlap of the indoor light source's and the solar source's emission, while offering high recombination resistance. In the cells of this chapter, the sensitizer that presented the best combination of the above factors was N719, with its ideal spectrum overlap and its relatively high R_{rec}.

Bibliographic references for chapter 3

[1] F. De Rossi, T. Pontecorvo, T.M. Brown, Characterization of photovoltaic devices for indoor light harvesting and customization of flexible dye solar cells to deliver superior efficiency under artificial lighting, Appl. Energy. 156 (2015) 413–422. https://doi.org/10.1016/j.apenergy.2015.07.031.

[2] 3GSolar product page, (n.d.). https://www.3gsolar.com/products.

[3] Fujikura, https://www.fujikura.co.uk/products/energy-and-environment/dye-sensitized-solar-cell, (n.d.).

[4] S. Mathew, A. Yella, P. Gao, R. Humphry-Baker, B.F.E. Curchod, N. Ashari-Astani, I. Tavernelli, U. Rothlisberger, M.K. Nazeeruddin, M. Grätzel, Dye-

sensitized solar cells with 13% efficiency achieved through the molecular engineering of porphyrin sensitizers, Nat. Chem. 6 (2014) 242–247. https://doi.org/10.1038/nchem.1861.

[5] G. V. Belessiotis, I. Ibrahim, C.S. Karagianni, P. Falaras, DSSCs for Indoor Environments: From Lab Scale Experiments to Real Life Applications, SVOA Mater. Sci. &Technology. 3 (2020) 01–05.

[6] Y. Cao, Y. Liu, S.M. Zakeeruddin, A. Hagfeldt, M. Grätzel, Direct Contact of Selective Charge Extraction Layers Enables High-Efficiency Molecular Photovoltaics, Joule. 2 (2018) 1108–1117. https://doi.org/10.1016/j.joule.2018.03.017.

[7] N.H. Reich, W. Van Sark, E. a Alsema, S.Y. Kan, S. Silvester, A. Van Der Heide, R.W. Lof, R. Schropp, Weak Light Performance and Spectral Response of Different Solar Cell Types, Proc 20th Eur. Photovolt. Sol. Energy ConfWIP. (2005) 4–7. http://scholar.google.com/scholar?hl=en&btnG=Search&q=intitle:WEAK+LIGHT+PERFORMANCE+AND+SPECTRAL+RESPONSE+OF+DIFFERENT+SOLAR+CELL+TYPES#0.

[8] Osram, L 18 W/930 data page, (n.d.). https://www.osram.com/ecat/LUMILUX DE LUXE T8-Fluorescent lamps T8-Fluorescent lamps-Lamps-Digital Systems/com/en/GPS01_1027895/PP_EUROPE_Europe_eCat/ZMP_60463/.

[9] S. Ito, Investigation of Dyes for Dye-Sensitized Solar Cells: Ruthenium-Complex Dyes, Metal-Free Dyes, Metal-Complex Porphyrin Dyes and Natural Dyes, Sol. Cells - Dye. Devices. (2011). https://doi.org/10.5772/19960.

[10] H. Michaels, M. Rinderle, R. Freitag, I. Benesperi, T. Edvinsson, R. Socher, A. Gagliardi, M. Freitag, Dye-sensitized solar cells under ambient light powering machine learning: Towards autonomous smart sensors for the internet of things, Chem. Sci. 11 (2020) 2895–2906. https://doi.org/10.1039/c9sc06145b.

[11] R. Cheng, C.C. Chung, H. Zhang, F. Liu, W.T. Wang, Z. Zhou, S. Wang, A.B. Djurišić, S.P. Feng, Tailoring Triple-Anion Perovskite Material for Indoor

Light Harvesting with Restrained Halide Segregation and Record High Efficiency Beyond 36%, Adv. Energy Mater. 9 (2019). https://doi.org/10.1002/aenm.201901980.

[12] https://gcell.com, GCell, (n.d.).

[13] A.G. Kontos, T. Stergiopoulos, V. Likodimos, D. Milliken, H. Desilvesto, G. Tulloch, P. Falaras, Long-term thermal stability of liquid dye solar cells, J. Phys. Chem. C. 117 (2013) 8636–8646. https://doi.org/10.1021/jp400060d.

[14] W. Sang-aroon, S. Tontapha, V. Amornkitbamrung, Photovoltaic performance of natural dyes for dye-sensitized solar cells: A combined experimental and theoretical study, Dye. Sol. Cells Math. Model. Mater. Des. Optim. (2019) 203–229. https://doi.org/10.1016/B978-0-12-814541-8.00006-9.

[15] J. Duan, Q. Xiong, H. Wang, J. Zhang, J. Hu, ZnO nanostructures for efficient perovskite solar cells, J. Mater. Sci. Mater. Electron. 28 (2017) 60–66. https://doi.org/10.1007/s10854-016-5492-3.

[16] Q. Wu, J. Hou, H. Zhao, Z. Liu, X. Yue, S. Peng, H. Cao, Charge recombination control for high efficiency CdS/CdSe quantum dot co-sensitized solar cells with multi-ZnS layers, Dalt. Trans. 47 (2018) 2214–2221. https://doi.org/10.1039/c7dt04356b.

[17] E. Gabrielsson, H. Ellis, S. Feldt, H. Tian, G. Boschloo, A. Hagfeldt, L. Sun, Convergent/divergent synthesis of a linker-varied series of dyes for dye-sensitized solar cells based on the D35 donor, Adv. Energy Mater. 3 (2013) 1647–1656. https://doi.org/10.1002/aenm.201300367.

[18] C.D. Elvidge, D.M. Keith, B.T. Tuttle, K.E. Baugh, Spectral identification of lighting type and character, Sensors. 10 (2010) 3961–3988. https://doi.org/10.3390/s100403961.

[19] Y. Li, Y. Lv, Y. Liu, H. Gao, Q. Shi, Y. Li, DFT and TD-DFT investigations of organic dye with different π-spacer used for solar cell, J. Mater. Sci. Mater. Electron. 28 (2017) 9642–9652. https://doi.org/10.1007/s10854-017-6714-z.

[20] N. Koumura, Z.S. Wang, S. Mori, M. Miyashita, E. Suzuki, K. Hara, Alkyl-functionalized organic dyes for efficient molecular photovoltaics, J. Am. Chem. Soc. 128 (2006) 14256–14257. https://doi.org/10.1021/ja0645640.

[21] Y. Li, C. Sun, P. Song, F. Ma, N. Kungwan, M. Sun, Physical insight on mechanism of photoinduced charge transfer in multipolar photoactive molecules, Sci. Rep. 8 (2018). https://doi.org/10.1038/s41598-018-28429-3.

[22] F. De Angelis, S. Fantacci, E. Mosconi, M.K. Nazeeruddin, M. Grätzel, Absorption spectra and excited state energy levels of the N719 dye on TiO2 in dye-sensitized solar cell models, J. Phys. Chem. C. 115 (2011) 8825–8831. https://doi.org/10.1021/jp111949a.

[23] P.J. Holliman, M. Mohsen, A. Connell, M.L. Davies, K. Al-Salihi, M.B. Pitak, G.J. Tizzard, S.J. Coles, R.W. Harrington, W. Clegg, C. Serpa, O.H. Fontes, C. Charbonneau, M.J. Carnie, Ultra-fast co-sensitization and tri-sensitization of dye-sensitized solar cells with N719, SQ1 and triarylamine dyes, J. Mater. Chem. 22 (2012) 13318–13327. https://doi.org/10.1039/c2jm31314f.

[24] R. Katoh, K. Yaguchi, A. Furube, Effect of dye concentration on electron injection efficiency in nanocrystalline TiO2 films sensitized with N719 dye, Chem. Phys. Lett. 511 (2011) 336–339. https://doi.org/10.1016/j.cplett.2011.06.046.

[25] B. O'Regan, L. Xiaoe, T. Ghaddar, Dye adsorption, desorption, and distribution in mesoporous TiO2 films, and its effects on recombination losses in dye sensitized solar cells, Energy Environ. Sci. 5 (2012) 7203–7215. https://doi.org/10.1039/c2ee21341a.

[26] Z.S. Wang, N. Koumura, Y. Cui, M. Takahashi, H. Sekiguchi, A. Mori, T. Kubo, A. Furube, K. Hara, Hexylthiophene-functionalized carbazole dyes for efficient molecular photovoltaics: Tuning of solar-cell performance by structural modification, Chem. Mater. 20 (2008) 3993–4003. https://doi.org/10.1021/cm8003276.

[27] A.N. Kabanakis, M. Bidikoudi, M.M. Elsenety, G.C. Vougioukalakis, P.

Falaras, Synthesis of novel semi-squaraine derivatives and application in efficient dye-sensitized solar cells, Dye. Pigment. 165 (2019) 308–318. https://doi.org/10.1016/j.dyepig.2019.02.028.

[28] Q. Liu, X. Lin, L. Mi, N. Gao, P. Song, F. Ma, Y. Li, Characterizations of efficient charge transfer and photoelectric performance in the cosensitization of solar cells, Appl. Sci. 8 (2018). https://doi.org/10.3390/app8071122.

[29] P. Liu, B. Xu, K.M. Karlsson, J. Zhang, N. Vlachopoulos, G. Boschloo, L. Sun, L. Kloo, The combination of a new organic D-π-A dye with different organic hole-transport materials for efficient solid-state dye-sensitized solar cells, J. Mater. Chem. A. 3 (2015) 4420–4427. https://doi.org/10.1039/c4ta05774k.

[30] F. Matar, T.H. Ghaddar, K. Walley, T. DosSantos, J.R. Durrant, B. O'Regan, A new ruthenium polypyridyl dye, TG6, whose performance in dye-sensitized solar cells is surprisingly close to that of N719, the "dye to beat" for 17 years, J. Mater. Chem. 18 (2008) 4246–4253. https://doi.org/10.1039/b808255c.

[31] R. Katoh, A. Furube, S. Mori, M. Miyashita, K. Sunahara, N. Koumura, K. Hara, Highly stable sensitizer dyes for dye-sensitized solar cells: Role of the oligothiophene moiety, Energy Environ. Sci. 2 (2009) 542–546. https://doi.org/10.1039/b900372j.

[32] W. Kubo, S. Kambe, S. Nakade, T. Kitamura, K. Hanabusa, Y. Wada, S. Yanagida, Photocurrent-determining processes in quasi-solid-state dye-sensitized solar cells using ionic gel electrolytes, J. Phys. Chem. B. 107 (2003) 4374–4381. https://doi.org/10.1021/jp034248x.

[33] K. Hara, Z.S. Wang, Y. Cui, A. Furube, N. Koumura, Long-term stability of organic-dye-sensitized solar cells based on an alkyl-functionalized carbazole dye, Energy Environ. Sci. 2 (2009) 1109–1114. https://doi.org/10.1039/b907486d.

[34] S.S.Y. Juang, P.Y. Lin, Y.C. Lin, Y.S. Chen, P.S. Shen, Y.L. Guo, Y.C. Wu, P. Chen, Energy harvesting under dim-light condition with dye-sensitized and perovskite solar cells, Front. Chem. 7 (2019).

https://doi.org/10.3389/fchem.2019.00209.

[35] D.P. Hagberg, X. Jiang, E. Gabrielsson, M. Linder, T. Marinado, T. Brinck, A. Hagfeldt, L. Sun, Symmetric and unsymmetric donor functionalization. comparing structural and spectral benefits of chromophores for dye-sensitized solar cells, J. Mater. Chem. 19 (2009) 7232–7238. https://doi.org/10.1039/b911397p.

[36] N. Balis, A.A. Zaky, D. Perganti, A. Kaltzoglou, L. Sygellou, F. Katsaros, T. Stergiopoulos, A.G. Kontos, P. Falaras, Dye Sensitization of Titania Compact Layer for Efficient and Stable Perovskite Solar Cells, ACS Appl. Energy Mater. 1 (2018) 6161–6171. https://doi.org/10.1021/acsaem.8b01221.

[37] M.M. Elsenety, A. Stergiou, L. Sygellou, N. Tagmatarchis, N. Balis, P. Falaras, Boosting perovskite nanomorphology and charge transport properties: Via a functional D-π-A organic layer at the absorber/hole transporter interface, Nanoscale. 12 (2020) 15137–15149. https://doi.org/10.1039/d0nr02562c.

[38] C. Bauer, G. Boschloo, E. Mukhtar, A. Hagfeldt, Electron injection and recombination in Ru(dcbpy)2(NCS)2 sensitized nanostructured Zno, J. Phys. Chem. B. 105 (2001) 5585–5588. https://doi.org/10.1021/jp004121x.

[39] Y. Tachibana, J.E. Moser, M. Grätzel, D.R. Klug, J.R. Durrant, Subpicosecond interfacial charge separation in dye-sensitized nanocrystalline titanium dioxide films, J. Phys. Chem. 100 (1996) 20056–20062. https://doi.org/10.1021/jp962227f.

Chapter 4 –Application of Cs_2SnI_6 Perovskite in quasi-solid DSSCs

4.1 Cs_2SnX_6 perovskites

Halide perovskite materials, especially, present extraordinary bulk photovoltaic properties with very high conversion efficiencies when used in Solar Cells [1,2] and at low cost due to the ease of their solution-processing [3]. Besides efficiency, the parameter of stability is equally important for their robust use. This chapter focuses on the structural characteristics of an exceptionally stable perovskite material, the effect of temperature variation on it and its utility in indoor operating DSSCs.

Predominantly, Pb halide perovskites were used for Perovskite Solar Cells (PCSs) providing the highest efficiency and chemical stability. Despite that, concerns on Pb toxicity have directed research community's attention towards robust Sn-based PSCs [4–6]. Divalent tin has been considered as proper alternative to the toxic Pb^{2+}, due to its similar ionic radius and electronic configuration. However, Sn(II) is easily oxidized to Sn(IV) [7], leading to the introduction of defects in the structure [8–10]. Thus, there has been increased interest in the properties of Sn(IV) vacancy-ordered double perovskites (also known as 'defect' perovskites that correspond to the K_2PtCl_6 structure type) [11] and especially, for the fully inorganic Cs_2SnX_6 compounds [11–13]. Hence, while in the case of $CsSnI_3$ the Sn^{2+} ion is not air stable, the Cs_2SnI_6 compound, which is an air-degradation product of $CsSnI_3$ [4,10] presents high oxidation resistance and -experimentally validated- air stability. Along with them it has a ~1.3-1.48 eV direct band gap [13,14], making it a promising material for solar cells -both as hole-transport [15,16] and as light-absorbing material [17,18]- photodetectors [19] and even for water splitting [20]. Due to these prospects, Cs_2SnI_6 has been recently examined for its vibrational and emission properties below room temperature [21]. Similar studies have been performed for the other Cs_2SnX_6 compounds including the mixed halide ones [22], allowing tunable band gaps from 1.3 to 3.9 eV upon halogen substitution from I to Br to Cl [20]. Currently, $CsSnBr_{3-x}I_x$ perovskites are also intensively examined as efficient thermoelectric materials due to their ultralow thermal conductivity [23]. These properties are attributed to scattering

of the heat-carrying phonons by low energy vibrations of the Cs cations with large amplitudes, rendering them interesting for their dynamic structural properties.

In terms of crystal structure, Cs_2SnX_6 perovskites can be thought of as molecular salts and as "0D" materials, as they are composed of discrete ions without an extended network arrangement [16,24]. Their structure [11] is similar to that of $CsSnX_3$, with the removal of every second Sn atom, while the Cs cations are positioned at the interstitials voids (Figure 4.1).

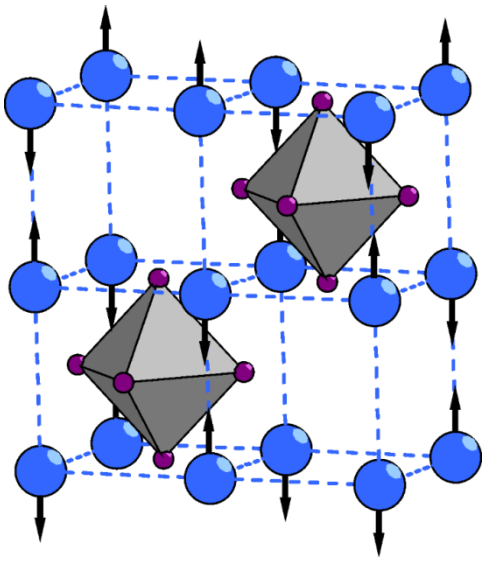

Fig. 4.1 Crystal structure of the defect perovskites Cs_2SnI_6. Sn atoms reside in the grey octahedra formed by I atoms (purple) and Cs atoms (blue) occupy the interstitial sites. The Raman-active Cs vibrations in the rigid $[SnI_6]$ lattice are indicated with black arrows.

All Cs_2SnX_6 compounds crystallize in the FCC phase at room temperature with no experimental evidence for any temperature induced phase transitions. Raman spectroscopy [25], a cornerstone of material characterization [26–28], is a sensitive probe of temperature effects on the structure and the dynamic disorder of perovskites [29], via the analysis of their vibrational modes [30,31]. In this chapter, Raman spectroscopy is applied to analyze the effects of temperature variation on the Cs_2SnI_6 compound and the potential of this air-stable perovskite in indoor operated DSSCs is evaluated, with a quasi-solid alternative to the previously proposed electrolyte formulation is presented.

4.2 Perovskite synthesis and characterization methods

4.2.1 Synthesis

The Cs_2SnI_6 material has been prepared according to bibliographic sources [16]: Briefly, SnI_4 and CsI were first mixed together in 1:2 molar ratio and then loaded into fused silica tubes under vacuum and annealed at 400 °C for 5 hours and then at 200 °C for 5 days before cooling slowly to room temperature. The compound is an air-stable polycrystalline material, having a distinct black color. It has been characterized by powder X-ray diffraction at room temperature, presenting the cubic symmetry (space group $Fm\bar{3}m$) [16].

4.2.2 Temperature dependent Raman measurements

The material's vibrational properties were investigated by micro-Raman spectroscopy using a Renishaw inVia Reflex microscope with a high power near-infrared (NIR) diode laser (λ = 785 nm) as excitation source. Temperature dependent Raman measurements were implemented inside a sealed THMS600PS Linkam temperature cell (heating−freezing stage) with optical windows allowing the recording of variable-temperature data. A 50x magnification lens with a focal distance of 8 mm was used for focusing the laser beam onto the samples. The scattered beam was filtered at 30 cm^{-1} with a double Rayleigh dielectric filter and analyzed through the 250-mm-focal length spectrometer, a 1200 lines/mm diffraction grating and a high-sensitivity CCD detector. An internal Si reference was used for frequency shift calibration. Raman spectra were fitted with multiple mixed Lorenzian-Gaussian curves via Wire software.

4.3 Temperature-variant Raman investigation of Cs_2SnI_6-type perovskites

Indicative Raman spectra of Cs_2SnI_6 acquired between -20 and 100°C and normalized to unity are shown in *Fig. 4.2*. Initially, the room temperature spectra (*Table 4.1*) were

used to identify the main Raman active vibrational modes of the compound in relation to refs. [16,32].

Table 4.1. Raman active modes for Cs_2SnI_6 at room temperature-ν(RT)

	ν (RT) (cm^{-1})	**Mode**
Cs_2SnI_6	40.1	ν^L (F_{2g})
	76.2	δ (F_{2g})
	89	ν (E_g)
	123.5	ν (A_{1g})
	-	ν (A_{1g})+δ (F_{2g})+ν^L (F_{2g})
	242.5	2ν (A_{1g})
	-	2ν (E_g)+δ (F_{2g})
	-	2ν (A_{1g})+δ (F_{2g})
	-	2ν (A_{1g})+ν (E_g)
	-	3ν (A_{1g})

Four 1st order Raman bands were observed, whereas three of them are related to vibrations inside SnX_6 octahedra: the -singly degenerate- ν (A_{1g}) due to the Sn-X symmetric stretching, the -doubly degenerate- ν (E_g) due to the Sn-X asymmetric stretching and the -triply degenerate- δ (F_{2g}) due to the X-Sn-X asymmetric bending. The lowest frequency Raman band is the -triply degenerate- ν^L(F_{2g}) lattice mode, involving vibrations of the Cs atoms in the rigid [SnX_6] lattice. In all cases, the vibrational frequencies vary in the following order: ν^L (F_{2g})<δ (F_{2g})<ν (E_g)<ν (A_{1g}) with the ν (A_{1g}) mode being the strongest amongst them. The ν^L (F_{2g}) peak was observed only above room temperature, at ~40 cm^{-1}. Furthermore, the compound, which was examined under resonance conditions (E_{gap}=1.3-1.48 eV<$E_{excitation}$=1.6 eV), exhibited the 2ν(A_{1g}) 2nd order mode, at around 250 cm^{-1}, clearly present at all temperatures. It is noteworthy that no sign of significant re-structuring or of a phase transformation for was observed across the examined temperature range. This is in accordance with the synchrotron powder X-ray diffraction study [33] and the vibrational spectroscopy study in [21].

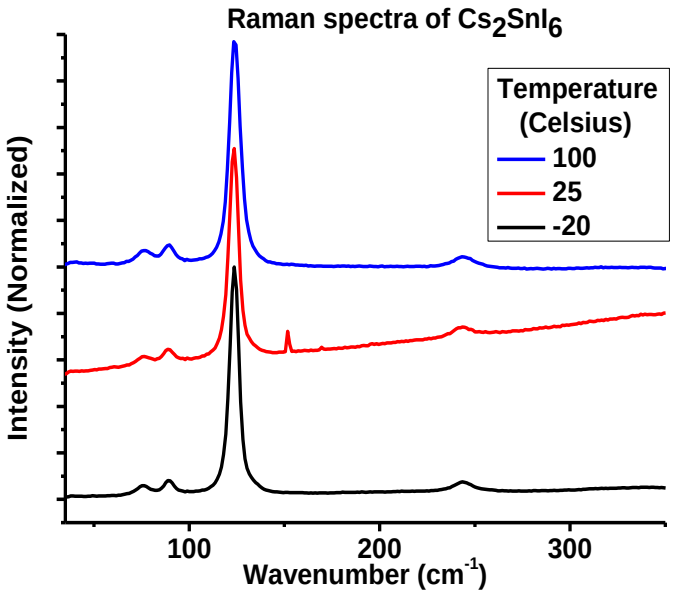

Fig. 4.2 Characteristic Raman spectra of Cs_2SnI_6 at various temperatures.

For the characteristic peak positions, a normal anharmonic behavior is observed with increase of the frequency with decreasing temperature due to hardening of the bonds by lattice contraction. Due to the small size of the Cs cation relative to the size of the cavity formed by the neighboring iodine anions, the Cs-SnI_6 interaction is weak and obstructs the ν^L (F_{2g}) phonon mode from appearing at low temperatures. However, it is possible that the anharmonic lattice dynamics in combination with the increased amplitude and energy of Cs-SnI_6 oscillation upon increasing the temperature induce a Raman cross section increase through a more efficient modulation of the polarizability, [(da/dQ)], by this specific "lattice mode". This leads to a clear appearance of this initially weak band in Cs_2SnI_6 at high temperatures. It is important to note that scattering by anharmonic optical phonons regulates the charge-carrier mobilities via electron-phonon coupling and consequently affects drastically the material's optoelectronic properties [34]. Moreover, very recently, the thermoelectric properties of Cs_2SnI_6 have been predicted by theoretical calculations [35] and experimental studies show a high dependence of the Seebeck coefficient of bulk materials on the presence of dopants, such as Sn^{2+} [36]. In this context, the low frequency Cs lattice vibrations under dynamic structural anharmonicity may strongly reduce the lattice contribution to the thermal conductivity of the compound. Thus Cs_2SnI_6, in addition to its use in optoelectronic devices such as solar cells and light

emitting diodes, may be an interesting candidate for thermoelectric applications, too [37].

4.3.1 Cs_2SnI_6-based electrolyte for quasi-solid indoor DSSCs

Perovksites can also be used as an efficient hole transport materials (HTMs) for solar cells. One of the key factors that limits the durability of electrolytes (including HTMs) in DSSCs is their chemical and physical stability. Even small structural changes at the interfaces of DSSCs can significantly affect their electrochemical characteristics. As discussed above, the stability of the Cs_2SnI_6 is evident. This non-toxic and lead-free analogue, in particular, has been considered promising for large-scale DSSC fabrication due to its oxygen/moisture stability (owing to tin's high oxidation state, Sn^{4+}). A Z907-DSSC with Cs_2SnI_6 as an HTM has been characterized under 1 sun exhibiting a 4.23% PCE, with further stability tests showing a constant PCE after storage (at room temperature, in the dark) [38,39].

To formulate the quasi-solid (gel-like) electrolyte solution [38] , TBP is added to a mixture of Cs_2SnI_6 (50 mg) and DMF (1 ml) at room temperature (1:26 μL/mg TBP:Cs_2SnI_6). Then 37.5 μL of a Li-TFSI/acetonitrile (170 mg/1 ml) solution are added. The final perovskite solution is deposited (dropwise) to a Z907-sensitized photoanode, which is, then, left to dry out in the atmosphere (Image 8). The Pt counter electrode also receives a drop of the perovskite solution and, after drying, the DSSC is put together.

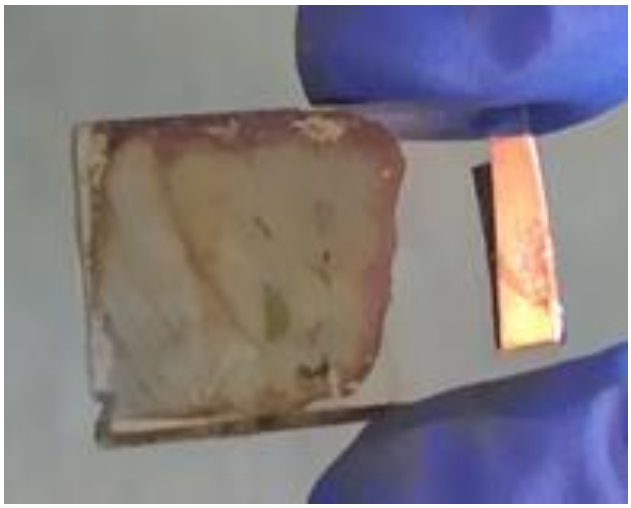

Image 8. The dried out (gel-like) Cs_2SnI_6-based electrolyte on top of the photoanode of the DSSC

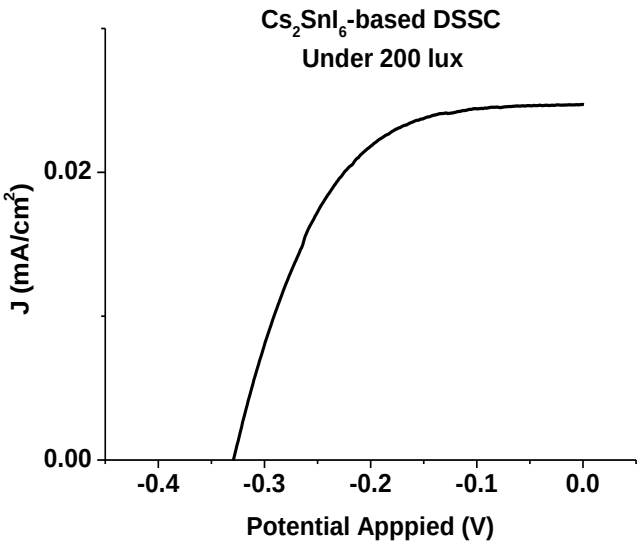

Fig. 4.3 JV curve of quasi-solid Cs_2SnI_6-based DSSC under 200 lux of indoor light

This quasi-solid Cs_2SnI_6-based DSSC was characterized under 200 lux of indoor light (Fig. 4.3), exhibiting a PCE of 7.28% (Jsc=24.7 μA/cm^2, Voc=330 mV, FF=55.2%). With a PCE=4.23% under 1 sun and a PCE=7.28% under 200 lux, it is obvious that the efficiency of this DSSC was lower than the champion panillumination DSSC of the previous chapters. However, evaporation/drying of the electrolyte in their cases would significantly impair the cell operation. Thus, what the Cs_2SnI_6-based DSSC lacks in efficiency, it makes up in stability due to its gel-like electrolyte. It can be concluded that each configuration holds its own advantages, whether a higher efficiency or a higher stability.

Bibliographic references for Chapter 4

[1] B. Chen, S.W. Baek, Y. Hou, E. Aydin, M. De Bastiani, B. Scheffel, A. Proppe, Z. Huang, M. Wei, Y.K. Wang, E.H. Jung, T.G. Allen, E. Van Kerschaver, F.P. García de Arquer, M.I. Saidaminov, S. Hoogland, S. De Wolf, E.H. Sargent, Enhanced optical path and electron diffusion length enable high-efficiency perovskite tandems, Nat. Commun. 11 (2020) 1257. https://doi.org/10.1038/s41467-020-15077-3.

[2] J.W. Lim, H. Kwon, S.H. Kim, Y.J. You, J.S. Goo, D.H. Ko, H.J. Lee, D. Kim, I. Chung, T.G. Kim, D.H. Kim, J.W. Shim, Unprecedentedly high indoor performance (efficiency > 34 %) of perovskite photovoltaics with controlled bromine doping, Nano Energy. 75 (2020) 104984. https://doi.org/10.1016/j.nanoen.2020.104984.

[3] A.G. Kontos, A. Kaltzoglou, E. Siranidi, D. Palles, G.K. Angeli, M.K. Arfanis, V. Psycharis, Y.S. Raptis, E.I. Kamitsos, P.N. Trikalitis, C.C. Stoumpos, M.G. Kanatzidis, P. Falaras, Structural Stability, Vibrational Properties, and Photoluminescence in CsSnI3 Perovskite upon the Addition of SnF2, Inorg. Chem. 56 (2017) 84–91. https://doi.org/10.1021/acs.inorgchem.6b02318.

[4] W. Ke, C.C. Stoumpos, M.G. Kanatzidis, "Unleaded" Perovskites: Status Quo and Future Prospects of Tin-Based Perovskite Solar Cells, Adv. Mater. 31 (2019) 1803230. https://doi.org/10.1002/adma.201803230.

[5] M.H. Kumar, S. Dharani, W.L. Leong, P.P. Boix, R.R. Prabhakar, T. Baikie, C. Shi, H. Ding, R. Ramesh, M. Asta, M. Graetzel, S.G. Mhaisalkar, N. Mathews, Lead-free halide perovskite solar cells with high photocurrents realized through vacancy modulation, Adv. Mater. 26 (2014) 7122–7127. https://doi.org/10.1002/adma.201401991.

[6] C.C. Stoumpos, C.D. Malliakas, M.G. Kanatzidis, Semiconducting tin and lead iodide perovskites with organic cations: Phase transitions, high mobilities, and near-infrared photoluminescent properties, Inorg. Chem. 52 (2013) 9019–9038. https://doi.org/10.1021/ic401215x.

[7] A.G. Kontos, A. Kaltzoglou, M.K. Arfanis, K.M. McCall, C.C. Stoumpos, B.W. Wessels, P. Falaras, M.G. Kanatzidis, Dynamic Disorder, Band Gap Widening, and Persistent Near-IR Photoluminescence up to at Least 523 K in ASnI3 Perovskites (A = Cs+, CH3NH3+ and NH2-CHNH2+), J. Phys. Chem. C. 122 (2018) 26353–26361. https://doi.org/10.1021/acs.jpcc.8b10218.

[8] T. Bin Song, T. Yokoyama, C.C. Stoumpos, J. Logsdon, D.H. Cao, M.R. Wasielewski, S. Aramaki, M.G. Kanatzidis, Importance of reducing vapor atmosphere in the fabrication of Tin-based perovskite solar cells, J. Am. Chem.

Soc. 139 (2017) 836–842. https://doi.org/10.1021/jacs.6b10734.

[9] Y. Takahashi, R. Obara, Z.Z. Lin, Y. Takahashi, T. Naito, T. Inabe, S. Ishibashi, K. Terakura, Charge-transport in tin-iodide perovskite CH3NH 3SnI3: Origin of high conductivity, Dalt. Trans. 40 (2011) 5563–5568. https://doi.org/10.1039/c0dt01601b.

[10] L. Dimesso, C. Das, M. Stöhr, T. Mayer, W. Jaegermann, Properties of cesium tin iodide (Cs-Sn-I) systems after annealing under different atmospheres, Mater. Chem. Phys. 197 (2017) 27–35. https://doi.org/10.1016/j.matchemphys.2017.05.018.

[11] Y. El Ajjouri, F. Locardi, M.C. Gélvez-Rueda, M. Prato, M. Sessolo, M. Ferretti, F.C. Grozema, F. Palazon, H.J. Bolink, Mechanochemical Synthesis of Sn(II) and Sn(IV) Iodide Perovskites and Study of Their Structural, Chemical, Thermal, Optical, and Electrical Properties, Energy Technol. 8 (2020) 1900788. https://doi.org/10.1002/ente.201900788.

[12] M. Krishnaiah, M.M.I. Khan, A. Kumar, S.H. Jin, Impact of CsI concentration, relative humidity, and annealing temperature on lead-free Cs2SnI6 perovskites: Toward visible light photodetectors application, Mater. Lett. 269 (2020) 127675. https://doi.org/10.1016/j.matlet.2020.127675.

[13] X. Nairui, T. Yehua, Q. Yali, L. Duoduo, W. Ke-Fan, One-step solution synthesis and stability study of inorganic perovskite semiconductor Cs2SnI6, Sol. Energy. 204 (2020) 429–439. https://doi.org/10.1016/j.solener.2020.04.079.

[14] X. Qiu, B. Cao, S. Yuan, X. Chen, Z. Qiu, Y. Jiang, Q. Ye, H. Wang, H. Zeng, J. Liu, M.G. Kanatzidis, From unstable CsSnI3 to air-stable Cs2SnI6: A lead-free perovskite solar cell light absorber with bandgap of 1.48 eV and high absorption coefficient, Sol. Energy Mater. Sol. Cells. 159 (2017) 227–234. https://doi.org/10.1016/j.solmat.2016.09.022.

[15] H.O. Shin, B.M. Kim, T. Jang, K.M. Kim, D.H. Roh, J.S. Nam, J.S. Kim, U.Y. Kim, B. Lee, Y. Pang, T.H. Kwon, Surface State-Mediated Charge Transfer of

Cs2SnI6 and Its Application in Dye-Sensitized Solar Cells, Adv. Energy Mater. 9 (2019) 1803243. https://doi.org/10.1002/aenm.201803243.

[16] A. Kaltzoglou, M. Antoniadou, A.G. Kontos, C.C. Stoumpos, D. Perganti, E. Siranidi, V. Raptis, K. Trohidou, V. Psycharis, M.G. Kanatzidis, P. Falaras, Optical-Vibrational Properties of the Cs2SnX6 (X = Cl, Br, I) Defect Perovskites and Hole-Transport Efficiency in Dye-Sensitized Solar Cells, J. Phys. Chem. C. 120 (2016) 11777–11785. https://doi.org/10.1021/acs.jpcc.6b02175.

[17] S. Ullah, J. Wang, M.H. Alvi, R. Chang, P. Yang, L. Liu, S.E. Yang, T. Xia, H. Guo, Y. Chen, Fabrication and characterization of lead-free Cs2SnI6 perovskite films for photovoltaic applications, Int. J. Energy Res. 45 (2021) 1720–1728. https://doi.org/10.1002/er.5838.

[18] B. Lee, Y. Ezhumalai, W. Lee, M.C. Chen, C.Y. Yeh, T.J. Marks, R.P.H. Chang, Cs2SnI6-Encapsulated Multidye-Sensitized All-Solid-State Solar Cells, ACS Appl. Mater. Interfaces. 11 (2019) 21424–21434. https://doi.org/10.1021/acsami.8b19778.

[19] D. Shao, W. Zhu, G. Xin, X. Liu, T. Wang, S. Shi, J. Lian, S. Sawyer, A high performance UV-visible dual-band photodetector based on an inorganic Cs2SnI6 perovskite/ZnO heterojunction structure, J. Mater. Chem. C. 8 (2020) 1819–1825. https://doi.org/10.1039/c9tc05940g.

[20] T.C. Dang, H.C. Le, D.L. Pham, S.H. Nguyen, T.T.O. Nguyen, T.T. Nguyen, T.D. Nguyen, Synthesis of perovskite Cs2SnI6 film via the solution processed approach: First study on the photoelectrochemical water splitting application, J. Alloys Compd. 805 (2019) 847–851. https://doi.org/10.1016/j.jallcom.2019.07.122.

[21] R. Luo, S. Zhang, S. Zhao, J. Li, F. Kang, K. Yu, G. Wei, Ultrasmall Blueshift of Near-Infrared Fluorescence in Phase-Stable Cs2Sn I6 Thin Films, Phys. Rev. Appl. 14 (2020) 014048. https://doi.org/10.1103/PhysRevApplied.14.014048.

[22] A. Kaltzoglou, M. Antoniadou, D. Perganti, E. Siranidi, V. Raptis, K. Trohidou, V. Psycharis, A.G. Kontos, P. Falaras, Mixed-halide Cs2SnI3Br3 perovskite as low resistance hole-transporting material in dye-sensitized solar cells, Electrochim. Acta. 184 (2015) 466–474. https://doi.org/10.1016/j.electacta.2015.10.030.

[23] H. Xie, S. Hao, J. Bao, T.J. Slade, G.J. Snyder, C. Wolverton, M.G. Kanatzidis, All-Inorganic Halide Perovskites as Potential Thermoelectric Materials: Dynamic Cation off-Centering Induces Ultralow Thermal Conductivity, J. Am. Chem. Soc. 142 (2020) 9553–9563. https://doi.org/10.1021/jacs.0c03427.

[24] M.M. Elsenety, A. Kaltzoglou, M. Antoniadou, I. Koutselas, A.G. Kontos, P. Falaras, Synthesis, characterization and use of highly stable trimethyl sulfonium tin(IV) halide defect perovskites in dye sensitized solar cells, Polyhedron. 150 (2018) 83–91. https://doi.org/10.1016/j.poly.2018.05.001.

[25] E. Smith, G. Dent, Modern Raman Spectroscopy - A Practical Approach, 2005. https://doi.org/10.1002/0470011831.

[26] M. Ledinský, P. Löper, B. Niesen, J. Holovský, S.J. Moon, J.H. Yum, S. De Wolf, A. Fejfar, C. Ballif, Raman spectroscopy of organic-inorganic halide perovskites, J. Phys. Chem. Lett. 6 (2015) 401–406. https://doi.org/10.1021/jz5026323.

[27] L.M. Malard, M.A. Pimenta, G. Dresselhaus, M.S. Dresselhaus, Raman spectroscopy in graphene, Phys. Rep. 473 (2009) 51–87. https://doi.org/10.1016/j.physrep.2009.02.003.

[28] I. Ibrahim, G. Belessiotis, M. Arfanis, C. Athanasekou, A. Philippopoulos, C. Mitsopoulou, G. Romanos, P. Falaras, Surfactant Effects on the Synthesis of Redox Bifunctional V2O5 Photocatalysts, Materials (Basel). 13 (2020) 4665. https://doi.org/10.3390/ma13204665.

[29] A.G. Kontos, G.K. Manolis, A. Kaltzoglou, D. Palles, E.I. Kamitsos, M.G. Kanatzidis, P. Falaras, Halogen-NH2+ Interaction, Temperature-Induced Phase Transition, and Ordering in (NH2CHNH2)PbX3 (X = Cl, Br, I) Hybrid

Perovskites, J. Phys. Chem. C. 124 (2020) 8479–8487. https://doi.org/10.1021/acs.jpcc.9b11334.

[30] M. Udagawa, T. Hasegawa, Y. Takasu, N. Ogita, K. Suekuni, M.A. Avila, T. Takabatake, Y. Ishikawa, N. Takeda, Y. Nemoto, T. Goto, H. Sugawara, D. Kikuchi, H. Sato, C. Sekine, I. Shirotani, J.I. Yamaura, Y. Nagao, Z. Hiroi, Guest ion motion in cage structure crystals investigated by Raman scattering, J. Phys. Soc. Japan. 77 (2008) 142–147. https://doi.org/10.1143/JPSJS.77SA.142.

[31] S. Christensen, L. Bjerg, A. Kaltzoglou, F. Juranyi, T. Fässler, T. Unruh, M. Christensen, Guest host interaction and low energy host structure dynamics in tin clathrates, J. Appl. Phys. 113 (2013) 084902. https://doi.org/10.1063/1.4793081.

[32] G. Bounos, M. Karnachoriti, A.G. Kontos, C.C. Stoumpos, L. Tsetseris, A. Kaltzoglou, X. Guo, X. Lü, Y.S. Raptis, M.G. Kanatzidis, P. Falaras, Defect Perovskites under Pressure: Structural Evolution of Cs2SnX6 (X = Cl, Br, I), J. Phys. Chem. C. 122 (2018) 24004–24013. https://doi.org/10.1021/acs.jpcc.8b08449.

[33] A.E. Maughan, A.M. Ganose, M.A. Almaker, D.O. Scanlon, J.R. Neilson, Tolerance Factor and Cooperative Tilting Effects in Vacancy-Ordered Double Perovskite Halides, Chem. Mater. 30 (2018) 3909–3919. https://doi.org/10.1021/acs.chemmater.8b01549.

[34] A.C. Ferreira, S. Paofai, A. Létoublon, J. Ollivier, S. Raymond, B. Hehlen, B. Rufflé, S. Cordier, C. Katan, J. Even, P. Bourges, Direct evidence of weakly dispersed and strongly anharmonic optical phonons in hybrid perovskites, Commun. Phys. 3 (2020) 48. https://doi.org/10.1038/s42005-020-0313-7.

[35] M. Huma, M. Rashid, Q. Mahmood, E. Algrafy, N.A. Kattan, A. Laref, A.S. Bhatti, Physical properties of lead-free double perovskites A2SnI6 (A= Cs, Rb) using ab-initio calculations for solar cell applications, Mater. Sci. Semicond. Process. 121 (2021) 105313. https://doi.org/10.1016/j.mssp.2020.105313.

[36] B. Lee, C.C. Stoumpos, N. Zhou, F. Hao, C. Malliakas, C.Y. Yeh, T.J. Marks,

M.G. Kanatzidis, R.P.H. Chang, Air-stable molecular semiconducting iodosalts for solar cell applications: Cs2SnI6 as a hole conductor, J. Am. Chem. Soc. 136 (2014) 15379–15385. https://doi.org/10.1021/ja508464w.

[37] G. V. Belessiotis, M.K. Arfanis, A. Kaltzoglou, V. Likodimos, Y.S. Raptis, P. Falaras, A.G. Kontos, Temperature dependence of the vibrational and emission spectra in the 0D vacancy-ordered Cs2SnI6 perovskite, Mater. Today Proc. (2022). https://doi.org/10.1016/j.matpr.2022.07.260.

[38] A. Kaltzoglou, M. Antoniadou, A.G. Kontos, C.C. Stoumpos, D. Perganti, E. Siranidi, V. Raptis, K. Trohidou, V. Psycharis, M.G. Kanatzidis, P. Falaras, Optical-Vibrational Properties of the Cs 2 SnX 6 (X = Cl, Br, I) Defect Perovskites and Hole-Transport Efficiency in Dye-Sensitized Solar Cells, J. Phys. Chem. C. 120 (2016) 11777–11785. https://doi.org/10.1021/acs.jpcc.6b02175.

[39] A. Kaltzoglou, D. Perganti, M. Antoniadou, A.G. Kontos, P. Falaras, Stress Tests on Dye-sensitized Solar Cells with the Cs2SnI6 Defect Perovskite as Hole-transporting Material, Energy Procedia. 102 (2016) 49–55. https://doi.org/10.1016/j.egypro.2016.11.317.

General Conclusions

5. Conclusions and Future perspectives

5.1 Conclusions

It is important for a light-activated photovoltaic cell to be able to operate well not only under ideal light conditions (e.g. direct solar light or with high energy photons), but to be able to take advantage of incident light of different wavelengths and intensities. Thus, the issue of the adaptability to different lighting conditions is an important one. For this study, low power artificial visible light sources were chosen as the target for optimization, while striving to prevent a single-focused strategy that would impair solar light performance. Specifically, the goal was for these systems to maintain their performance under the usual lighting environments while being able to take advantage of such challenging light sources, the challenge found in the radical difference in intensity, wavelength of emission or in both. DSSCs were chosen as they were a suitable 3rd generation PV technology with proven potential when operating under indoor light sources. In their effort for solar light or indoor light optimization, many bibliographic attempts sacrifice one for the other due to the indoor lighting conditions being radically different from the Standard Test Conditions (STC) and due to different parameters being more significant in one case versus the other. Therefore, a tailored architecture with optimized components was attempted.

As a first step, the optimized electrolyte formulation allowed for good DSSC performance maintained across different lighting types and illumination intensities. A universal electrolyte solution was formulated for good performance under both outdoor and indoor lighting conditions. A tailored combination of the necessary low iodine concentration with the most suitable additives in a transparent low viscosity solvent mixture (acetonitrile/butyronitrile), ensure an ideal synergy. As evidenced through optical and IPCE characterization, the almost complete transparency of the electrolyte -achieved through the choice of solvent and the weakly absorbing electrolyte components- negated any significant competitive absorption effects, thereby allowing the harvesting of lower wavelength region photons, a significant emission region for indoor lamps. Despite the low iodine content, the optimized electrolyte displayed excellent mass transport properties. No diffusion-imposed limitation occurs on the photocurrent and all electrochemical interfaces are

sufficiently optimized to permit fast charge transfer and ion transport, along with suppressed recombination, regardless of the operating conditions for the cell. The optimized electrolyte formulation allowed for proper performance being maintained between radically different light intensity levels.

In the next step, through an absorber study, the optimum sensitizer (N719) was determined based not only on its spectral characteristics but also its role against recombination, one of the more important issues for indoor PV. A series of sensitizers were tested in DSSC to study their effects during operation under solar and indoor light. Their performance under 1 sun, 0.1 sun of solar illuminated light and 200 lux of indoor fluorescent light was characterized, highlighting the significance of two factors for optimal "pan-illumination" sensitizer performance: Recombination suppression and spectral agreement. A good spectral agreement between absorber and emission source was found to be important for good utilization of the incident light from either source, while recombination suppression was found to be especially critical during operation under low intensity light, with poor suppression nullifying the advantages of a good absorption spectrum.

Finally, in order to formulate a less volatile electrolyte formulation, an air-stable perovskite material was studied. A variable temperature Raman spectroscopic investigation on Cs_2SnI_6 air-stable was undertaken in order to elucidate its vibrational properties. Upon lowering the temperature, a blue shift and narrowing of the SnI_6 stretching and bending bands was observed and attributed to lattice anharmonicity, with no signs of phase transitions across the studied temperature range. Furthermore, the $\nu^L(F_{2g})$ phonon was observed only above room temperature, pointing to anharmonic lattice dynamics in combination with the increase in oscillation energy overcoming the obstacle of weak interaction between Cs^+ with the I^- cage ions. A quasi-solid electrolyte based on this perovskite was tested in DSSCs and while a significantly lower efficiency was achieved, compared to the aforementioned acetonitrile/butyronitrile-based I^-/I_3^- electrolyte, the perovskite offers a more stable alternative to the aforementioned volatile DSSC electrolyte.

To sum up, in this work, an optimization strategy for DSSCs has been presented, specifically in the electrolyte and sensitizer components, all in an effort to minimize recombination issues and maximize charge/ion transport in the semiconductor devices under both solar and low intensity visible light. Two optimum configurations were presented, focused either on photo conversion efficiency or device stability: The first one employing a Ru dye and a finely tuned liquid electrolyte reached the top bibliographic indoor efficiency for iodide-based DSSCs while maintaining a good performance under 1 sun (higher than the reference DSSC) and the other one employing a Ru dye and a quasi-solid Cs_2SnI_6-based electrolyte mixture sacrificed a degree of efficiency for higher stability, as it is able to retain its efficiency during storage. Cells with these configurations, prepared with common, low cost and available materials, manage to maintain good performance under all tested lighting conditions from 1 sun solar simulated illumination to 100 lux of indoor fluorescent light (0.03% of 1 sun irradiance) with a consistently high fill factor, paving the way for the manufacturing of PVs that are able to operate well, under all environments and lighting conditions.

5.2 Future perspectives

Under low light conditions, the produced power density is considered to be a more appropriate performance evaluation metric than the usual PCE value [1]. For DSSCs operating under 200 lux, power densities in the range of ~4-8 $\mu W/cm^2$ have been reported by industry sources [1–4]. The synergetic strategies for the optimized device presented in this work has allowed values very close to the characteristic 200 lux PV values found in I^-/I_3^- electrolyte indoor optimization studies [2] and in industrial indoor DSSC products [4], with a power density of 8 $\mu W/cm^2$, while maintaining a solid performance under 1 sun. DSSC have been known to outperform other PV technologies under non-ideal light conditions, and are an excellent choice for BIPV, since they present better performance under non-direct light (e.g. indoors and/or diffuse solar lighting conditions) [5]. An adaptable DSSC should be able to perform well under both high and low light intensity levels for robust operation under clear sky but also under cloudy weather and indoor lighting. Concerning PIPV, power densities in the magnitude of $\mu W/cm^2$ can be produced by a module of a few cm^2 and

can be used for powering low power electronic devices such as sensors, cameras etc [2]. Furthermore, PVs with good adaptability to different light conditions can be used to power not only low energy drain products, but also more demanding devices (e.g. tablets, laptops, smartphones) with varying power draw profiles depending on their usage [6], by utilizing light regardless of the user environment (outdoors/indoors). Thus, a PV device that presents good adaptability during the changing of lighting conditions under which it operates (ranging from intense 1 sun to low power indoor light conditions) is very promising for BIPV and PIPV applications and the "pan-illumination" configuration of this work, is a step in the right direction as it offers DSSCs a degree of usage flexibility and adaptability. Further, optimization is required not only for the cells themselves but also for their integration into the BIPV/PIPV systems.

The area of DSSCs for indoor lighting environments is very attractive and relatively new, meaning there is a lot of potential for interesting future works. For DSSCs, focus should be primarily placed on electrolyte optimization. Besides the classic I_3^-/I^- electrolyte studied in this dissertation, electrolytes based on cobalt and copper have emerged for some time and have proven highly efficient as they are currently the more common applied electrolytes and have led to the latest record braking efficiencies under 1 sun. Thus, optimization studies focused on these newer electrolytes and their "pan-illumination" targeted operation is a rich area for future research. Additionally, on the sensitizer front, co-sensitization strategies can be tailored for panillumination purposes, with the aim of achieving both a panchromatic response and a good panillumination performance. This can be challenging as an effort to increase the absorption spectra for the device may not have a significant impact on indoor performance: indoor light sources are more limited in their emission spectra (compared to solar light) and it is possible that an extended absorptions spectrum may go to waste depending on the sensitizers and irradiating source. A successful balance between panchromatic and panillumination pursuits however will significantly increase the efficiency and adaptability of such devices in different light conditions. Furthermore, for a wider array of applications, it is important for a PV device to be transparent or at least semi-transparent and DSSCs are in a unique

position for optimization in this area, with a focus on the transparency of the entire device.

Finally, for a robust "panillumination" application of PVs, both stability and efficiency are needed. Stability is required to assure a constant performance by the cell and the device it is integrated into, while efficiency is required to assure a wider application in industrial products. A significant number of electronic products, such as wireless sensor networks or portable devices, require power in the range of 10nW-20μW [7]. Thus, a photovoltaic cell with such level of produced power during operation under indoor light sources is suitable for an array of real life products such as sensors or tablets [2,6], especially when considering an equally impressive efficiency under 1 sun which leads to much greater usage flexibility for the device, especially when it can be utilized equally well in radically different lighting environments. Therefore, a strategy to simultaneously achieve high efficiencies and stability by studying solid state charge transfer media for DSSCs is suggested, starting from a point of assured stability and enhancing its interfacial charge transfer properties. Perovskites and other solid media are a good choice for this path. Alternatively, optimization of sealing technologies can assure stability even for liquid electrolyte-based DSSCs. Finally, similar research goals can be set for Perovskite Solar Cells which are capable of achieving even higher efficiencies. Research focused towards rendering photovoltaic cells stable and efficient under any possible light condition will pave the way for devices that not only fully utilize solar light but also achieve maximum re-use of the energy consumed for artificial lighting, thereby reaching a significant milestone in the effort for sustainability and renewable energy.

Bibliographic references for Chapter 5

[1] Solar cell description. Section: "Electrical performance". https://gcell.com/gcell-products/custom-solar-cell, GCell, n.d.

[2] F. De Rossi, T. Pontecorvo, T.M. Brown, Characterization of photovoltaic devices for indoor light harvesting and customization of flexible dye solar cells to deliver superior efficiency under artificial lighting, Appl. Energy. 156 (2015) 413–422. https://doi.org/10.1016/j.apenergy.2015.07.031.

[3] Ricoh, https://www.ricoh.com/technology/tech/066_dssc, (n.d.).

[4] Indoor energy solutions product data sheet, 3Gsolar. (n.d.). https://static.wixstatic.com/media/dcad42_6376bc7b15b64c28afaa6b60c27a5a3e~mv2.png/v1/fill/w_945,h_625,al_c,q_90,usm_0.66_1.00_0.01/dcad42_6376bc7b15b64c28afaa6b60c27a5a3e~mv2.webp.

[5] A.G. Kontos, T. Stergiopoulos, V. Likodimos, D. Milliken, H. Desilvesto, G. Tulloch, P. Falaras, Long-term thermal stability of liquid dye solar cells, J. Phys. Chem. C. 117 (2013) 8636–8646. https://doi.org/10.1021/jp400060d.

[6] C.J. Traverse, R. Pandey, M.C. Barr, R.R. Lunt, Emergence of highly transparent photovoltaics for distributed applications, Nat. Energy. 2 (2017) 849–860. https://doi.org/10.1038/s41560-017-0016-9.

[7] J. Dagar, S. Castro-Hermosa, G. Lucarelli, F. Cacialli, T.M. Brown, Highly efficient perovskite solar cells for light harvesting under indoor illumination via solution processed SnO2/MgO composite electron transport layers, Nano Energy. 49 (2018) 290–299. https://doi.org/10.1016/j.nanoen.2018.04.027.